Structures and Reactions of Diplatinum Complexes

Thesis by
Tania V. Darnton

In Partial Fulfillment of the Requirements for the degree of
Doctor of Philosophy

CALIFORNIA INSTITUTE OF TECHNOLOGY
Pasadena, California

2017
Defended August 1, 2016

ACKNOWLEDGMENTS

First things first: Harry, you've been an amazing advisor. I feel so incredibly lucky to have had the privilege of being your student. At every turn, you have been nothing but supportive, encouraging, and understanding, while also being an unfailing advocate for my health and happiness. Thank you for taking me into your group, and thank you for encouraging me to take on leadership roles in outreach - I feel like you knew I would become a teacher before I had any inkling of it. You saw how happy I was working with the kids in CCI outreach when I couldn't even see it myself yet. Thank you for encouraging me to pursue a path in teaching; thank you for supporting and backing my decision to take a leave of absence from grad school; thank you for your indefatigable good humor. Thank you for caring about me, and thank you for taking care of all of us.

To my committee – you are my dream team. Thank you for your excitement about my chosen career, and for your commitment to getting me out "on time." You've been kind, insightful, supportive, and encouraging. I can't thank you enough for how staunchly you have committed to me completing my Ph.D., even though it meant scrapping some research plans and pushing out this thesis on an extraordinarily condensed timeline.

To Jack Richards – thank you for consistently being there for me, for always coming to my group meetings, and for having excellent suggestions for my project even if they didn't pan out. I miss you, and I wish you were here to see this.

To Maggie, Felicia, and Dana – I truly mean it when I say that I could not have done this without you. Without your friendship and unwavering support, I would have left Caltech

before my second year. Thank you for listening, for helping in every way you could, and for being there no matter what. I will miss you dearly.

To the Caltech Grad Office, the Health Center, and the Counseling Center – thank you for your help, support, and flexibility before, during, and after my leave of absence. I can't imagine a place that takes better care of its students, and you all contribute to that. Thank you for making me feel valued and cared for.

Huge gratitude and thanks go out to my research mentors in the Gray group, especially Maraia Ener, Kana Takematsu, Oliver Shafaat, Yan-Choi Lam, Gretchen Keller, Bryan Hunter, and Wes Sattler. Thank you for showing me how to be a good scientist, both by example and by instruction, and thank you for the hours you've spent over the years answering my questions, helping me on the laser, and reading my drafts!

To all my compadres and/or colleagues in the Gray group – it's been a pleasure working with you, and I mean it when I say that you made coming to work fun. Thank you for your help, jokes, and all-around good attitudes: Bryan Hunter, Stephanie Laga, Wes Sattler, Aaron Sattler, James Blakemore, Maraia Ener, Gretchen Keller, Jeff Warren, Oliver Shafaat, Kana Takematsu, Paul Bracher, Sarah Del Ciello, Mike Lichterman, Yan-Choi Lam, Brad Brennan, Nicole Bouley-Ford, Chris Roske, Carl Blumenfeld, Josef Schwann, James McKone, Peter Agbo, Daniel Konopka, Judy Lattimer, and all the members of Team Fun.

To Paul Bracher – thank you for being a champion of chemistry education, and for demonstrating to me that deciding to dedicate the majority of one's time to teaching can be a Good Idea. I'm proud to count you among my personal friends, but I wish you were closer!

To Rick Jackson and Catherine May – thank you for taking care of the group, and for always keeping the fourth floor stocked with pastries, coffee, water, tea, and the all-important half-and-half. I'll miss swinging by to chat with you and attempting to do word jumbles with Larry and Professor Marsh. Rick, may you always have an orchid in bloom!

To Mike, Alli, and Shaunae- you are some of the only people in my life who will ever understand how much completing this degree really means to me. Thank you for being there, for listening, and for always having good advice.

Mutti and Vati – it's finally over! Thank you for being supportive through all this, and for standing behind my decision to stay at Caltech even (or especially) when things looked impossibly bleak. Thank you for driving out to Pasadena and taking me out to breakfast so many times, and for helping out in any way you could whenever I asked you. You both mean the world to me, and I hope to get to see more of you now that I have a job with a set schedule!

Roxanne – I love how with every year that goes by, our relationship gets better and stronger. I couldn't imagine a better sister, and I'm so happy to have you in my life and (relatively) nearby! Thank you for coming up to hang out for no reason, for inspiring me with your commitment to your physical well-being, and for standing with me as an advocate for familial transformation. Jason – you're the greatest brother-in-law. Thanks for your punny sense of humor, for taking care of my sister, and for always looking out for my digital welfare. Lots and lots of lob to both of you from PTT.

To Greg – meeting you just as I entered the most stressful and difficult period of my entire life is not the timing I would have chosen, but I will always choose you. Thank you for believing in me, for doing everything in your power to make me happy, for committing to us, and for being my partner in everything from spur-of-the-moment Death Valley trips to catching Pokémon.

Now, on to the next adventure!

ABSTRACT

A d^8–d^8 complex $[Pt_2(\mu\text{-}P_2O_5(BF_2)_4]^{4-}$ (abbreviated $Pt(pop\text{-}BF_2)^{4-}$) undergoes two $1e^-$ reductions at $E_{1/2} = -1.68$ and $E_p = -2.46$ V (vs Fc^+/Fc) producing reduced $Pt(pop\text{-}BF_2)^{5-}$ and superreduced $Pt(pop\text{-}BF_2)^{6-}$ species, respectively. The EPR spectrum of $Pt(pop\text{-}BF_2)^{5-}$ and UV−vis spectra of both the reduced and the superreduced complexes, together with TD-DFT calculations, reveal successive filling of the 6pσ orbital accompanied by gradual strengthening of Pt−Pt bonding interactions and, because of 6pσ delocalization, of Pt−P bonds in the course of the two reductions. Both reduction steps proceed without changing either d^8 Pt electronic configuration, making the superreduced $Pt(pop\text{-}BF_2)^{6-}$ a very rare $6p^2$ σ-bonded binuclear complex. However, the Pt−Pt σ bonding interaction is limited by the relatively long bridging-ligand-imposed Pt−Pt distance accompanied by repulsive electronic congestion. $Pt(pop\text{-}BF_2)^{4-}$ is predicted to be a very strong photooxidant (potentials of +1.57 and +0.86 V are estimated for the singlet and triplet dσ*pσ excited states, respectively).

Further study of the electronic excited states of $Pt(pop\text{-}BF_2)^{4-}$ in the presence of luminescence quenchers revealed Stern-Volmer type dynamic quenching of the triplet state by trialkyl and triaryl amines. Quenching of the singlet as well as the triplet was observed in the presence of Co^{II} trisbipyridine complexes, but sample decomposition and the observed presence of simultaneous static and dynamic quenching behaviors hampered quantitative analysis.

PUBLISHED CONTENT AND CONTRIBUTIONS

Darnton, T. V. et al. (2016). “Reduced and Superreduced Diplatinum Complexes.” In: *Journal of the American Chemical Society*, 138.17, pp. 5699-5705. DOI: 10.1021/jacs.6b02559

T.V.D. participated in the conception of the project; conducted absorption, electron paramagnetic resonance, electrochemical, and spectroelectrochemical experiments; prepared and analyzed data; and participated in the writing of the manuscript.

TABLE OF CONTENTS

CHAPTER 1: INTRODUCTION TO D^8-D^8 SYSTEMS

1.1 Background and history

Coordination compounds based on metals with a d^8 electron configuration have been of interest to chemists for nearly two hundred years. In 1830, Heinrich Magnus first reported the discovery of a green salt prepared from aqueous solutions of $[Pt(NH_3)_4]^{2+}$ and $[PtCl_4]^{2-}$; in 1957, it was discovered that Magnus' salt, rather than being a single molecule like Peyrone chloride (*cis*-$PtCl_2(NH_3)_2$), was in fact a polymer consisting of alternating $[PtCl_4]^{2-}$ anions and $[Pt(NH_3)_4]^{2+}$ cations.[1] This "polymer" could also be described as a series of d^8 square planar metal atoms interacting with each other along the coordination axis.

In the 1960s and 70s, the study of d^8 coordination chemistry was undertaken in earnest by groups such as Gray, Mann, Miskowski, Connick, and others. Researchers began to find that d^8 compounds, and particularly binuclear d^8-d^8 compounds, have access to a range of electronically excited states. This corresponds to a wealth of unique luminescence properties. Although thermal reactivity has always been one of the fundamental tenets of chemistry, the reactivity and applications of electronically excited states has greatly increased in importance and impact since the inception of the field in the mid-1900s.

1.2 Photochemistry of binuclear d^8-d^8 metal complexes

D^8 metal complexes commonly adopt a square-planar geometry with four coordinating ligands.[2] In a face-to-face dimeric structure of this type, transition metals such as Rh, Ir, and Pt exhibit a significant amount of metal-metal bonding character in their electronically excited states. This contributes to a rich photochemistry.

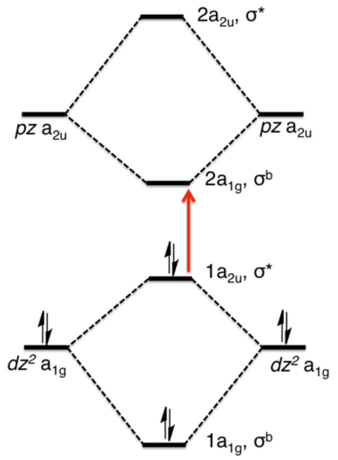

Figure 1: MO diagram of the HOMO to LUMO transition in d^8-d^8 complexes.[3]

The intense photochemical activity of face-to-face D_{4h} d^8-d^8 complexes is readily explained by a simplified molecular orbital (MO) diagram, as shown in Figure 1. Extensive spectroscopic and theoretical studies have demonstrated that the highest occupied molecular orbital (HOMO) is a $d\sigma^*$ (with respect to M-M bonding) orbital of a_{2u} symmetry and d_{z^2} parentage; specifically, it is a molecular orbital that results from the overlap of the two metal d_{z^2} (a_{1g}) atomic orbitals. The lowest energy transition is to an orbital of a_{1g} symmetry and p_z parentage. As this excitation is from an orbital of σ-antibonding character to one of σ-bonding character, the promotion results in the formation of a full metal-metal bond in the excited state as well as the formation of a "hole" at an open coordination site on a metal atom (Figure 2).[4] The $^3(d\sigma^*p\sigma)$ excited state is capable of performing a variety of reactions that would be thermodynamically disfavored for the ground state, including atom abstraction and intermolecular electron transfer.

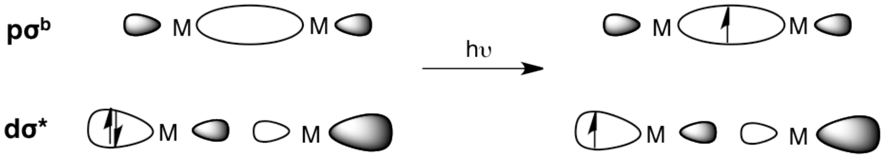

Figure 2: Electron localization on metal MOs.[4]

The study of d^8-d^8 dimeric compounds has long been a theme in the Gray group. In 1976, researchers in the Gray group first synthesized a dimeric Rh^I complex ligated by four 1,3-diisocyanopropane (“bridge”) moieties. This compound, when irradiated at 546 nm in an aqueous solution of HCl, was found to produce hydrogen gas with concomitant oxidation of the complex to form $[Rh_2(bridge)_4Cl_2]^{2+}$. In 1990, Fox and coworkers studied the kinetics of photoinduced electron transfer d^8-d^8 Ir_2 phosphonite complexes and demonstrated the existence of an inverted free-energy dependence of electron transfer kinetics at high driving forces. This was one of the first examples of a Marcus “inverted region” in chemical kinetics.[5]

1.3 Remarkable properties of pyrophosphito-bridged diplatinum(II) compounds

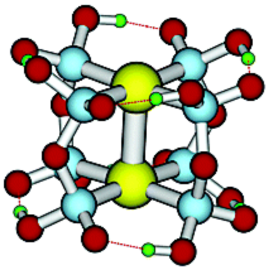

Figure 3: Structure of Pt(pop)$^{4-}$ [6]

One compound that has garnered particular attention is tetrakis(μ-pyrophosphito) diplatinate(II)$^{4-}$, also known as $^{4-}$ due to its bridging P-O-P moieties. The compound consists of two d^8 square planar ML_4 fragments supported by pyrophosphito bridges. The two halves are eclipsed, giving rise to a lantern-like complex with D_{4h} symmetry (Figure 3). In the ground state, the Pt-Pt distance is 2.93 Å; while generally this distance is too long to be considered a bond and the molecular orbital (MO) diagram indicates a formal bond order of zero, resonance Raman studies as well as recent theoretical work show that there is indeed some degree of bonding in the ground state due to favorable mixing of the (n)d_{z^2} and (n+1)p_z orbitals.[8,9]

1.3.1 *Photophysical properties*

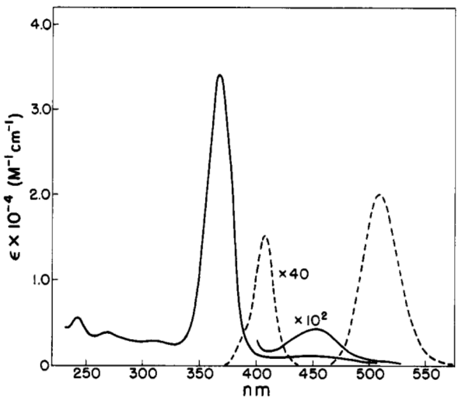

Figure 4: Absorption (solid) and emission (dashed) spectra of the potassium salt of Pt(pop)$^{4-}$ in water.[7]

The absorption spectrum of the tetra-*n*-butylammonium salt of Pt(pop)$^{4-}$ in MeCN shows an intense electronic absorption band at 372 nm (ε = 33400 M^{-1} cm^{-1}) which is assigned to the $^1A_{1g} \rightarrow {}^1A_{2u}$ transition ($d\sigma^* \rightarrow p\sigma$). A much weaker absorption at 454 nm (ε = 155 M^{-1} cm^{-1}) is assigned to the spin-forbidden triplet transition, $^1A_{1g} \rightarrow {}^3A_{2u}$.[10] Fluorescence from the $^1(d\sigma^*p\sigma)$ state decays on the picosecond timescale and is quite dependent on temperature and solvent, while remarkably long-lived phosphorescence (on the order of 10 μs with a quantum yield of 50%) is observed from the $^3(d\sigma^*p\sigma)$ state in a variety of solvents (Figure 4).[10-12]

The lowest energy transition for Pt(pop)$^{4-}$, as in other d^8-d^8 complexes, promotes an electron from a Pt-Pt antibonding (n)$d\sigma^*$ orbital to an (n+1)$p\sigma$ orbital, leading to an increase in the formal bond order and a contraction of the Pt-Pt distance by ≈0.24 Å.[13] In addition to X-ray studies, the presence of a Pt-Pt bond upon excitation has been investigated by a Franck-Condon analysis of the vibronic progression measured by resonance Raman in the $d\sigma^* \rightarrow p\sigma$ absorption bands in single crystals at low temperatures.[8]

1.3.2 Electron transfer

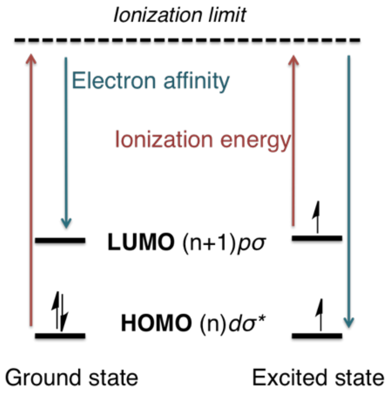

Figure 5: Graphical representation of the enhanced oxidizing (blue) and reducing power (red) of a d^8-d^8 compound's excited state.[11]

Photoexcitation (i.e. promotion of an electron from the HOMO to the LUMO) of Pt(pop)$^{4-}$ generates a species that is both a more powerful oxidant *and* reductant than the ground state species. The reducing power of a species (or, its ability to be oxidized and lose an electron) is defined as the energy required to remove its highest-energy electron (i.e. the ionization energy). The excited state of Pt(pop)$^{4-}$ is a better reductant than the ground state because its highest energy electron is in the (n+1)$p\sigma$ orbital rather than the (n)$d\sigma^*$ orbital, making that electron easier to remove by an amount of energy equal to the spectroscopic transition.

By a parallel argument, the excited state of Pt(pop)$^{4-}$ is a stronger oxidant than the ground state because the oxidizing power of a species is defined by its electron affinity. Since the excited state of Pt(pop)$^{4-}$ has a "hole" at the (n)$d\sigma^*$ level, transferring an electron there is more favored than transferring an electron into the LUMO of the ground state, which is the higher energy (n+1)$p\sigma$ level. These arguments are illustrated in Figure 5.

These general properties of Pt(pop)$^{4-}$ combined with the microsecond lifetime of the triplet excited state combine to form a compound that reacts readily with many substrates, including hydrocarbons, alkyl halides, and alcohols.[14] Mechanisms of these reactions may be described as inner-sphere electron transfer processes or as photochemical oxidative addition involving transfer of hydrogen or halogen atoms.

1.3.3 Known reactions of Pt(pop)$^{4-}$

Pt(pop)$^{4-}$ undergoes thermal two-electron, two-center oxidative additions of halogens or alkyl halides to produce axially substituted diplatinum(III) complexes Pt_2X_2 or Pt_2RX. These diamagnetic complexes possess an intermetallic bond joining the Pt^{III} centers. These complexes may also be synthesized by the chemical oxidation of Pt(pop)$^{4-}$ in the presence of halide ions. Mixed valence species of the type Pt_2X have also been observed transiently.

Excited-state studies demonstrated that ^{3}[Pt(pop)$^{4-}$]* is a one-electron reductant in aqueous solution; it may also be quenched by halogen- or hydrogen-atom transfer by alkyl and aryl halides or by hydrogen-atom donors like alcohols, silanes, and stannanes. Pt(pop)$^{4-}$ is also known to catalytically produce hydrogen gas, as in the photochemical conversion of isopropyl alcohol to acetone and an equivalent of hydrogen. Furthermore, alkenes and alkynes both react with ^{3}[Pt(pop)$^{4-}$]*, either by energy transfer to effect photoisomerization or by hydrogen-atom abstraction to form an organic radical and Pt_2H.

1.4 Structural control of $^1A_{2u}$-to-$^3A_{2u}$ intersystem crossing (ISC) in Pt(pop) by BF_2 functionalization

Due to its symmetric and relatively uncomplicated structure, Pt(pop)$^{4-}$ does not offer many opportunities for functionalization or derivatization. Replacement of the oxygen atoms in the P-O-P bridges by a methylene group curtails the reactive (and therefore greatly desired) $^3(d\sigma^*p\sigma)$ lifetime to only 55 ns.[15] However, in 2011 Yan-Choi Lam and collaborators in the Bercaw group synthesized a derivative of Pt(pop)$^{4-}$ in which all eight hydrogen atoms of the pyrophosphito groups are replaced with electron-withdrawing BF_2 groups, each of which links the oxygen atoms of two different bridges to form a cage-like structure (Figure 6).[14]

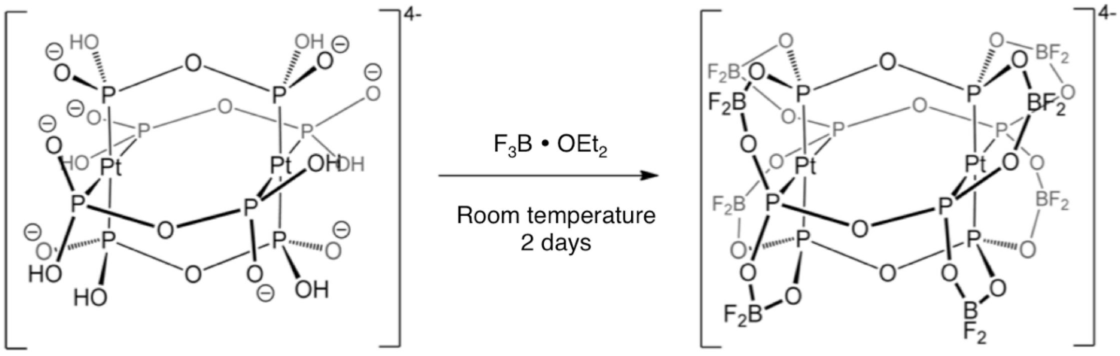

Figure 6: Synthesis of $Pt(pop\text{-}BF_2)^{4-}$

This compound, per(difluoroboro)tetrakis(μ-pyrophosphito)diplatinate(II)$^{4-}$, will be referred to as $Pt(pop\text{-}BF_2)^{4-}$ for the remainder of this work. The electron-withdrawing nature of the BF_2 groups has the effect of removing electron density from the phosphorus atoms that are directly ligated to the Pt^{II} centers. This stabilizes the $d\pi$ levels in $Pt(pop\text{-}BF_2)^{4-}$ compared to $Pt(pop)^{4-}$, making it a stronger oxidant than the parent compound.

1.5 Photophysical implications of BF_2 functionalization

The "perfluoroboration" of Pt(pop) has dramatic effects on its photophysical properties. Table 1 compares the absorption and emission properties of $Pt(pop)^{4-}$ and $Pt(pop\text{-}BF_2)^{4-}$.[14]

Table 1: Comparison of $Pt(pop)^{4-}$ and $Pt(pop\text{-}BF_2)^{4-}$

$Pt(pop\text{-}BF_2)^{4-}$	**$Pt(pop)^{4-}$**	**Assignment**

Absorption, nm (ε, M^{-1} cm^{-1})		
233 (7880)	246 (3770)	LMMCT
260 (3180)	285 (2550)	LMMCT
291 (2110)	315 (1640)	LMMCT
365 (37500)	372 (33400)	$^{1}(d\sigma^{*}\rightarrow p\sigma)$ $^{1}A_{1g}\rightarrow {}^{1}A_{2u}$
454 (140)	454 (155)	$^{3}(d\sigma^{*}\rightarrow p\sigma)$ $^{1}A_{1g}\rightarrow {}^{3}A_{2u}$
Emission, nm (Lifetime at 21 °C)		
393 (1.6 ns)	398 (~8 ps)	$^{1}(p\sigma\rightarrow d\sigma^{*})$ $^{1}A_{2u}\rightarrow {}^{1}A_{1g}$
512 (8.4 μs)	511 (9.4 μs)	$^{3}(p\sigma\rightarrow d\sigma^{*})$ $^{3}A_{2u}\rightarrow {}^{1}A_{1g}$
Emission Stokes Shift, cm^{-1}		
1760	2230	Fluorescence
2460	2500	Phosphorescence
E_a for ISC (cm^{-1})		
2230	1190	$^{1}A_{2u}$-$^{3}E_{u}$ S-O coupling

The metal-centered absorption features (the $d\sigma^{*}\rightarrow p\sigma$ transitions) of Pt(pop-BF_2)$^{4-}$ are similar to those of Pt(pop)$^{4-}$; shifts of only about five hundred wavenumbers are observed. This is expected, as the BF_2 functionalization should not affect the $d \rightarrow p$ absorption features; the effect of the BF_2 groups is instead to stabilize the metal-centered orbitals as a whole. The most intense band at 365 nm (27397 cm^{-1}) results from the $d\sigma^{*} \rightarrow p\sigma$ ($^{1}A_{1g} \rightarrow {}^{1}A_{2u}$) transition; the same transition in Pt(pop)$^{4-}$ occurs at 372 nm (26881 cm^{-1}). The much more weakly absorbing spin forbidden singlet-to-triplet

($^1A_{1g} \rightarrow {}^3A_{2u}$) transition occurs at 454 nm in Pt(pop-BF$_2$), the same as in the original compound (Figure 7and Figure 4). All of the ligand-to-metal/metal charge transfer (LMMCT) absorption

bands in Pt(pop-BF$_2$)$^{4-}$ are blue-shifted by several thousand wavenumbers compared to Pt(pop)$^{4-}$. This indicates that the ligand orbital energies are decreasing with respect to the metal orbitals. As the highest-energy occupied ligand orbitals are likely of oxygen origin, it stands to reason that an electron-withdrawing BF$_2$ group would decrease their energy and therefore raise the LMMCT transition energy. Although the BF$_2$ groups are also stabilizing the Pt centers, given the spectroscopically observed blue shift their effect on the ligand orbitals must be more dramatic.

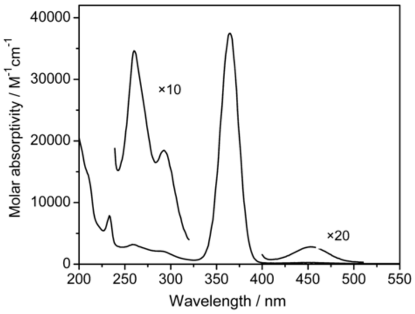

Figure 7: Absorption spectrum of Pt(pop-BF$_2$).[14]

Compared to the absorbance spectra, the emission spectra of Pt(pop)$^{4-}$ and Pt(pop-BF$_2$)$^{4-}$ differ greatly. While both compounds exhibit very strong, long-lived phosphorescence at room temperature at ~512 nm, Pt(pop-BF$_2$)$^{4-}$ has nearly equally strong fluorescence at 393 nm, while the corresponding fluorescence of Pt(pop)$^{4-}$ at 398 nm is three orders of magnitude weaker as measured by emission quantum yields.[14] Furthermore, the 1.6 ns fluorescence lifetime for Pt(pop-BF$_2$)$^{4-}$ is over 500 times longer than the corresponding values of ~3 ps previously reported for Pt(pop)$^{4-}$;[16-18] this indicates that intersystem crossing (ISC) in Pt(pop-BF$_2$)$^{4-}$ is much slower than in Pt(pop)$^{4-}$.

Direct intersystem crossing (ISC) between states of identical symmetries (for example, $^1A_{2u} \rightarrow {}^3A_{2u}$) is allowable only in point groups where one of the rotation components belongs to the totally symmetric representation; therefore, it is forbidden in the D_{4h} point group of Pt(pop)$^{4-}$ and

$Pt(pop\text{-}BF_2)^{4-}$. However, ISC may become partially allowed via spin-orbit coupling with higher triplet states. In $Pt(pop)^{4-}$ and $Pt(pop\text{-}BF_2)^{4-}$, this higher triplet state of interest is likely the ^3E_u of LMMCT origin. By undergoing symmetry-allowed spin-orbit coupling with the ^3E_u state, the $^1A_{2u}$ state is able to cross to the $^3A_{2u}$ state, thus leading to the long-lived phosphorescence observed in both the Pt_2^{4-} complexes.

The 500-fold less rapid ISC in $Pt(pop\text{-}BF_2)^{4-}$ versus $Pt(pop)^{4-}$ is attributable to the fact that ISC results from spin-orbit coupling to an LMMCT state. The BF_2 groups lower the energy of the ligand states, as evidenced by the higher-energy LMMCT bands in the absorption spectra. A higher energy ^3E_u state makes spin-orbit coupling with the $^1A_{2u}$ state less favorable, thereby slowing the rate of ISC in $Pt(pop\text{-}BF_2)^{4-}$. Furthermore, solvent vibrations are quite important for acting as energy-accepting modes during ISC, as evidenced by the strong solvent dependence of $Pt(pop)^{4-}$ decay kinetics.[17] Given that BF_2 groups are both bulkier than the O–H···O– groups and that they form a rigid covalent cage rather than a more flexible hydrogen bonded one, one would expect that solvent interactions would be diminished. By that reasoning, the ability of the solvent to provide vibrational coupling between the singlet and triplet states is reduced for $Pt(pop\text{-}BF_2)^{4}$. The dramatic reduction in the rate of intersystem crossing and the concomitant increase in ISC activation energy, from 1190 cm^{-1} for $Pt(pop)^{4-}$ to 2230 cm^{-1} for $Pt(pop\text{-}BF_2)^{4-}$, is the reason for the much longer lived singlet in the perfluoroborated compound (1.6 ns vs 8 ps).

1.6 Electrochemical implications of BF_2 functionalization

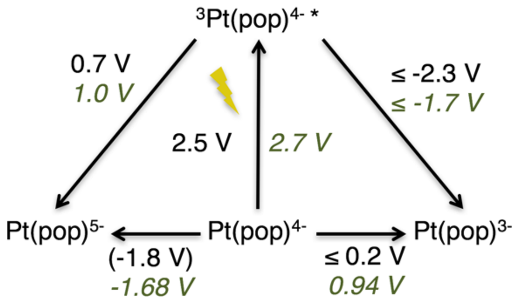

Figure 9: Latimer diagram for $Pt(pop)^{4-}$ and *$Pt(pop\text{-}BF_2)^{4-}$*. Reduction potentials (all reported versus Fc^+/Fc)[i] for Pt(pop) are written in black;[11] reduction potentials for $Pt(pop\text{-}BF_2)$ are written in *green italics*.[19]

As discussed in section 1.4, the BF_2 groups were predicted to make $Pt(pop\text{-}BF_2)^{4-}$ a stronger oxidant. Recent research published by myself and Bryan Hunter et al. places the potential of the reversible $Pt(pop\text{-}BF_2)^{4-/5-}$ couple at -1.68 V vs Fc^+/Fc while also predicting the existence of an even more reduced compound, $Pt(pop\text{-}BF_2)^{6-}$, due to a second irreversible reduction wave at -2.46 V.[19] As expected, the single electron reduction potential for $Pt(pop\text{-}BF_2)^{4-}$ lies at a more positive potential than that of $Pt(pop)^{4-}$. A Latimer diagram illustrating the electrochemical differences between the two compounds is presented in Figure 9. The excited state reduction potential for $^3[Pt(pop\text{-}BF_2)^{4-}]^*$ is estimated based on spectroscopic data to be approximately 1.0 V, which makes it comparable in oxidative strength to compounds like $[NO]^+$ ($E^{o\prime}$ = 1.0 V vs Fc/Fc^+ in CH_2Cl_2) and $[Ru(phen)_3]^{3+}$ ($E^{o\prime}$ ≈ 0.87 V vs Fc/Fc^+ in CH_3CN).[20] Meanwhile, $^1[Pt(pop\text{-}BF_2)^{4-}]^*$ is expected to have even *more* oxidizing power, as the spectroscopic difference between the absorption peaks for the triplet and the singlet is ≈5000 cm^{-1}, which corresponds to a 620 mV more positive potential. Given the short lifetime of the singlet state, it is improbable that this oxidizing power could be utilized in a diffusional solution setting; however, the possibilities for direct charge- or energy-transfer to substrates are substantial.

---

[i] Historic values for $Pt(pop)^{4-}$ were reported by Harvey in acetonitrile with respect to NHE; potentials were converted to a ferrocene reference by adding 0.64 V.

1.7 Applications

The oxidative strength of $[\mathrm{Pt(pop\text{-}BF_2)^{4-}}]^*$ and its steric bulk, combined with the fact that the production of the excited state is phototriggered, make it an attractive candidate for probing reactivity via transient absorption (TA) spectroscopy. As previously mentioned, canonical $\mathrm{Pt(pop)^{4-}}$ is capable of performing a variety of organic transformations on its own due to the rotational flexibility of the terminal hydroxyl groups. This flexibility leaves the metal centers unblocked, and these open axial coordination sites on each Pt atom allow "docking" of various substrates with subsequent atom abstraction. The much more hindered and rigidly covalent $\mathrm{BF_2}$ cage precludes this type of reactivity in $\mathrm{Pt(pop\text{-}BF_2)^{4-}}$. Unpublished results in the Gray Group obtained by Yan-Choi Lam indicate that $\mathrm{Pt(pop\text{-}BF_2)^{4-}}$ possesses very little, if any, of the inherent reactivity of $\mathrm{Pt(pop)^{4-}}$ discussed in 1.3.3. For example, $\mathrm{Pt(pop)^{4-}}$ reacts rapidly with iodomethane to form the oxidative addition product, but $\mathrm{Pt(pop\text{-}BF_2)^{4-}}$ is wholly unreactive toward such powerful electrophiles.[21] However, considering the case where *only* electron transfer is desired from $\mathrm{Pt(pop\text{-}BF_2)^{4-}}$ to trigger reactivity in a *different* molecule, this lack of reactivity is actually quite a boon. Given its relative inertness, $\mathrm{Pt(pop\text{-}BF_2)^{4-}}$ is hoped to act as an outer sphere electron transfer agent only, with little or no inherent reactivity of its own. Meanwhile, the reduced (5-) and superreduced (6-) states are expected to be much more reactive than the parent compound and may act directly as catalytic agents. Initial studies in these areas will be discussed.

REFERENCES

(1) Atoji, M.; Richardson, J. W.; Rundle, R. E. *J. Am. Chem. Soc.* **1957**, *79*, 3017.

(2) Yam, V. W.-W.; Au, V. K.-M.; Leung, S. Y.-L. *Chem. Rev.* **2015**, *115*, 7589.

(3) Mann, K. R.; Gordon, J. G.; Gray, H. B. *J. Am. Chem. Soc.* **1975**, *97*, 3553.

(4) Smith, D. C.; Gray, H. B. *Coord. Chem. Rev.* **1990**, *100*, 169.

(5) Fox, L. S.; Kozik, M.; Winkler, J. R.; Gray, H. B. *Science* **1990**, *247*, 1069.

(6) Pan, Q.-J.; Fu, H.-G.; Yu, H.-T.; Zhang, H.-X. *Inorg. Chem.* **2006**, *45*, 8729.

(7) Che, C. M.; Butler, L. G.; Gray, H. B. *J. Am. Chem. Soc.* **1981**, *103*, 7796.

(8) Che, C. M.; Butler, L. G.; Gray, H. B.; Crooks, R. M.; Woodruff, W. H. *J. Am. Chem. Soc.* **1983**, *105*, 5492.

(9) Bercaw, J. E.; Durrell, A. C.; Gray, H. B.; Green, J. C.; Hazari, N.; Labinger, J. A.; Winkler, J. R. *Inorg. Chem.* **2010**, *49*, 1801.

(10) Stiegman, A. E.; Rice, S. F.; Gray, H. B.; Miskowski, V. M. *Inorg. Chem.* **1987**, *26*, 1112.

(11) Harvey, E. L. Dissertation (Ph.D.), California Institute of Technology, 1990.

(12) Heuer, W. B.; Totten, M. D.; Rodman, G. S.; Hebert, E. J.; Tracy, H. J.; Nagle, J. K. *J. Am. Chem. Soc.* **1984**, *106*, 1163.

(13) Christensen, M.; Haldrup, K.; Bechgaard, K.; Feidenhans'l, R.; Kong, Q.; Cammarata, M.; Russo, M. L.; Wulff, M.; Harrit, N.; Nielsen, M. M. *J. Am. Chem. Soc.* **2008**, *131*, 502.

(14) Durrell, A. C.; Keller, G. E.; Lam, Y.-C.; Sykora, J.; Vlček, A.; Gray, H. B. *J. Am. Chem. Soc.* **2012**, *134*, 14201.

(15) King, C.; Auerbach, R. A.; Fronczek, F. R.; Roundhill, D. M. *J. Am. Chem. Soc.* **1986**, *108*, 5626.

(16) van der Veen, R. M.; Cannizzo, A.; van Mourik, F.; Vlček, A.; Chergui, M. *J. Am. Chem. Soc.* **2010**, *133*, 305.

(17) Milder, S. J.; Brunschwig, B. S. *J. Phys. Chem.* **1992**, *96*, 2189.

(18) Vlček, A. 2016.

(19) Darnton, T. V.; Hunter, B. M.; Hill, M. G.; Záliš, S.; Vlček, A.; Gray, H. B. *J. Am. Chem. Soc.* **2016**, *138*, 5699.

(20) Connelly, N. G.; Geiger, W. E. *Chem. Rev.* **1996**, *96*, 877.

(21) Lam, Y.-C.; Darnton, T. Unpublished results.

CHAPTER 2: SYNTHESIS AND CHARACTERIZATION OF $Pt(POP-BF_2)^{4-}$

As discussed in Chapter 1, $Pt(pop)^{4-}$ participates in and facilitates a wide array of reactions. In its excited state, $[Pt(pop)^{4-}]^*$ is able to abstract hydrogen atoms from a variety of substrates including stannanes, silanes, alcohols, and hydrocarbons. It also reacts readily with alkyl and aryl halides (R or RX) to form the axially substituted Pt^{III}-Pt^{III} oxidative addition product (i.e. $[Pt(pop)-RX]^{4-}$ or $[Pt(pop)-X_2]^{4-}$) and, in the case of dihalide, the corresponding organic radical coupling product R_2.

In the late 1980s, Harvey prepared a fluoroborated analog of $Pt(pop)^{4-}$ by reaction with gaseous BF_3; however, the method replaced on average only six of the protons with BF_2 groups rather than the full eight replacements needed to form a complete covalent cage of bridging BF_2 groups. Unsurprisingly, the mix of constitutional isomers produced (Figure 1) via partial fluoroboration made the compound troublesome to purify. Presumably, this also explains why

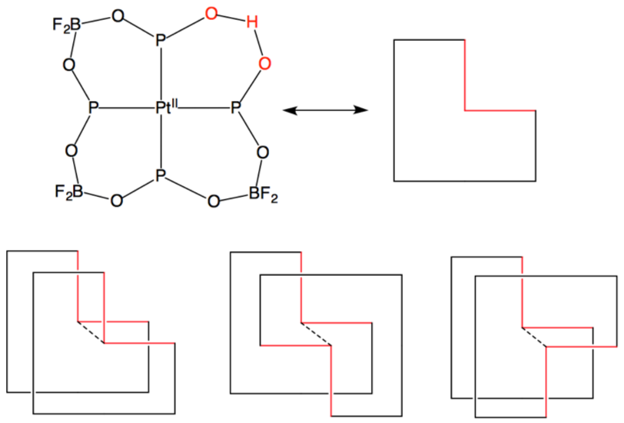

Figure 1: Schematic representation of the possible isomers resulting from the replacement of six of Pt(pop)'s eight protons with BF_2 groups, assuming neither half of the Pt_2 dimer experiences full replacement.[1]

Harvey was not able at the time to rigorously determine the compound's properties, particularly with respect to NMR signatures.[1]

In 2011, Yan-Choi Lam and collaborators in the lab of John Bercaw developed a more robust and reliable synthetic method for producing Pt(pop-BF_2)$^{4-}$ by stirring Pt(pop)$^{4-}$ in neat boron trifluoride diethyletherate (BF_3•Et_2O) for several days.[2] Initial experiments performed by Durrell, Lam, and Keller indicated that Pt(pop-BF_2)$^{4-}$, as predicted by Harvey, possessed unique luminescence properties that clearly differentiated it from its parent, Pt(pop)$^{4-}$.[2] In late 2012, intrigued by this relatively new and unexplored compound, I decided to devote my doctoral research to its study.

2.1 Synthetic developments

Before embarking on more complex analytical studies of Pt(pop-BF_2)$^{4-}$'s luminescence and reactivity, I first endeavored to corroborate the basic synthetic and luminescence results reported by Durrell and coworkers. As a result, I further developed Lam's synthesis of Pt(pop-BF_2)$^{4-}$ by improving the glassware setup and work-up techniques to decrease the possibility of exposure to BF_3•Et_2O or its hydration product, hydrofluoric acid (see section 2.4.6).

During this process, the tetraphenylphosphonium (Ph_4P^+) salt of Pt(pop-BF_2)$^{4-}$ was crystallized and characterized via X-ray diffraction for the first time (Figure 2). Prior to this point, only the tetrabutylammonium ($(n\text{-Bu})_4N^+$) salt had been reported in the literature, although the tetraphenylarsonium (Ph_4As^+) salt had also been accessed by Lam.[2-4] In $[Ph_4P]_4$[Pt(pop-BF_2)], the distance between the largest electron density maxima is 2.85 Å, which corresponds to the Pt-Pt distance. However, the compound crystallizes in the monoclinic space group $P2_1/n$ with only half of the molecule and two tetraphenylphosphonium cations in the asymmetric unit. Attempts to refine the density maxima as a second platinum position were unsuccessful; this could account for the slight discrepancy between this 2.85 Å distance and Lam's previously reported value of 2.89 Å for the tetraphenylarsonium salt of Pt(pop-BF$_2$)$^{4-}$.[4] Both the Pt-Pt distance values for salts of Pt(pop-BF$_2$)$^{4-}$ are significantly smaller than the value of 2.93 Å reported for K$_4$Pt(pop); this could be attributed to the overall contraction of the Pt-Pt unit due to the rigidity of the BF$_2$ covalent "cage."[4,5] X-ray data are tabulated in Table 1 through Table 5 in section 2.6.

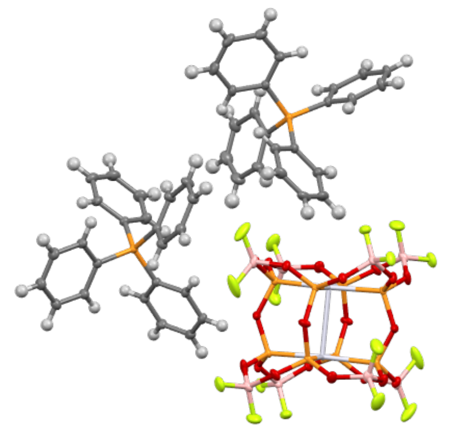

Figure 2: Crystal structure of [Ph$_4$P]$_4$[Pt(pop-BF$_2$)].

2.2 Basic luminescence properties

With the goal of duplicating the values for E_a, k_r and k_0 obtained by Durrell and coworkers, solutions of Pt(pop-BF$_2$)$^{4-}$ in acetonitrile were analyzed via both time-resolved and steady-state techniques to obtain values for fluorescence lifetime and quantum yield. With values for fluorescence lifetime and quantum yield in hand, values for E_a, k_r, and k_0 can be calculated. These new data were compared directly to the values published in 2012.

2.2.1 Theoretical basis

In their 1992 publication probing the luminescence lifetimes of Pt(pop)$^{4-}$, Milder and Brunschwig presented an elegant series of experiments and equations for combining time-resolved and steady-state data taken at various temperatures to determine the activation energy of intersystem crossing between the singlet and triplet excited states, as well as the rates of radiative and nonradiative decay from the singlet state. These equations were applied to $Pt(pop\text{-}BF_2)^{4-}$ by Durrell and coworkers.

In $Pt(pop\text{-}BF_2)^{4-}$, analogously to $Pt(pop)^{4-}$, an electron in the singlet excited state has several pathways available by which to return to the ground state. It may nonradiatively decay (that is, decay without emitting a photon) or radiatively decay by emitting a photon (fluorescence). Nonradiative decay may occur either by intersystem crossing to the triplet state or by nonemissive decay to the ground state (for example, due to energy loss from solvent interactions). The rate of nonemissive decay to the ground state is represented by the rate constant k_d while the rate of intersystem crossing is represented by the rate constant k_{ISC}; the rate of radiative decay is denoted by k_r. Therefore, the total amount of nonradiative decay may be represented by the sum of k_d and k_{ISC}. As proposed by Milder and Brunschwig for $Pt(pop)^{4-}$, k_{ISC} for $Pt(pop\text{-}BF_2)^{4-}$ is presumed to follow Arrhenius-like behavior.

$$k_{nr} = k_d + k_{ISC} = k_d + \left(k_0 + \frac{A}{\sqrt{k_B T}} e^{-\frac{E_a}{k_B T}}\right) \qquad (1)$$

Meanwhile, the fluorescence lifetime (τ_{fl}) is inversely proportional to the rates of the decay paths out of the excited state:

$$\frac{1}{\tau_{fl}} = k_r + k_{nr} = k_r + k_d + k_0 + \frac{A}{\sqrt{k_B T}} e^{-\frac{E_a}{k_B T}} \qquad (2)$$

The lifetime τ_{fl} may be extracted from a luminescence-decay plot. By observing τ_{fl} at various temperatures, the following relation derived from equation (2) used with an appropriate fitting program may be used to find values for the unknowns A, E_a, and $k_r + k_d + k_0$.

$$y = \frac{1}{\tau_{fl}}$$

$$x = \frac{1}{T}$$

$$y = \alpha + \frac{\beta\sqrt{x}}{\sqrt{0.695}} e^{\frac{-\gamma x}{0.695}} \qquad (3)$$

in which

$$\alpha = k_r + k_d + k_0 \approx k_r + k_0$$

$$\beta = A$$

$$\gamma = E_a$$

Finally, the quantum yield (Φ) of a radiation-induced process is the number of times a specific event occurs per photon absorbed by the system. In this case, the quantum yield describes the ratio of photons emitted through fluorescence to total photons absorbed. Photons emitted through fluorescence can be equated to the radiative decay rate k_r, while total photon absorption is equal to the sum of the rates of all decay pathways: $k_r + k_{nr}$.

$$\Phi_{fl} = \frac{k_r}{k_r + k_{nr}} \qquad (4)$$

Equations (1) and (4) can be combined to give an expression for quantum yield that is dependent on k_r, k_d, k_0, E_a, and the temperature T.

$$\frac{1}{\Phi_{fl}} = \frac{k_{nr} + k_r}{k_r} = 1 + \frac{k_{nr}}{k_r} = 1 + \frac{k_d + k_0}{k_r} + \frac{A}{k_r\sqrt{k_B T}} e^{-\frac{E_a}{k_B T}} \qquad (5)$$

Φ_{fl} is difficult to directly observe, but in an optically dilute sample, the method of Williams, Winfield, and Miller may be used to calculate the quantum yield of un unknown Φ_x. In this method, the emission intensity of the unknown is compared to that of a reference possessing a known quantum yield Φ_r.[6-9] This comparison is based on Beer's law and is detailed in equation (6).

$$\Phi_x = \Phi_r \left(\frac{A_r(\lambda_r)}{A_x(\lambda_x)}\right)\left(\frac{I(\lambda_r)}{I(\lambda_x)}\right)\left(\frac{n_x^2}{n_r^2}\right)\left(\frac{D_x}{D_r}\right) \qquad (6)$$

in which

$$\Phi_x = quantum\ yield\ of\ unknown$$

$$\Phi_r = quantum\ yield\ of\ reference\ compound\ (tabulated)$$

$$A(\lambda) = absorbance\ per\ cm\ of\ solution\ at\ excitation\ wavelength\ \lambda$$

$$I(\lambda) = relative\ intensity\ of\ excitation\ light\ at\ \lambda$$

$$n = average\ refractive\ index\ of\ solvent$$

$$D = integrated\ area\ under\ emission\ spectrum$$

With temperature-dependent quantum yield data in hand, the following function extracted from equation (5) used with an appropriate fitting program may be used to extract relations for $k_0, k_r, A,$ and E_a.

$$y = \frac{1}{\Phi_{fl}} \qquad x = \frac{1}{T} \qquad y = 1 + a + \frac{b\sqrt{x}}{\sqrt{0.695}} e^{\frac{-cx}{0.695}} \qquad (7)$$

in which

$$a = \frac{k_d + k_0}{k_r} \approx \frac{k_0}{k_r}$$

$$b = \frac{A}{k_r}$$

$$c = E_a$$

The values calculated for the fitting parameters $a, b, c, \alpha, \beta,$ and γ using equations (3) and (7) can then be combined to obtain values for the unknowns $k_r, k_0, A,$ and E_a:

$$k_r = \frac{\beta}{b}$$

$$k_0 = \frac{\beta a}{b} \qquad (8)$$

$$A = \beta$$

$$E_a = \gamma = c$$

2.2.2 *Comparison to Durrell results*

Fluorescence lifetime and quantum yield data were acquired at temperatures ranging from 283 to 333 K.[i] Given that the quantum yield fitting program was written newly for this project (see Appendix 1) and relied on quantum yields derived from equation (6) using anthracene as the standard, the same fitting program used to fit our data was used to fit Durrell et al.'s raw data. These results were compared to Durrell's published results in order to assure the validity of our fitting program, and good agreement was found.[2] Results are summarized in Figure 3.

Fit parameter	**Value (2015 experiments)**	**Durrell value (with 2015 fitting program)**	**Durrell value (published, 2012)**
a	0.4269	0.5789	0.6 ± 0.1
b ($cm^{1/2}$)	2.547×10^{6}	1.73×10^{6}	1.73×10^{6}
c (cm^{-1})	2347	2232	2233 ± 75
α (s^{-1})	1.214×10^{8}		$(2.55 \pm 0.007) \times 10^{8}$
β ($cm^{1/2}$)	1.5×10^{14}		$(3.0 \pm 0.2) \times 10^{14}$
γ (cm^{-1})	2018		2229 ± 20

Figure 3: Temperature-dependent fluorescence lifetime and quantum yield fitting

With confidence in the validity of our fitting programs, we obtained several full sets of steady-state and time-resolved data. Values for a, b, and c were obtained using the absorbance and steady-state luminescence data presented in Figure 4; values for α, β, and γ were obtained using the time-resolved luminescence data presented in Figure 5. Our values are plotted against those obtained by Durrell et al. in Figure 6.

---

[i] Lifetime data were acquired with the kind assistance of Kana Takematsu.

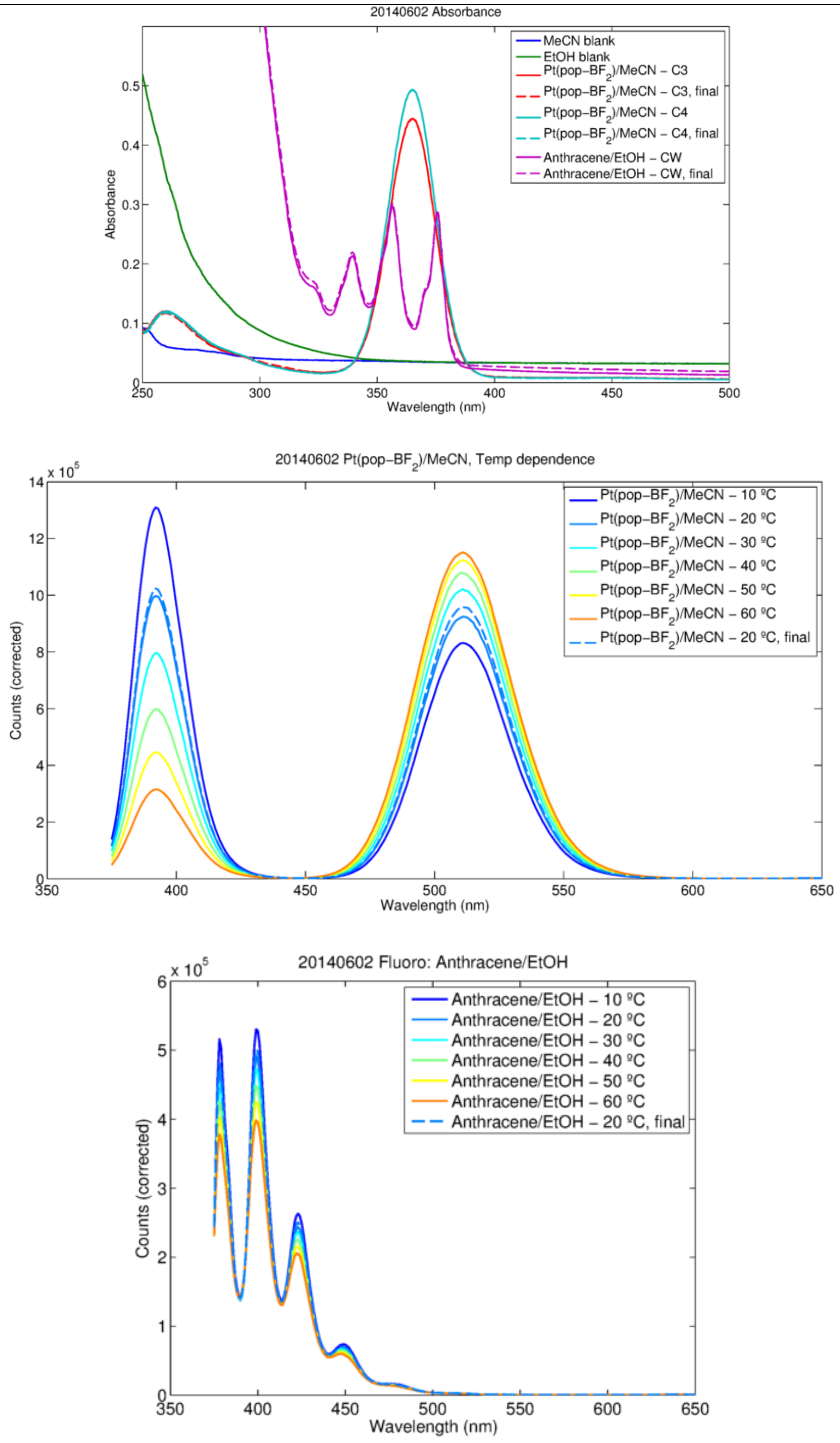

Figure 4: Absorbance data for Pt(pop-BF$_2$)$^{4-}$ and anthracene quantum yield standard (top) with steady-state luminescence data for Pt(pop-BF$_2$)$^{4-}$ (middle) and anthracene (bottom).

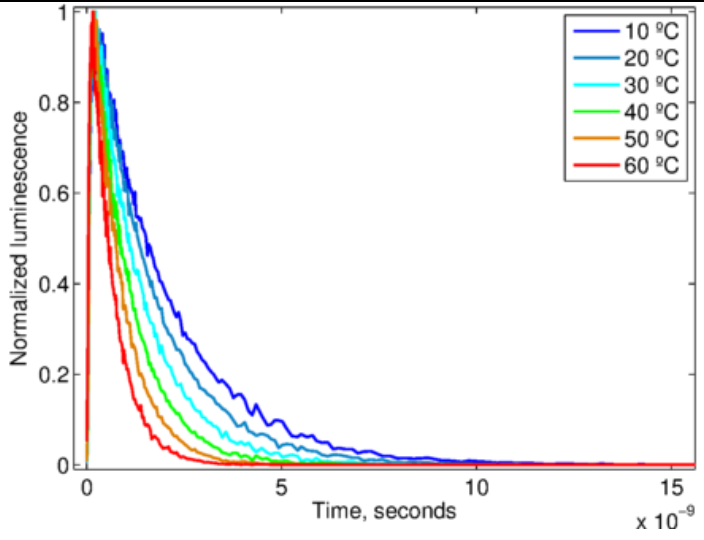

Figure 5: Temperature-dependent fluorescence lifetime data for Pt(pop-BF$_2$)$^{4-}$.

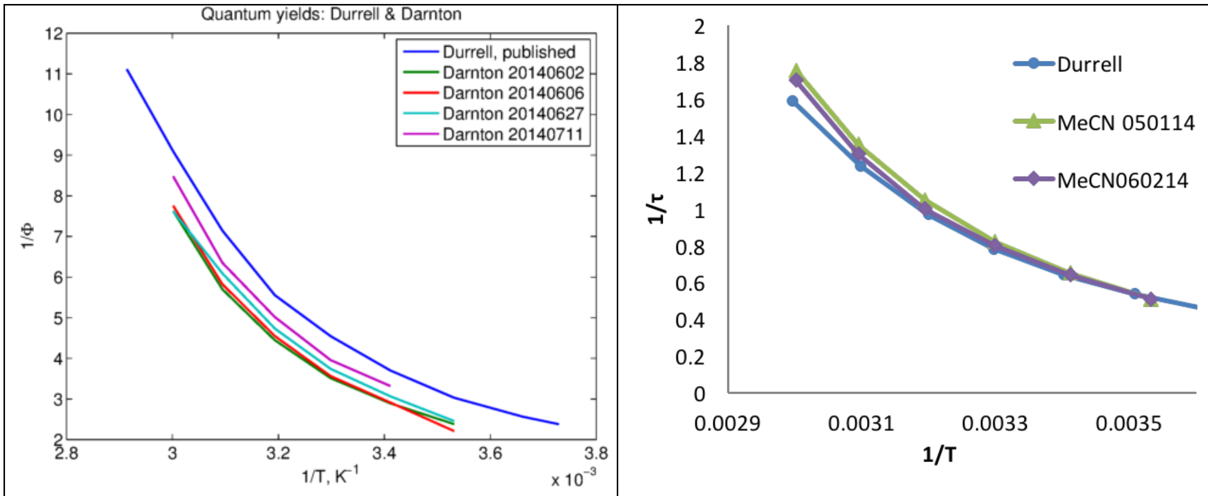

Figure 6: Data acquired in 2015 by Darnton & Takematsu vs. Durrell et al.; quantum yields (left), fluorescence lifetimes (right).

Anthracene was chosen as a quantum yield standard due to its well-documented behavior as well as the fact that it emits in the same region as Pt(pop-BF$_2$)$^{4-}$.[7,9-14] To ensure that equation (6) was being employed correctly, quinine sulfate was also employed as a standard to calculate both the quantum yield of Pt(pop-BF$_2$)$^{4-}$ and the quantum yield of anthracene itself; these data are presented in Figure 7 and summarized in Figure 8. Based on these results, it was concluded that anthracene was an appropriate standard for calculating the quantum yield of Pt(pop-BF$_2$)$^{4-}$ emission.

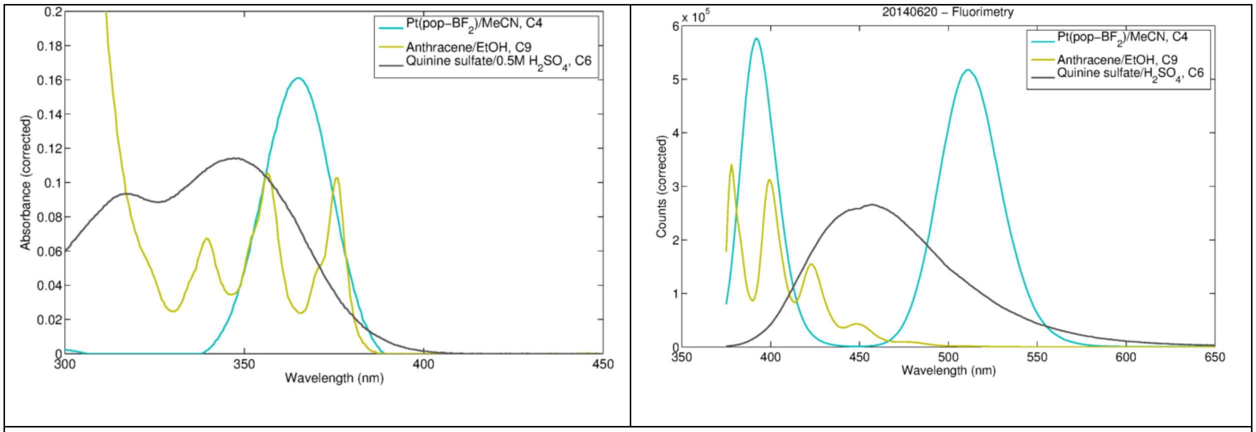

Figure 7: Pt(pop-BF$_2$)$^{4-}$, anthracene, and quinine sulfate absorbance (left) and luminescence (right) spectra.

Reference used	**Φ_{fl} (T=298 K)**	
	Pt(pop-BF$_2$)$^{4-}$	**Anthracene**
Anthracene	0.35	n/a
Quinine sulfate	0.31	0.22

Accepted values: Φ_{fl} Pt(pop-BF$_2$)$^{4-}\approx$ 0.35; Φ_{fl} (anthracene) = 0.27[13]

Figure 8: Quantum yield tests

2.3 Pt(pop-BF$_2$)$^{4-}$ luminescence in different solvents

A study published in the early 1990s by Brunchschwig and Milder found that the rate of nonradiative decay for the singlet excited state in Pt(pop)$^{4-}$ had a strong dependency on solvent, particularly with regards to solvent polarity and the presence of exchangeable protons. After significant analysis, they concluded that the vibrations coupling the singlet and triplet state in

$Pt(pop)^{4-}$ are solvent modes and/or modes representing the interaction of the solvent with the $^1A_{2u}$ and $^3A_{2u}$ states of the complex along the Pt-Pt axial coordinate.[15]

It was expected that the rigidity and steric bulk of $Pt(pop\text{-}BF_2)^{4-}$, along with its lack of exchangeable ligands, would afford more protection from solvents. However, initial results reported by collaborator Tony Vlček indicated that Pt-Pt vibrational coherence in $Pt(pop\text{-}BF_2)^{4-}$ survived intersystem crossing and that the time constants were approximately equal to those found for $Pt(pop)^{4-}$. This raised the possibility that the Pt atoms in $Pt(pop\text{-}BF_2)^{4-}$ were not as well-shielded as we had previously thought them to be, and were perhaps still exposed to solvent molecules. With this in mind, experiments were undertaken to quantify the effect of solvent on $Pt(pop\text{-}BF_2)^{4-}$ excited state dynamics.

2.3.1 *Solvent choice and solvent stability*

Unfortunately, $Pt(pop\text{-}BF_2)^{4-}$ is much less soluble in common solvents than $Pt(pop)^{4-}$. All previous experiments involving $Pt(pop\text{-}BF_2)^{4-}$ were completed in acetonitrile, in which it is quite soluble. It is insoluble in less polar solvents like diethyl ether, toluene, and tetrahydrofuran, and decomposes in dichloromethane. While $Pt(pop\text{-}BF_2)^{4-}$ is soluble in dimethyl sulfoxide and dimethylformamide, such solvents are exceedingly difficult to keep anhydrous and uncontaminated due to their extreme polarity, in addition to being costly when purchased in the requisite high purities.

The greatest effects on the excited state dynamics of $Pt(pop)^{4-}$ were noted by Milder et al. in methanol and ethanol. As such, samples of ethanol and methanol were purified and dried according to published protocols.[16] $Pt(pop\text{-}BF_2)^{4-}$ proved to be insoluble in ethanol and only sparingly soluble in methanol, and it decomposed significantly in both methanol and methanol/acetonitrile mixtures as noted by significant broadening of the characteristic absorbance maximum at 365 nm. This was followed by a loss of absorption intensity and a slight blue-shift in wavelength over 24 hours (Figure 9).

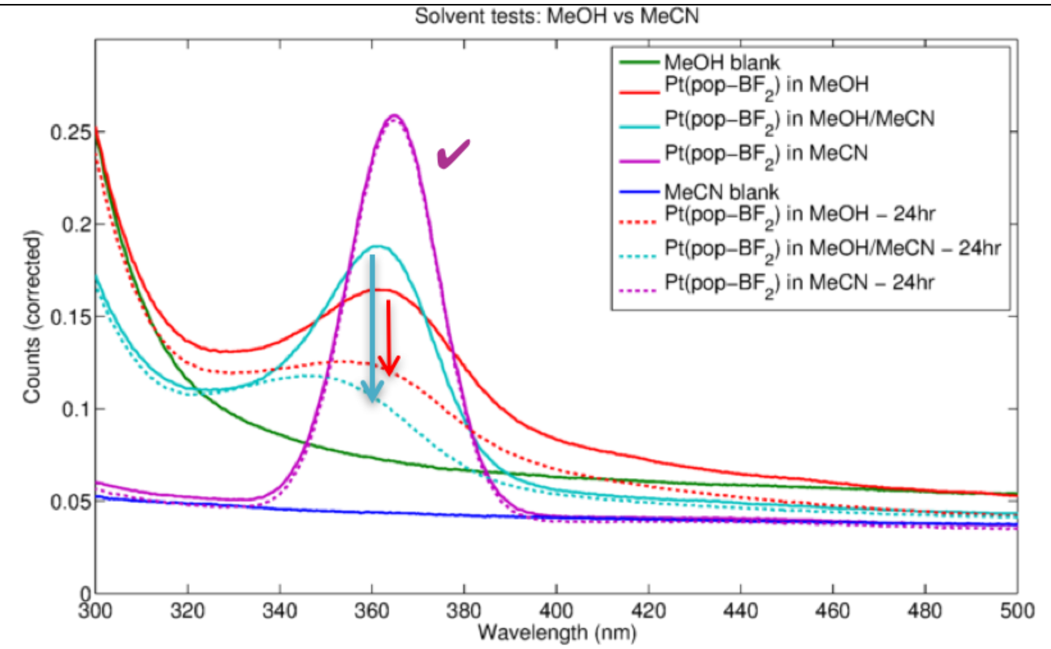

Figure 9: Stability of Pt(pop-BF$_2$)$^{4-}$ over 24 hours in acetonitrile, acetonitrile/methanol, and methanol. Absorbance profile is maintained in acetonitrile (purple); immediate peak broadening and loss of intensity over time noted in acetonitrile/methanol (blue) and methanol (red).

This decomposition in methanol is attributed, at least initially, to removal of the BF$_2$ groups by protonation to reform Pt(pop)$^{4-}$. This is supported by steady-state fluorescence data obtained in the same solvents; the emission maxima and the relative sizes of the fluorescence and phosphorescence peaks in neat methanol and in methanol mixed with acetonitrile are characteristic of Pt(pop)$^{4-}$. The control sample measured in acetonitrile maintains the signatures of Pt(pop-BF$_2$)$^{4-}$. In Pt(pop-BF$_2$)$^{4-}$ the fluorescence and phosphorescence emission peaks are nearly equal in intensity; in Pt(pop)$^{4-}$ the phosphorescence peak is ~40x more intense than the fluorescence peak. Accepted values for the emission maxima of Pt(pop)$^{4-}$ and Pt(pop-BF$_2$)$^{4-}$ are presented in Figure 10[2,4,17] together with the steady-state emission spectra of Pt(pop-BF$_2$)$^{4-}$ in the discussed solvent mixtures.

	λ_{max}, fluorescence	**λ_{max}, phosphorescence**
Pt(pop)$^{4-}$	398 nm	511 nm
Pt(pop-BF$_2$)$^{4-}$	393 nm	512 nm

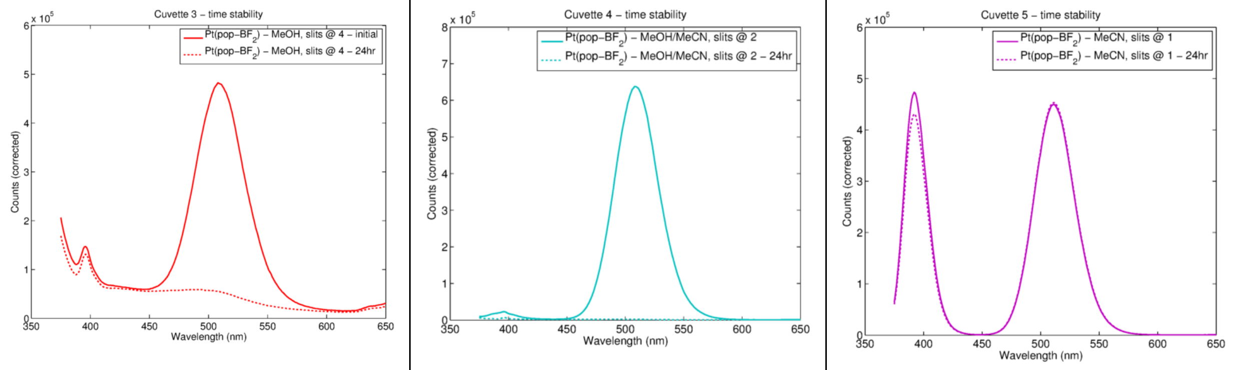

MeOH
$\lambda_{\text{max, fl}} = 396$ nm
$\lambda_{\text{max, phos}} = 509$ nm

MeOH/MeCN
$\lambda_{\text{max, fl}} = 396$ nm
$\lambda_{\text{max, phos}} = 509$ nm

MeCN
$\lambda_{\text{max, fl}} = 392$ nm
$\lambda_{\text{max, phos}} = 511$ nm

Figure 10: Steady-state emission spectra of Pt(pop-BF$_2$)$^{4-}$ in various solvents; decomposition to Pt(pop)$^{4-}$ noted in the presence of methanol.

Other solvents investigated for stability include 2-methyltetrahydrofuran (MeTHF), butyronitrile (BuCN), and propionitrile (PrCN); Pt(pop-BF$_2$)$^{4-}$ is soluble in BuCN and PrCN and sparingly soluble in MeTHF. Quantities of these three solvents were dried and purified.[16] However, Pt(pop-BF$_2$)$^{4-}$ proved to be unstable in a 1:1 mixture of MeCN:MeTHF (such a mixture was required for complete solubility) as noted by a significant decrease in both absorption intensity and singlet emission intensity during the course of a series of fluorimetry experiments.

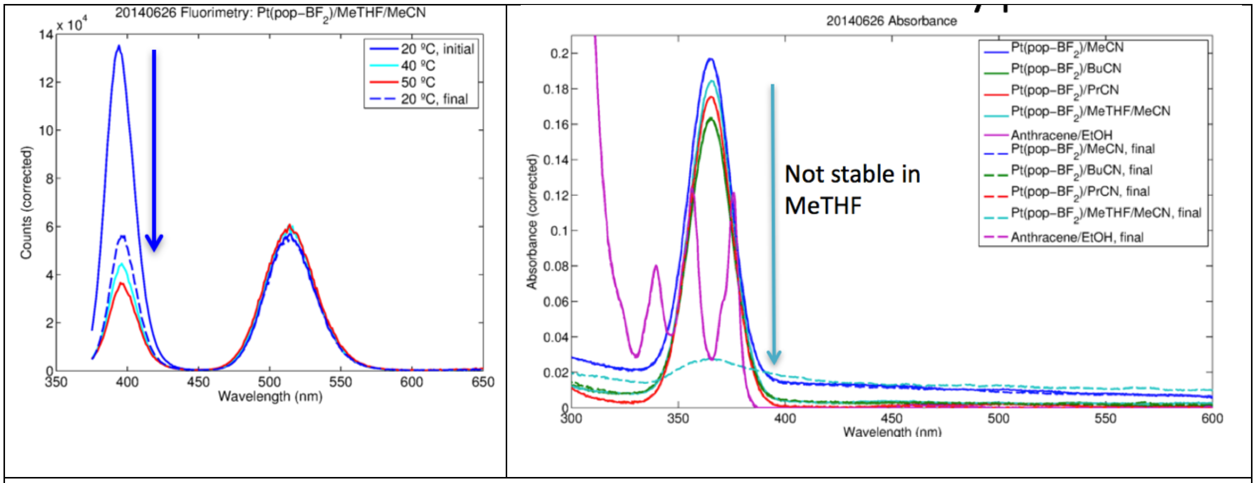

Figure 11: Decomposition of Pt(pop-BF$_2$)$^{4-}$ in MeCN/MeTHF during variable temperature fluorimetry experiments showing decrease in singlet emission intensity (left) with a concomintant decrease in absorption intensity (right).

While solutions of Pt(pop-BF$_2$)$^{4-}$ proved to be stable (as measured by absorption intensity) in BuCN and PrCN over temperatures ranging from 278 – 333 K for 48 hours (Figure 12), decomposition was noted following the laser measurements needed to obtain values for τ. This decomposition was noted both as a decrease in calculated quantum yield before and after the laser measurements due to overall decreases in luminescence intensity (Figure 13), as well as by decreases in absorption intensity (Figure 14). While the sample in MeCN also exhibited a decrease in luminescence intensity following the time-resolved laser experiments, the calculated quantum yield was the same; this indicates that the observed decrease for MeCN could be due to instrument fluctuation. However, the decreases observed for BuCN and PrCN solutions resulted in significantly different quantum yields, which shows that the change in intensity was not due to a systematic instrument error effective across all wavelengths. This is indicative of actual changes in the sample and cannot be attributed to instrument fluctuations. While during this experiment slightly longer lifetimes were observed in BuCN and PrCN as compared to MeCN, these data cannot be relied upon due to the sample decomposition.

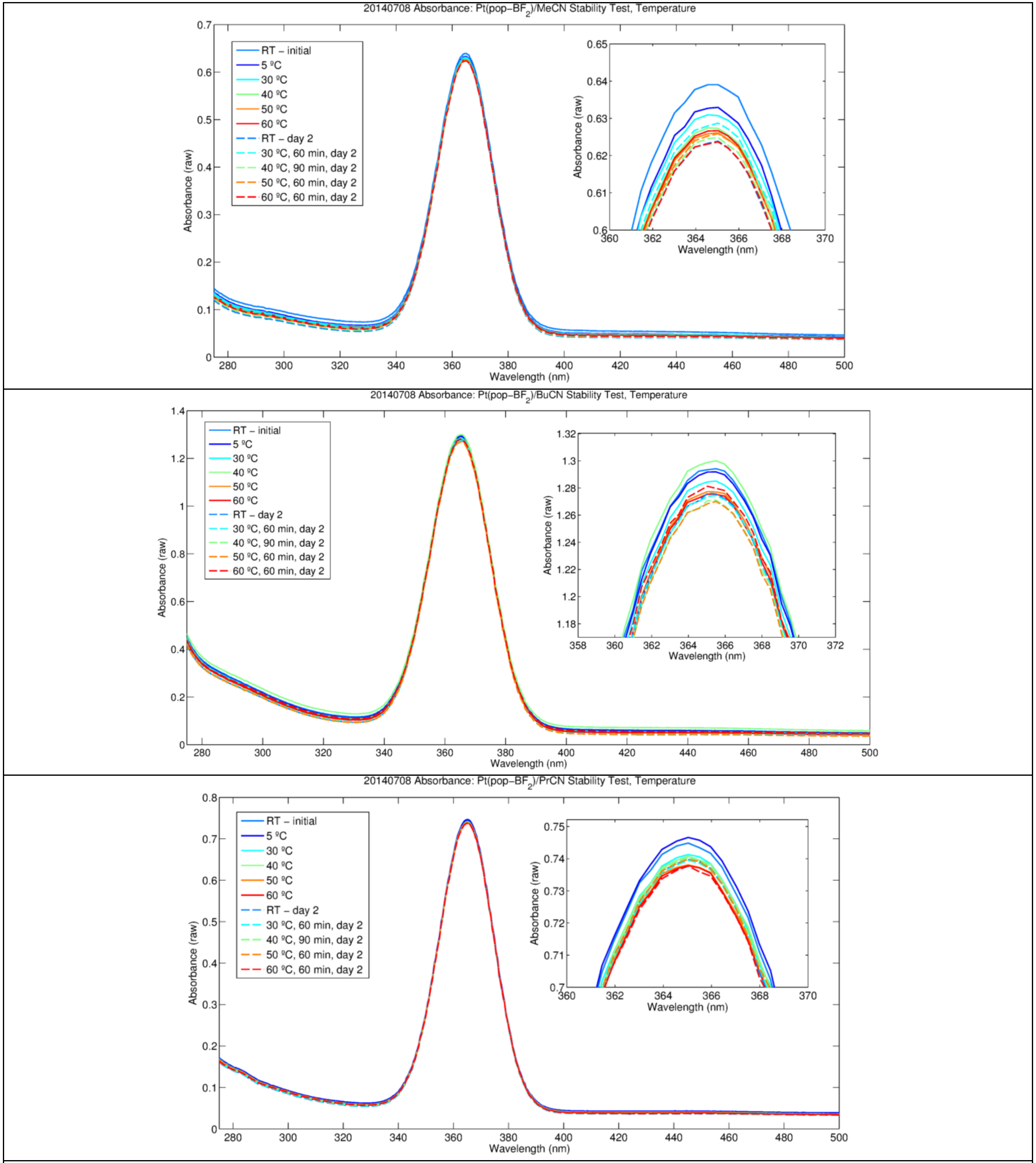

Figure 12: Absorption profile of Pt(pop-BF$_2$)$^{4-}$ in MeCN (top), BuCN (middle), and PrCN(bottom) at temperatures from 278 – 333 K over 48 hours (day 1 values are solid lines; day 2 values are dashed lines). Insets show the region of maximum absorption.

	Φ_{fl}, initial, 20 ºC	Φ_{fl}, final, 20 ºC (after laser measurements)
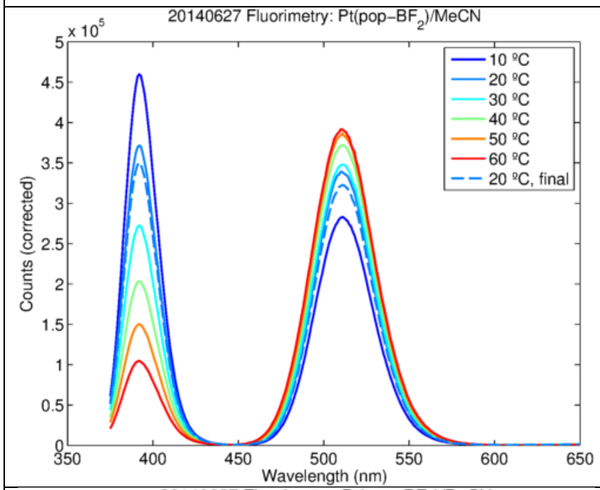	0.33	0.33
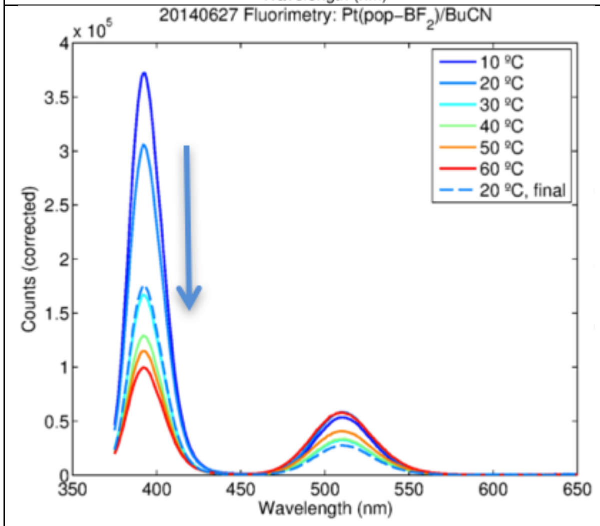	0.34	0.21
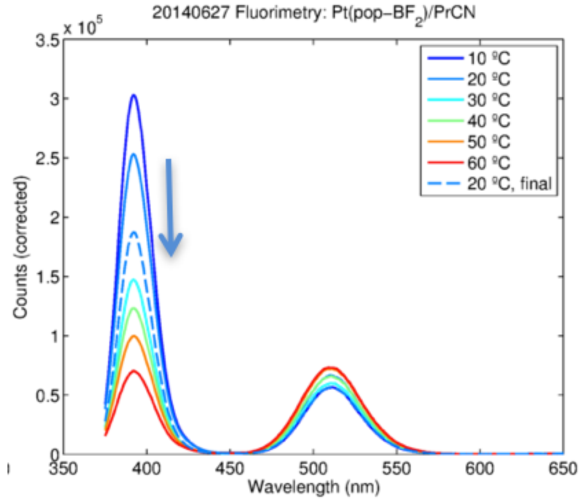	0.39	0.31

Figure 13: Decreases in luminescence intensity from before laser experiments (solid lines) to after (dashed lines), for solutions of Pt(pop-BF$_2$)$^{4-}$ in MeCN (top), BuCN (middle), and PrCN(bottom).

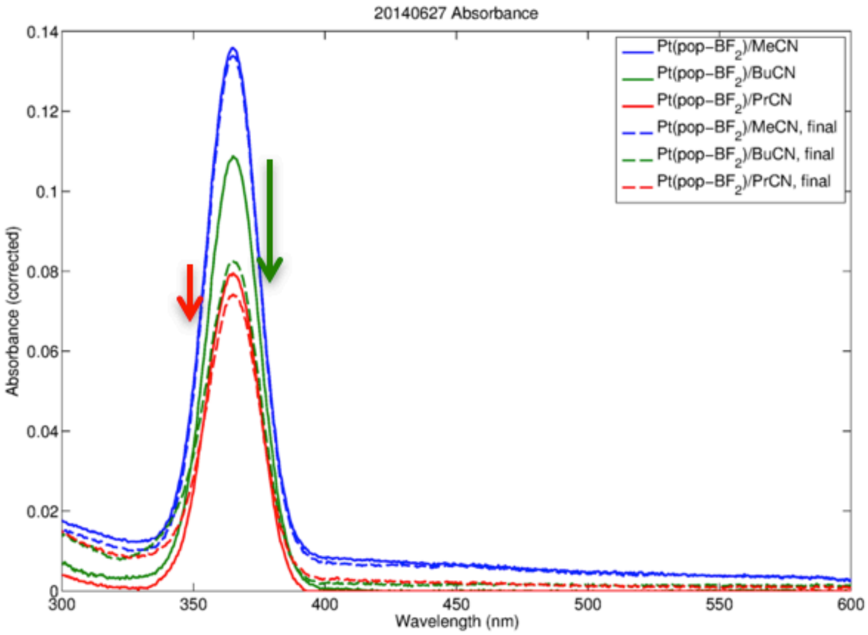

Figure 14: Changes in absorption intensity from before laser experiments (solid lines) to after (dashed lines), for solutions of Pt(pop-BF$_2$)$^{4-}$ in MeCN (blue), BuCN (green), and PrCN (red).

The noted sample decomposition can be attributed solely to laser exposure, as this experiment was repeated including every step except the time-resolved laser measurements. Absorption and luminescence profiles remained constant over the course of the steady-state fluorimetry measurements at temperatures from 293 to 333 K (Figure 15).

Steady-state luminescence spectra	Absorption spectra
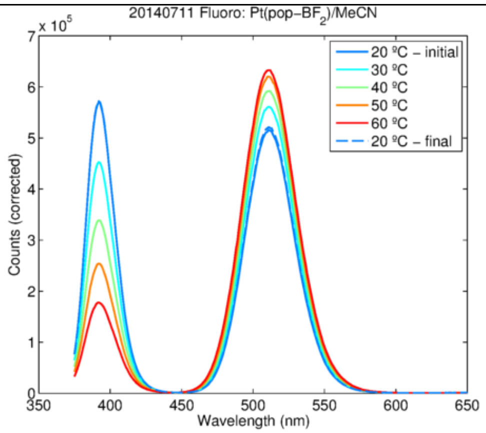	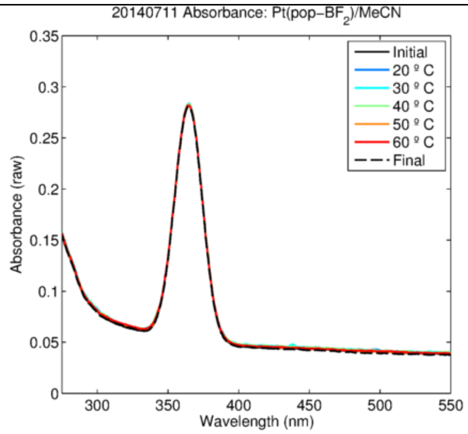
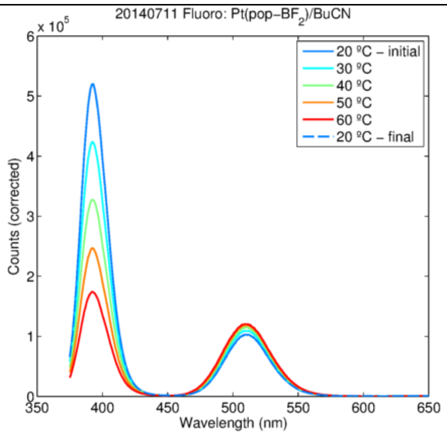	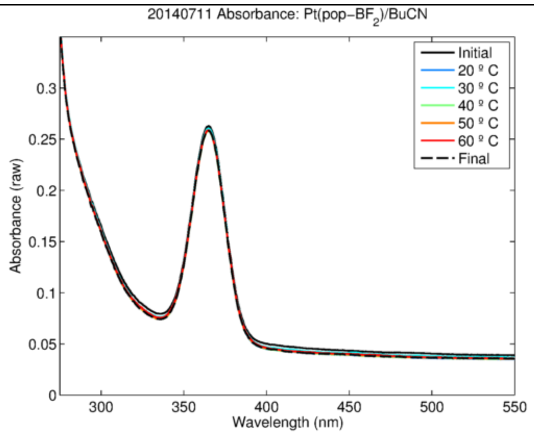
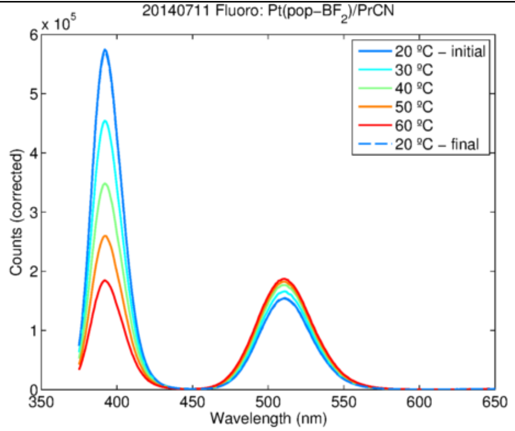	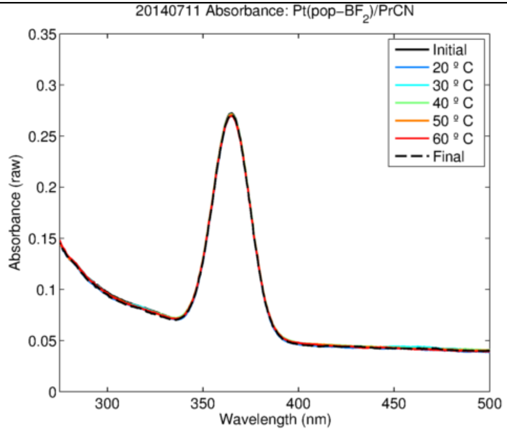

Figure 15: Temperature-dependent measurements excluding the time-resolved laser experimental portion indicates Pt(pop-BF$_2$)$^{4-}$ stability in MeCN (top), BuCN (middle), and PrCN (bottom).

2.4 Materials and methods

Unless otherwise noted, all reagents were obtained from Sigma-Aldrich and used without further purification; all water used was deionized. All manipulations involving $\mathrm{Pt(pop\text{-}BF_2)^{4-}}$ were carried out with standard air-free techniques in an inert-atmosphere glovebox or by utilizing a vacuum manifold. Solvents were dried using activated alumina columns according to Grubbs' method.[18] Anhydrous acetonitrile was stored over activated 3 Å molecular sieves; all other anhydrous solvents were stored over activated 4 Å molecular sieves.[16] Molecular sieves were activated by heating to 200 ºC under reduced pressure for 4 hours.

2.4.1 Phosphorous acid, H_3PO_3

$$\mathrm{PCl_3 + 3\,H_2O \xrightarrow{CH_2Cl_2} H_3PO_3 + 3\,HCl}$$

Phosphorous acid was prepared by adding 15.6 g phosphorus trichloride (PCl_3) to 40 mL dichloromethane in a round-bottom flask in an ice bath. 6 mL water was added to a dropping funnel and added to the stirring solution of PCl_3 over 30 minutes. The flask was removed from the ice bath and stirred at room temperature for 90 minutes. The dichloromethane was removed under reduced pressure and the remaining fluffy white solid was transferred to a vial and stored in a desiccator.

It is important to use a slight excess of PCl_3 in order to obtain a solid product. Excess water in the reaction will result in the formation of a thick, colorless oil; the H_3PO_3 product may be recovered from this oil via multiple solvent extractions using CH_2Cl_2.

The ^{31}P NMR exhibits a single peak at 5.86 ppm.

This reaction has been successfully scaled up to produce ~40 g of H_3PO_3 at a time; however, extreme care must be taken to add the water slowly to avoid dangerous exotherms. Furthermore, given the large amount of HCl gas produced at this scale, it is recommended to route the evolved gas through a bubbler filled with ice and an aqueous solution of either sodium bicarbonate or sodium hydroxide.

2.4.2 $K_4Pt(pop)$

$$2K_2PtCl_4 + 8\ H_3PO_3 \xrightarrow[100\ ^{\circ}C]{H_2O} K_4[Pt_2(P_2O_5H_2)_4] + 2\ H_2O + 8\ HCl$$

The water-soluble potassium salt of $Pt(pop)^{4-}$ was prepared by dissolving 0.326 g potassium tetrachloroplatinate (K_2PtCl_4) in 10 mL water. 1.48 g phosphorus acid (as prepared in 2.4.1) was dissolved in another 10 mL of water.[ii] The two solutions were mixed in a petri dish to give a light red solution; this was held over a boiling water bath for three hours to yield a lightly-colored yellow-brown solution. The petri dish was refilled with water every 30 minutes to maintain solution volume. The dish was transferred to a modified vacuum oven set to 110 ºC for three hours. This modified oven, rather than pulling vacuum, blew a constant stream of air through the oven to purge out evolved hydrochloric acid. The resulting bright yellow solid was suspended in methanol, isolated on a glass frit, and rinsed with copious methanol and diethyl ether. The isolated solid was collected and dried under vacuum. The isolated solid may range in color from bright yellowish-green to dark purple; when dissolved in water, the expected yellow-green

---

[ii] Commercially available phosphorous acid is often contaminated with water, as phosphorous acid is quite hygroscopic. Purchased phosphorous acid may be used for this synthesis, but yields may be adversely affected.

luminescent solution is reliably obtained. It has been proposed that the dark purple color is caused by a small amount of a highly colored impurity.[5]

^{31}P NMR exhibits a singlet at 67.1 ppm flanked by satellite peaks at 76.6 and 57.6 ppm caused by coupling to the compound’s ^{195}Pt atoms ($^{1}J_{Pt\text{-}P}$ = 3025 Hz, 33% abundance).

2.4.3 *[TBA]$_4$[Pt(pop)]*

$$K_4[Pt_2(P_2O_5H_2)_4] + 4\ [(n\text{-}Bu)_4N]Cl \xrightarrow{H_2O} [(n\text{-}Bu)_4N]_4[Pt_2(P_2O_5H_2)_4] + 4\ KCl$$

The tetrabutylammonium (TBA) salt of Pt(pop) was prepared by dissolving 0.35 g K_4[Pt(pop)] in 4 mL water. 2.5 g (a 30-fold excess) tetrabutylammonium chloride ([(n-Bu)$_4$N]Cl) was added to the solution and stirred for one hour at room temperature. In the dark, the syrupy aqueous solution was extracted with three 50 mL aliquots of dichloromethane and the organic layer was concentrated under vacuum to a volume of 5 mL. 50 mL ethyl acetate was added to induce precipitation of a bright yellow-green powder. The powder was isolated on a glass frit and dried under vacuum.

^{31}P NMR exhibits a single peak at 67.8 ppm flanked with the previously described ^{195}Pt coupling satellites. In the presence of light, Pt(pop)$^{4-}$ reacts with dichloromethane to form the chloride adduct, which exhibits a single peak at 30.1 ppm in the ^{31}P NMR spectrum.[19] The presence of this peak indicates a crude product which must be purified via recrystallization in the dark from a concentrated CH_2Cl_2 solution layered with ethyl acetate.

2.4.4 *[Ph$_4$P]$_4$[Pt(pop)]*

$$K_4[Pt_2(P_2O_5H_2)_4] + 4\ [Ph_4P]Cl \xrightarrow{H_2O} [Ph_4P]_4[Pt_2(P_2O_5H_2)_4] + 4\ KCl$$

The tetraphenylphosphonium (Ph_4P^+) salt of $Pt(pop)^{4-}$ may be prepared by a similar salt metathesis procedure to that described in 2.4.3. Briefly, 1.2 g Ph_4PCl was dissolved in 20 mL water and 0.28 g $K_4Pt(pop)$ was dissolved in 50 mL water; both solutions were sparged with nitrogen for 15 minutes. The tetraphenylphosphonium chloride solution was then added to the $Pt(pop)^{4-}$ solution and a light yellow solid precipitated immediately. The solid was isolated via vacuum filtration through fine glass-fiber filter paper and dried under vacuum.

Crystals suitable for X-ray diffraction analysis (bright yellow-green needles) were grown from slow evaporation of a dilute methanol solution of the product. The ^{31}P NMR exhibited a single peak at 66.83 ppm, flanked by the previously discussed ^{195}Pt satellite peaks.

2.4.5 $[Ph_4As]_4[Pt(pop)]$

The tetraphenylarsonium (Ph_4As^+) salt of $Pt(pop)^{4-}$ may be prepared in a similar salt metathesis procedure to that described in 2.4.4. Briefly, 0.93 g Ph_4AsCl was dissolved in 20 mL water and 0.34 g $K_4Pt(pop)$ was dissolved in 50 mL water; both solutions were sparged with nitrogen for 15 minutes. The tetraphenylphosphonium solution was then added to the $Pt(pop)^{4-}$ solution and a light yellow solid precipitated immediately. The solid was isolated via vacuum filtration through fine glass-fiber filter paper and dried under vacuum.

The ^{31}P NMR exhibited a single peak at 67.1 ppm, flanked by the previously discussed ^{195}Pt satellite peaks.

2.4.6 $[Pt(pop\text{-}BF_2)]^{4-}$

$$[R]_4[Pt_2(P_2O_5H_2)_4] + BF_3{\bullet}Et_2O \longrightarrow [R]_4[Pt_2(P_2O_5B_2F_4)_4] + HF$$

$$R = (n\text{-}Bu)_4N^+,\ Ph_4P^+,\ Ph_4As^+$$

$[R]_4[Pt(pop\text{-}BF_2)]$, where R = Ph_4P^+, $(n\text{-}Bu)_4N^+$, or Ph_4As^+, was prepared by adding 0.3 – 0.6 g of the appropriate $Pt(pop)^{4-}$ salt to a 10 mL Schlenk flask. After sparging with dry argon for 15 minutes, a syringe was used to add 3.5 mL boron trifluoride diethyletherate ($BF_3{\bullet}Et_2O$) to the flask through a rubber septum. Under positive argon flow, the rubber septum was replaced with a ground-glass stopper; the reaction was then left stirring under a static blanket of argon for six hours (although the reaction may be left stirring for multiple days with no decomposition). The remaining $BF_3{\bullet}Et_2O$ was removed under reduced pressure in a 40 ºC water bath. The $BF_3{\bullet}Et_2O$ was condensed into an ice-cooled pre-trap immediately in line after the Schlenk flask. If a pre-trap is not used, $BF_3{\bullet}Et_2O$ will condense inside the vacuum tubing and/or the Schlenk line itself, causing contamination and presenting a significant health and safety hazard to researchers. Removal of solvent yielded a bright yellow-green powder. The Schlenk flask containing the product was sealed under nitrogen and taken into an inert-atmosphere glovebox; the product was then suspended in dry tetrahydrofuran (THF), filtered through a glass frit, and rinsed with copious THF. The isolated product was dried under vacuum and recrystallized via slow evaporation of diethylether into a saturated acetonitrile solution to yield bright yellow-green luminescent crystalline blocks.

The ^{31}P NMR exhibits a single peak at ≈58.8 ppm (depending on the cation; see section 2.5) together with the aforementioned ^{195}Pt coupling satellite peaks ($^1J_{Pt\text{-}P} \cong$ 3126 – 3136 Hz). The ^{19}F NMR exhibits two doublets at 133.5 ppm (^1J = 60 Hz) and 138.7 ppm (^1J = 60 Hz).

2.4.7 *X-ray structure determination of $[Ph_4P]_4[Pt(pop\text{-}BF_2)]$*

Low-temperature diffraction data (ϕ-and ω-scans) were collected on a Bruker three-circle diffractometer coupled to a Bruker Smart 1000 CCD detector with graphite monochromated Mo

K_α radiation (λ = 0.71073 Å) for the structure of $[Ph_4P]_4[Pt(pop\text{-}BF_2)]$. The structure was solved by direct methods using SHELXS[20] and refined against F^2 on all data by full-matrix least squares with SHELXL-2013[21] using established refinement techniques.[22] All non-hydrogen atoms were refined anisotropically. All hydrogen atoms were included into the model at geometrically calculated positions and refined using a riding model. The isotropic displacement parameters of all hydrogen atoms were fixed to 1.2 times the U value of the atoms they are linked to (1.5 times for methyl groups). Data are presented in section 2.6.

2.4.8 *Steady-state quenching experiments*

Steady-state emission spectra were recorded on a Jobin Yvon Spex Fluorolog-3-11. A 450-W xenon arc lamp was used as the excitation source with a single monochromator providing wavelength selection. Right-angle light emission was sorted using a single monochromator and fed into a Hamamatsu R928P photomultiplier tube with photon counting. Short and long pass filters were used where appropriate. Spectra were recorded on Datamax software.[2] Variable-temperature experiments were performed using a Peltier-cooled circulating water bath.

2.4.9 *Temperature-dependent lifetime experiments: Picosecond laser data*[2]

An IBH 5000 U instrument equipped with a cooled Hamamatsu R3809U-50 microchannel plate photomultiplier was used. Samples were excited at 355 nm with an IBH NanoLED-03 diode laser (~80 ps fwhm, repetition rate 500 kHz). For fluorescence decay measurements, the emission monochromator was set to ≈405 ± 4 nm, preceded by a 390 nm long-pass cutoff filter to remove stray excitation light. Magic angle between the excitation and emission polarization directions was used for all experiments. Variable-temperature experiments were performed using a Peltier-cooled circulating water bath. Data manipulation was performed and plotted using MATLAB R2015a (Mathworks, Inc.).

2.5 NMR spectra

All NMR spectra were recorded in the Caltech Liquid NMR facility using a Varian 400 MHz spectrometer with a broadband auto-tune OneProbe ("Siena"). All ^{31}P spectra were externally referenced to 85% phosphoric acid. Spectra were processed using the MestReNova software suite.[23]

<table>
<tr><th colspan="2">$K_4Pt(pop)$</th></tr>
<tr><td>^1H</td><td>^{31}P</td></tr>
<tr><td>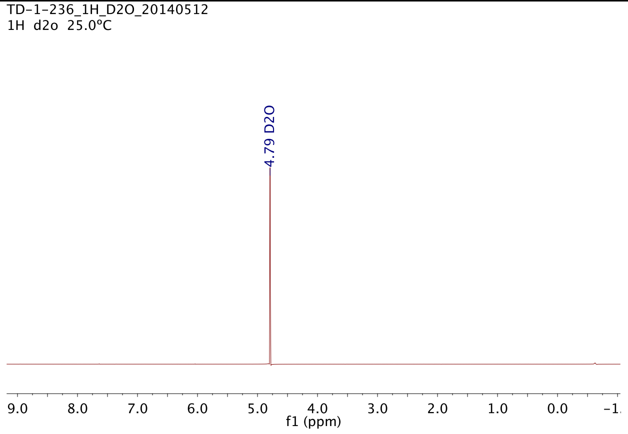
</td><td>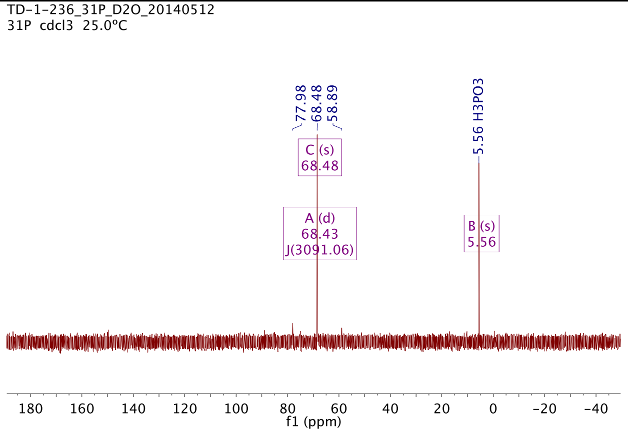
</td></tr>
<tr><th colspan="2">$[(n\text{-}Bu)_4P]_4[Pt(pop\text{-}BF_2)]$</th></tr>
<tr><td>^1H</td><td>^{31}P</td></tr>
</table>

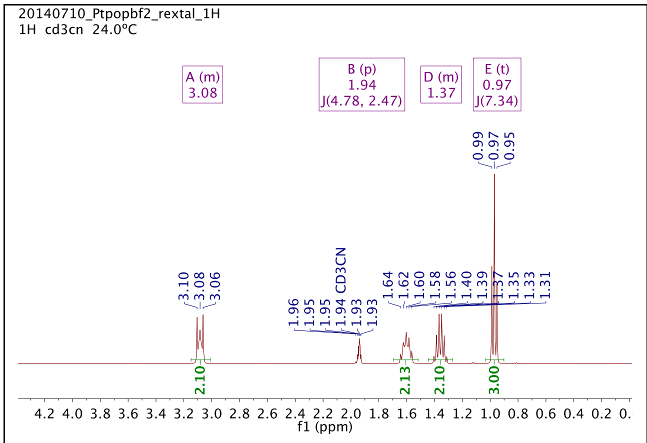

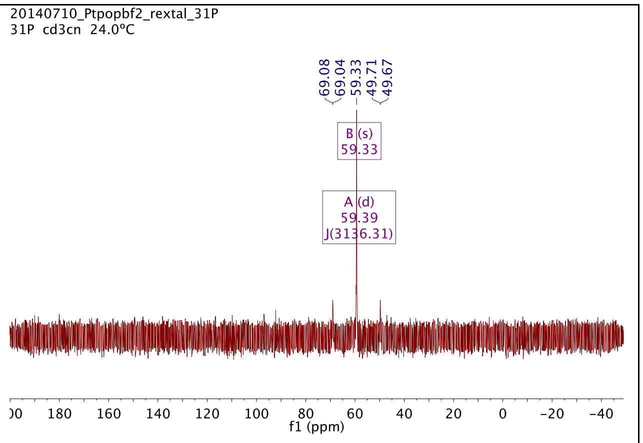

^{19}F

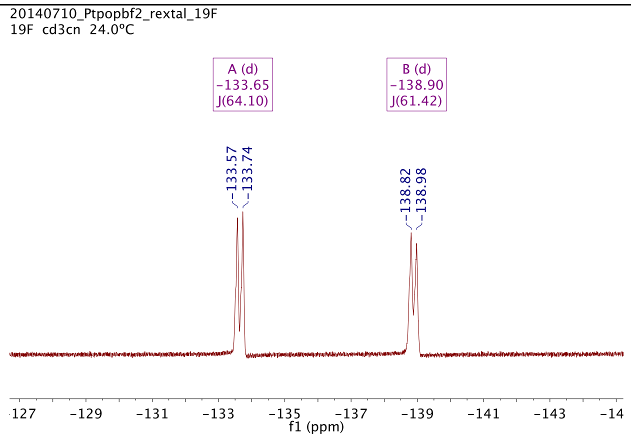

[Ph$_4$P]$_4$[Pt(pop-BF$_2$)]

^{1}H

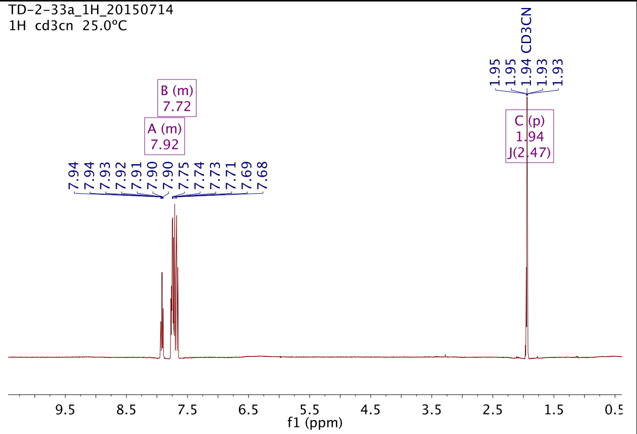

^{31}P

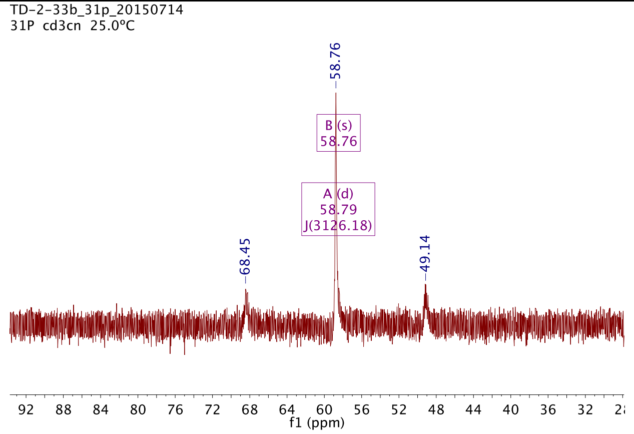

^{19}F

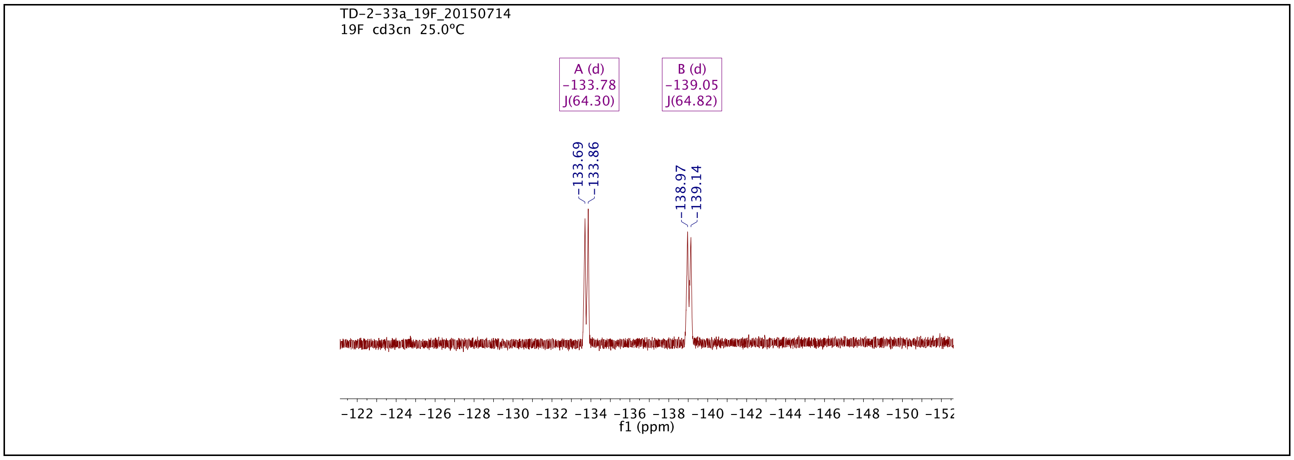

2.6 X-ray data for $[Ph_4P]_4[Pt(pop\text{-}BF_2)]$

Table 1: Crystal data and structure refinement for S13045.

Identification code	S13045	
Empirical formula	C96 H80 B8 F16 O20 P12 Pt2	
Formula weight	2705.90	
Temperature	100(2) K	
Wavelength	0.71073 Å	
Crystal system	Monoclinic	
Space group	P 21/n	
Unit cell dimensions	a = 15.8751(6) Å	a= 90°.
	b = 17.2490(6) Å	b= 98.5184(18)°.
	c = 18.6455(7) Å	g = 90°.
Volume	5049.4(3) $Å^3$	
Z	2	
Density (calculated)	1.780 Mg/m^3	
Absorption coefficient	3.058 mm^{-1}	
F(000)	2672	
Crystal size	0.400 x 0.300 x 0.300 mm^3	
Theta range for data collection	1.617 to 36.377°.	
Index ranges	-26<=h<=26, -28<=k<=28, -31<=l<=30	
Reflections collected	149401	
Independent reflections	24436 [R(int) = 0.0435]	
Completeness to theta = 25.242°	100.0 %	

Absorption correction	Semi-empirical from equivalents
Max. and min. transmission	0.7471 and 0.4555
Refinement method	Full-matrix least-squares on F^2
Data / restraints / parameters	24436 / 0 / 694
Goodness-of-fit on F^2	1.098
Final R indices [I>2sigma(I)]	R1 = 0.0329, wR2 = 0.0745
R indices (all data)	R1 = 0.0502, wR2 = 0.0843
Extinction coefficient	n/a
Largest diff. peak and hole	4.106 and -1.695 e.Å^{-3}

Table 2: Atomic coordinates (x 10^4) and equivalent isotropic displacement parameters (Å^{2}x 10^3) for S13045. U(eq) is defined as one third of the trace of the orthogonalized U^{ij} tensor.

	x	y	z	U(eq)
Pt(1)	9405(1)	5584(1)	5154(1)	10(1)
P(1)	10469(1)	6423(1)	5622(1)	13(1)
O(1)	10476(1)	6693(1)	6409(1)	20(1)
B(1)	9955(2)	6477(2)	6981(2)	18(1)
F(1)	10439(1)	6602(1)	7643(1)	29(1)
F(2)	9224(1)	6917(1)	6894(1)	36(1)
O(2)	9723(1)	5642(1)	6933(1)	25(1)
P(2)	9395(1)	5106(1)	6298(1)	12(1)
O(3)	8546(1)	4766(1)	6459(1)	20(1)
B(2)	7701(2)	4764(2)	5989(1)	17(1)
F(3)	7387(1)	5517(1)	5925(1)	26(1)
F(4)	7180(1)	4280(1)	6308(1)	25(1)
O(4)	7765(1)	4454(1)	5260(1)	16(1)
O(5)	8616(1)	3990(1)	4344(1)	19(1)
P(3)	8305(1)	4772(1)	4700(1)	11(1)
O(6)	7664(1)	5131(1)	4091(1)	17(1)
B(3)	7778(2)	5571(2)	3428(1)	21(1)
F(5)	7048(1)	5986(2)	3220(1)	48(1)

F(6)	7936(2)	5054(1)	2905(1)	53(1)
O(7)	8499(1)	6125(1)	3550(1)	18(1)
O(8)	9968(1)	5623(1)	3541(1)	22(1)
P(4)	9377(1)	6106(1)	4018(1)	12(1)
O(9)	9694(1)	6949(1)	3993(1)	21(1)
B(4)	10448(2)	7337(2)	4408(2)	20(1)
F(7)	10361(1)	8113(1)	4301(1)	40(1)
F(8)	11185(1)	7060(2)	4179(1)	40(1)
O(10)	10521(1)	7184(1)	5200(1)	21(1)
P(5)	9558(1)	8187(1)	1153(1)	15(1)
C(1)	8687(1)	7969(1)	1629(1)	17(1)
C(2)	8310(2)	8544(2)	2001(2)	24(1)
C(3)	7631(2)	8345(2)	2358(2)	31(1)
C(4)	7350(2)	7588(2)	2365(2)	26(1)
C(5)	7729(2)	7018(2)	1999(2)	22(1)
C(6)	8392(2)	7207(2)	1620(1)	21(1)
C(11)	10533(1)	7784(1)	1620(1)	16(1)
C(12)	10527(2)	7269(1)	2200(1)	18(1)
C(13)	11292(2)	6954(2)	2543(1)	21(1)
C(14)	12055(2)	7155(2)	2317(1)	22(1)
C(15)	12068(2)	7682(2)	1749(1)	21(1)
C(16)	11310(2)	7994(2)	1402(1)	19(1)
C(21)	9306(2)	7764(1)	264(1)	17(1)
C(22)	9926(2)	7397(2)	-79(1)	20(1)
C(23)	9702(2)	7082(2)	-768(1)	23(1)
C(24)	8865(2)	7133(2)	-1117(2)	25(1)
C(25)	8250(2)	7498(2)	-781(2)	26(1)
C(26)	8465(2)	7814(2)	-90(1)	21(1)
C(31)	9693(2)	9215(1)	1105(1)	17(1)
C(32)	9219(2)	9643(2)	548(1)	21(1)
C(33)	9288(2)	10448(2)	554(2)	26(1)
C(34)	9826(2)	10823(2)	1099(2)	29(1)
C(35)	10305(2)	10396(2)	1648(2)	28(1)
C(36)	10234(2)	9595(2)	1658(2)	24(1)
P(6)	7680(1)	9757(1)	4861(1)	15(1)
C(41)	8545(2)	10091(2)	4419(1)	19(1)

C(42)	8629(2)	10881(2)	4280(1)	23(1)
C(43)	9257(2)	11132(2)	3887(2)	28(1)
C(44)	9784(2)	10592(2)	3621(2)	32(1)
C(45)	9701(2)	9805(2)	3756(2)	33(1)
C(46)	9083(2)	9548(2)	4159(2)	26(1)
C(51)	6716(2)	10144(1)	4372(1)	17(1)
C(52)	6605(2)	10098(2)	3615(1)	21(1)
C(53)	5825(2)	10283(2)	3221(2)	28(1)
C(54)	5159(2)	10521(2)	3572(2)	29(1)
C(55)	5279(2)	10601(2)	4320(2)	26(1)
C(56)	6060(2)	10413(2)	4726(2)	21(1)
C(61)	7626(2)	8717(1)	4825(1)	18(1)
C(62)	7022(2)	8336(2)	4327(1)	21(1)
C(63)	6999(2)	7528(2)	4315(2)	27(1)
C(64)	7577(2)	7108(2)	4794(2)	30(1)
C(65)	8185(2)	7485(2)	5282(2)	31(1)
C(66)	8219(2)	8283(2)	5299(2)	26(1)
C(71)	7756(2)	10051(1)	5791(1)	17(1)
C(72)	7326(2)	9619(2)	6261(1)	22(1)
C(73)	7305(2)	9880(2)	6962(1)	25(1)
C(74)	7704(2)	10571(2)	7195(1)	23(1)
C(75)	8134(2)	10996(2)	6733(1)	22(1)
C(76)	8162(2)	10743(2)	6028(1)	19(1)

Table 3: Bond lengths [Å] and angles [°] for S13045.

Pt(1)-P(2)	2.2880(6)
Pt(1)-P(1)	2.2958(5)
Pt(1)-P(4)	2.2966(6)
Pt(1)-P(3)	2.3003(5)
Pt(1)-Pt(1)#1	2.87596(16)
P(1)-O(1)	1.5376(18)
P(1)-O(10)	1.5400(19)

P(1)-O(5)#1	1.6110(18)
O(1)-B(1)	1.490(3)
B(1)-F(1)	1.371(3)
B(1)-F(2)	1.377(3)
B(1)-O(2)	1.486(3)
O(2)-P(2)	1.5318(18)
P(2)-O(3)	1.5392(18)
P(2)-O(8)#1	1.6145(18)
O(3)-B(2)	1.491(3)
B(2)-F(4)	1.372(3)
B(2)-F(3)	1.388(3)
B(2)-O(4)	1.478(3)
O(4)-P(3)	1.5453(17)
O(5)-P(1)#1	1.6110(18)
O(5)-P(3)	1.6134(18)
P(3)-O(6)	1.5389(17)
O(6)-B(3)	1.483(3)
B(3)-F(5)	1.368(4)
B(3)-F(6)	1.373(4)
B(3)-O(7)	1.483(3)
O(7)-P(4)	1.5308(17)
O(8)-P(2)#1	1.6146(18)
O(8)-P(4)	1.6156(19)
P(4)-O(9)	1.5431(18)
O(9)-B(4)	1.485(3)
B(4)-F(7)	1.357(3)
B(4)-F(8)	1.388(4)
B(4)-O(10)	1.487(3)
P(5)-C(31)	1.789(2)
P(5)-C(1)	1.791(2)
P(5)-C(11)	1.799(2)
P(5)-C(21)	1.801(2)
C(1)-C(6)	1.395(3)
C(1)-C(2)	1.395(3)
C(2)-C(3)	1.390(4)
C(2)-H(2)	0.9500

C(3)-C(4)	1.381(4)
C(3)-H(3)	0.9500
C(4)-C(5)	1.383(4)
C(4)-H(4)	0.9500
C(5)-C(6)	1.391(3)
C(5)-H(5)	0.9500
C(6)-H(6)	0.9500
C(11)-C(12)	1.401(3)
C(11)-C(16)	1.402(3)
C(12)-C(13)	1.396(3)
C(12)-H(12)	0.9500
C(13)-C(14)	1.384(4)
C(13)-H(13)	0.9500
C(14)-C(15)	1.398(4)
C(14)-H(14)	0.9500
C(15)-C(16)	1.388(3)
C(15)-H(15)	0.9500
C(16)-H(16)	0.9500
C(21)-C(22)	1.402(3)
C(21)-C(26)	1.403(3)
C(22)-C(23)	1.391(4)
C(22)-H(22)	0.9500
C(23)-C(24)	1.394(4)
C(23)-H(23)	0.9500
C(24)-C(25)	1.386(4)
C(24)-H(24)	0.9500
C(25)-C(26)	1.393(4)
C(25)-H(25)	0.9500
C(26)-H(26)	0.9500
C(31)-C(32)	1.400(3)
C(31)-C(36)	1.403(4)
C(32)-C(33)	1.393(4)
C(32)-H(32)	0.9500
C(33)-C(34)	1.387(4)
C(33)-H(33)	0.9500
C(34)-C(35)	1.392(4)

C(34)-H(34)	0.9500
C(35)-C(36)	1.388(4)
C(35)-H(35)	0.9500
C(36)-H(36)	0.9500
P(6)-C(51)	1.791(2)
P(6)-C(71)	1.793(2)
P(6)-C(61)	1.797(3)
P(6)-C(41)	1.797(3)
C(41)-C(42)	1.398(4)
C(41)-C(46)	1.401(4)
C(42)-C(43)	1.390(4)
C(42)-H(42)	0.9500
C(43)-C(44)	1.391(5)
C(43)-H(43)	0.9500
C(44)-C(45)	1.390(5)
C(44)-H(44)	0.9500
C(45)-C(46)	1.393(4)
C(45)-H(45)	0.9500
C(46)-H(46)	0.9500
C(51)-C(56)	1.393(3)
C(51)-C(52)	1.399(3)
C(52)-C(53)	1.381(4)
C(52)-H(52)	0.9500
C(53)-C(54)	1.385(5)
C(53)-H(53)	0.9500
C(54)-C(55)	1.385(4)
C(54)-H(54)	0.9500
C(55)-C(56)	1.392(4)
C(55)-H(55)	0.9500
C(56)-H(56)	0.9500
C(61)-C(62)	1.396(3)
C(61)-C(66)	1.407(4)
C(62)-C(63)	1.395(4)
C(62)-H(62)	0.9500
C(63)-C(64)	1.387(4)
C(63)-H(63)	0.9500

C(64)-C(65)	1.385(5)
C(64)-H(64)	0.9500
C(65)-C(66)	1.379(4)
C(65)-H(65)	0.9500
C(66)-H(66)	0.9500
C(71)-C(76)	1.397(3)
C(71)-C(72)	1.402(3)
C(72)-C(73)	1.388(4)
C(72)-H(72)	0.9500
C(73)-C(74)	1.389(4)
C(73)-H(73)	0.9500
C(74)-C(75)	1.384(4)
C(74)-H(74)	0.9500
C(75)-C(76)	1.392(3)
C(75)-H(75)	0.9500
C(76)-H(76)	0.9500
P(2)-Pt(1)-P(1)	88.81(2)
P(2)-Pt(1)-P(4)	177.48(2)
P(1)-Pt(1)-P(4)	90.95(2)
P(2)-Pt(1)-P(3)	90.79(2)
P(1)-Pt(1)-P(3)	177.92(2)
P(4)-Pt(1)-P(3)	89.368(19)
P(2)-Pt(1)-Pt(1)#1	91.728(15)
P(1)-Pt(1)-Pt(1)#1	92.871(15)
P(4)-Pt(1)-Pt(1)#1	90.787(15)
P(3)-Pt(1)-Pt(1)#1	89.183(14)
O(1)-P(1)-O(10)	103.68(11)
O(1)-P(1)-O(5)#1	102.59(10)
O(10)-P(1)-O(5)#1	106.25(11)
O(1)-P(1)-Pt(1)	117.06(7)
O(10)-P(1)-Pt(1)	115.83(7)
O(5)#1-P(1)-Pt(1)	110.13(7)
B(1)-O(1)-P(1)	132.87(16)
F(1)-B(1)-F(2)	111.7(2)
F(1)-B(1)-O(2)	107.9(2)

F(2)-B(1)-O(2)	109.3(2)
F(1)-B(1)-O(1)	108.0(2)
F(2)-B(1)-O(1)	108.9(2)
O(2)-B(1)-O(1)	111.0(2)
B(1)-O(2)-P(2)	133.14(17)
O(2)-P(2)-O(3)	106.65(11)
O(2)-P(2)-O(8)#1	101.19(12)
O(3)-P(2)-O(8)#1	102.03(11)
O(2)-P(2)-Pt(1)	117.08(8)
O(3)-P(2)-Pt(1)	116.54(7)
O(8)#1-P(2)-Pt(1)	111.28(7)
B(2)-O(3)-P(2)	128.56(15)
F(4)-B(2)-F(3)	112.1(2)
F(4)-B(2)-O(4)	107.8(2)
F(3)-B(2)-O(4)	109.4(2)
F(4)-B(2)-O(3)	107.02(19)
F(3)-B(2)-O(3)	109.2(2)
O(4)-B(2)-O(3)	111.26(18)
B(2)-O(4)-P(3)	127.80(15)
P(1)#1-O(5)-P(3)	133.11(11)
O(6)-P(3)-O(4)	105.61(9)
O(6)-P(3)-O(5)	104.04(10)
O(4)-P(3)-O(5)	102.45(10)
O(6)-P(3)-Pt(1)	114.17(7)
O(4)-P(3)-Pt(1)	115.76(7)
O(5)-P(3)-Pt(1)	113.45(6)
B(3)-O(6)-P(3)	132.22(16)
F(5)-B(3)-F(6)	111.9(3)
F(5)-B(3)-O(6)	107.5(2)
F(6)-B(3)-O(6)	108.6(2)
F(5)-B(3)-O(7)	108.0(2)
F(6)-B(3)-O(7)	108.0(2)
O(6)-B(3)-O(7)	112.89(19)
B(3)-O(7)-P(4)	133.61(16)
P(2)#1-O(8)-P(4)	134.28(12)
O(7)-P(4)-O(9)	103.65(10)

O(7)-P(4)-O(8)	104.57(10)
O(9)-P(4)-O(8)	104.47(11)
O(7)-P(4)-Pt(1)	115.25(7)
O(9)-P(4)-Pt(1)	115.83(7)
O(8)-P(4)-Pt(1)	111.83(7)
B(4)-O(9)-P(4)	130.59(17)
F(7)-B(4)-F(8)	111.5(2)
F(7)-B(4)-O(9)	108.1(2)
F(8)-B(4)-O(9)	109.6(2)
F(7)-B(4)-O(10)	108.1(2)
F(8)-B(4)-O(10)	107.4(2)
O(9)-B(4)-O(10)	112.1(2)
B(4)-O(10)-P(1)	131.03(16)
C(31)-P(5)-C(1)	109.89(11)
C(31)-P(5)-C(11)	107.84(11)
C(1)-P(5)-C(11)	110.57(11)
C(31)-P(5)-C(21)	111.49(11)
C(1)-P(5)-C(21)	106.81(11)
C(11)-P(5)-C(21)	110.26(11)
C(6)-C(1)-C(2)	120.6(2)
C(6)-C(1)-P(5)	118.29(18)
C(2)-C(1)-P(5)	121.14(19)
C(3)-C(2)-C(1)	118.8(3)
C(3)-C(2)-H(2)	120.6
C(1)-C(2)-H(2)	120.6
C(4)-C(3)-C(2)	120.8(3)
C(4)-C(3)-H(3)	119.6
C(2)-C(3)-H(3)	119.6
C(3)-C(4)-C(5)	120.2(3)
C(3)-C(4)-H(4)	119.9
C(5)-C(4)-H(4)	119.9
C(4)-C(5)-C(6)	120.1(3)
C(4)-C(5)-H(5)	120.0
C(6)-C(5)-H(5)	120.0
C(5)-C(6)-C(1)	119.5(2)
C(5)-C(6)-H(6)	120.3

C(1)-C(6)-H(6)	120.3
C(12)-C(11)-C(16)	119.6(2)
C(12)-C(11)-P(5)	121.00(18)
C(16)-C(11)-P(5)	119.36(18)
C(13)-C(12)-C(11)	119.7(2)
C(13)-C(12)-H(12)	120.1
C(11)-C(12)-H(12)	120.1
C(14)-C(13)-C(12)	120.3(2)
C(14)-C(13)-H(13)	119.9
C(12)-C(13)-H(13)	119.9
C(13)-C(14)-C(15)	120.4(2)
C(13)-C(14)-H(14)	119.8
C(15)-C(14)-H(14)	119.8
C(16)-C(15)-C(14)	119.7(2)
C(16)-C(15)-H(15)	120.1
C(14)-C(15)-H(15)	120.1
C(15)-C(16)-C(11)	120.2(2)
C(15)-C(16)-H(16)	119.9
C(11)-C(16)-H(16)	119.9
C(22)-C(21)-C(26)	119.8(2)
C(22)-C(21)-P(5)	121.85(18)
C(26)-C(21)-P(5)	118.36(19)
C(23)-C(22)-C(21)	119.7(2)
C(23)-C(22)-H(22)	120.1
C(21)-C(22)-H(22)	120.1
C(22)-C(23)-C(24)	120.2(2)
C(22)-C(23)-H(23)	119.9
C(24)-C(23)-H(23)	119.9
C(25)-C(24)-C(23)	120.3(2)
C(25)-C(24)-H(24)	119.8
C(23)-C(24)-H(24)	119.8
C(24)-C(25)-C(26)	120.2(2)
C(24)-C(25)-H(25)	119.9
C(26)-C(25)-H(25)	119.9
C(25)-C(26)-C(21)	119.8(2)
C(25)-C(26)-H(26)	120.1

C(21)-C(26)-H(26)	120.1
C(32)-C(31)-C(36)	120.1(2)
C(32)-C(31)-P(5)	120.34(19)
C(36)-C(31)-P(5)	119.37(19)
C(33)-C(32)-C(31)	119.2(3)
C(33)-C(32)-H(32)	120.4
C(31)-C(32)-H(32)	120.4
C(34)-C(33)-C(32)	120.7(3)
C(34)-C(33)-H(33)	119.7
C(32)-C(33)-H(33)	119.7
C(33)-C(34)-C(35)	120.2(3)
C(33)-C(34)-H(34)	119.9
C(35)-C(34)-H(34)	119.9
C(36)-C(35)-C(34)	120.0(3)
C(36)-C(35)-H(35)	120.0
C(34)-C(35)-H(35)	120.0
C(35)-C(36)-C(31)	119.9(3)
C(35)-C(36)-H(36)	120.1
C(31)-C(36)-H(36)	120.1
C(51)-P(6)-C(71)	108.47(11)
C(51)-P(6)-C(61)	108.71(11)
C(71)-P(6)-C(61)	108.29(11)
C(51)-P(6)-C(41)	107.51(11)
C(71)-P(6)-C(41)	113.97(11)
C(61)-P(6)-C(41)	109.77(12)
C(42)-C(41)-C(46)	120.4(2)
C(42)-C(41)-P(6)	119.87(19)
C(46)-C(41)-P(6)	119.4(2)
C(43)-C(42)-C(41)	119.8(3)
C(43)-C(42)-H(42)	120.1
C(41)-C(42)-H(42)	120.1
C(42)-C(43)-C(44)	119.7(3)
C(42)-C(43)-H(43)	120.1
C(44)-C(43)-H(43)	120.1
C(45)-C(44)-C(43)	120.7(3)
C(45)-C(44)-H(44)	119.6

C(43)-C(44)-H(44)	119.6
C(44)-C(45)-C(46)	120.1(3)
C(44)-C(45)-H(45)	120.0
C(46)-C(45)-H(45)	120.0
C(45)-C(46)-C(41)	119.2(3)
C(45)-C(46)-H(46)	120.4
C(41)-C(46)-H(46)	120.4
C(56)-C(51)-C(52)	120.4(2)
C(56)-C(51)-P(6)	121.73(18)
C(52)-C(51)-P(6)	117.56(19)
C(53)-C(52)-C(51)	119.5(3)
C(53)-C(52)-H(52)	120.3
C(51)-C(52)-H(52)	120.3
C(52)-C(53)-C(54)	120.3(3)
C(52)-C(53)-H(53)	119.8
C(54)-C(53)-H(53)	119.8
C(53)-C(54)-C(55)	120.2(2)
C(53)-C(54)-H(54)	119.9
C(55)-C(54)-H(54)	119.9
C(54)-C(55)-C(56)	120.3(3)
C(54)-C(55)-H(55)	119.9
C(56)-C(55)-H(55)	119.9
C(55)-C(56)-C(51)	119.2(2)
C(55)-C(56)-H(56)	120.4
C(51)-C(56)-H(56)	120.4
C(62)-C(61)-C(66)	119.8(2)
C(62)-C(61)-P(6)	121.26(19)
C(66)-C(61)-P(6)	118.9(2)
C(63)-C(62)-C(61)	119.7(3)
C(63)-C(62)-H(62)	120.2
C(61)-C(62)-H(62)	120.2
C(64)-C(63)-C(62)	119.9(3)
C(64)-C(63)-H(63)	120.1
C(62)-C(63)-H(63)	120.1
C(65)-C(64)-C(63)	120.6(3)
C(65)-C(64)-H(64)	119.7

C(63)-C(64)-H(64)	119.7
C(66)-C(65)-C(64)	120.3(3)
C(66)-C(65)-H(65)	119.8
C(64)-C(65)-H(65)	119.8
C(65)-C(66)-C(61)	119.8(3)
C(65)-C(66)-H(66)	120.1
C(61)-C(66)-H(66)	120.1
C(76)-C(71)-C(72)	120.0(2)
C(76)-C(71)-P(6)	120.61(18)
C(72)-C(71)-P(6)	119.03(18)
C(73)-C(72)-C(71)	119.9(2)
C(73)-C(72)-H(72)	120.1
C(71)-C(72)-H(72)	120.1
C(72)-C(73)-C(74)	120.0(2)
C(72)-C(73)-H(73)	120.0
C(74)-C(73)-H(73)	120.0
C(75)-C(74)-C(73)	120.3(2)
C(75)-C(74)-H(74)	119.9
C(73)-C(74)-H(74)	119.9
C(74)-C(75)-C(76)	120.6(2)
C(74)-C(75)-H(75)	119.7
C(76)-C(75)-H(75)	119.7
C(75)-C(76)-C(71)	119.3(2)
C(75)-C(76)-H(76)	120.3
C(71)-C(76)-H(76)	120.3

Symmetry transformations used to generate equivalent atoms:

#1 -x+2,-y+1,-z+1

Table 4: Anisotropic displacement parameters (Å^{2}x 10^3) for S13045. The anisotropic displacement factor exponent takes the form: -2p^2[h^2 a*^{2}U^{11} + ... + 2 h k a* b* U^{12}]

	U^{11}	U^{22}	U^{33}	U^{23}	U^{13}	U^{12}
Pt(1)	11(1)	10(1)	10(1)	0(1)	3(1)	0(1)
P(1)	14(1)	11(1)	12(1)	-1(1)	3(1)	-2(1)
O(1)	22(1)	22(1)	17(1)	-10(1)	6(1)	-6(1)
B(1)	20(1)	21(1)	16(1)	-6(1)	5(1)	-3(1)
F(1)	34(1)	35(1)	16(1)	-9(1)	2(1)	-10(1)
F(2)	25(1)	42(1)	44(1)	-3(1)	12(1)	11(1)
O(2)	41(1)	24(1)	11(1)	-3(1)	4(1)	-13(1)
P(2)	13(1)	15(1)	9(1)	-1(1)	3(1)	-1(1)
O(3)	15(1)	30(1)	14(1)	6(1)	3(1)	-3(1)
B(2)	14(1)	22(1)	14(1)	1(1)	5(1)	1(1)
F(3)	26(1)	25(1)	26(1)	0(1)	3(1)	10(1)
F(4)	19(1)	39(1)	19(1)	3(1)	8(1)	-9(1)
O(4)	14(1)	20(1)	14(1)	1(1)	3(1)	-5(1)
O(5)	14(1)	17(1)	26(1)	-10(1)	3(1)	-1(1)
P(3)	11(1)	13(1)	10(1)	0(1)	3(1)	-1(1)
O(6)	13(1)	20(1)	16(1)	4(1)	1(1)	-2(1)
B(3)	20(1)	26(1)	14(1)	6(1)	-2(1)	-8(1)
F(5)	18(1)	64(2)	58(1)	41(1)	-4(1)	-5(1)
F(6)	94(2)	44(1)	27(1)	-18(1)	27(1)	-39(1)
O(7)	15(1)	21(1)	18(1)	6(1)	-1(1)	-3(1)
O(8)	26(1)	28(1)	14(1)	6(1)	8(1)	12(1)
P(4)	12(1)	13(1)	12(1)	2(1)	2(1)	-1(1)
O(9)	25(1)	17(1)	19(1)	5(1)	-1(1)	-6(1)
B(4)	25(1)	17(1)	20(1)	2(1)	4(1)	-6(1)
F(7)	55(1)	20(1)	39(1)	10(1)	-9(1)	-13(1)
F(8)	24(1)	67(2)	31(1)	-5(1)	10(1)	-3(1)
O(10)	29(1)	13(1)	20(1)	0(1)	0(1)	-5(1)
P(5)	15(1)	15(1)	15(1)	2(1)	2(1)	0(1)
C(1)	18(1)	18(1)	18(1)	2(1)	4(1)	2(1)
C(2)	31(1)	19(1)	27(1)	2(1)	14(1)	3(1)

C(3)	40(2)	24(1)	34(2)	2(1)	23(1)	6(1)
C(4)	27(1)	28(1)	27(1)	7(1)	13(1)	3(1)
C(5)	21(1)	23(1)	24(1)	4(1)	5(1)	-2(1)
C(6)	21(1)	20(1)	23(1)	0(1)	6(1)	-1(1)
C(11)	17(1)	16(1)	16(1)	1(1)	2(1)	1(1)
C(12)	20(1)	17(1)	16(1)	3(1)	2(1)	0(1)
C(13)	25(1)	18(1)	18(1)	2(1)	-2(1)	1(1)
C(14)	22(1)	23(1)	21(1)	-3(1)	-2(1)	5(1)
C(15)	16(1)	26(1)	21(1)	-2(1)	1(1)	2(1)
C(16)	18(1)	21(1)	18(1)	2(1)	3(1)	0(1)
C(21)	18(1)	17(1)	16(1)	1(1)	2(1)	1(1)
C(22)	19(1)	22(1)	19(1)	0(1)	4(1)	1(1)
C(23)	25(1)	24(1)	21(1)	-3(1)	6(1)	-1(1)
C(24)	29(1)	26(1)	21(1)	-3(1)	2(1)	-1(1)
C(25)	23(1)	30(1)	22(1)	-2(1)	-4(1)	0(1)
C(26)	19(1)	23(1)	21(1)	-2(1)	0(1)	4(1)
C(31)	17(1)	15(1)	20(1)	2(1)	3(1)	1(1)
C(32)	17(1)	21(1)	24(1)	6(1)	3(1)	3(1)
C(33)	24(1)	22(1)	34(1)	9(1)	8(1)	5(1)
C(34)	30(1)	18(1)	41(2)	2(1)	13(1)	1(1)
C(35)	31(1)	20(1)	34(1)	-3(1)	4(1)	-4(1)
C(36)	26(1)	19(1)	25(1)	1(1)	-1(1)	-1(1)
P(6)	18(1)	16(1)	12(1)	-1(1)	2(1)	1(1)
C(41)	20(1)	21(1)	16(1)	-2(1)	4(1)	1(1)
C(42)	28(1)	22(1)	20(1)	-1(1)	7(1)	-4(1)
C(43)	34(1)	27(1)	26(1)	0(1)	10(1)	-9(1)
C(44)	25(1)	42(2)	33(1)	-1(1)	11(1)	-8(1)
C(45)	25(1)	39(2)	39(2)	-3(1)	16(1)	3(1)
C(46)	24(1)	26(1)	31(1)	1(1)	10(1)	4(1)
C(51)	19(1)	16(1)	15(1)	-1(1)	0(1)	0(1)
C(52)	26(1)	22(1)	15(1)	1(1)	0(1)	0(1)
C(53)	31(1)	29(1)	21(1)	4(1)	-7(1)	-3(1)
C(54)	22(1)	27(1)	34(1)	12(1)	-6(1)	-4(1)
C(55)	19(1)	24(1)	34(1)	6(1)	4(1)	1(1)
C(56)	19(1)	22(1)	22(1)	1(1)	4(1)	2(1)
C(61)	22(1)	19(1)	16(1)	1(1)	5(1)	1(1)

C(62)	25(1)	17(1)	22(1)	1(1)	5(1)	-1(1)
C(63)	33(1)	18(1)	34(1)	-4(1)	13(1)	-4(1)
C(64)	41(2)	16(1)	37(2)	2(1)	23(1)	5(1)
C(65)	41(2)	22(1)	32(1)	6(1)	13(1)	12(1)
C(66)	31(1)	26(1)	21(1)	1(1)	3(1)	9(1)
C(71)	18(1)	20(1)	13(1)	-1(1)	1(1)	-1(1)
C(72)	28(1)	23(1)	16(1)	-1(1)	4(1)	-8(1)
C(73)	31(1)	28(1)	16(1)	-2(1)	6(1)	-7(1)
C(74)	30(1)	26(1)	13(1)	-3(1)	2(1)	-2(1)
C(75)	28(1)	20(1)	16(1)	-3(1)	0(1)	-3(1)
C(76)	22(1)	20(1)	16(1)	-2(1)	1(1)	-2(1)

Table 5: Hydrogen coordinates (x 10^4) and isotropic displacement parameters ($Å^2$x 10^3) for S13045.

	x	y	z	U(eq)
H(2)	8513	9063	2011	29
H(3)	7357	8735	2600	37
H(4)	6896	7458	2622	32
H(5)	7536	6497	2007	27
H(6)	8642	6820	1356	25
H(12)	10005	7134	2360	21
H(13)	11289	6600	2933	25
H(14)	12572	6934	2549	27
H(15)	12594	7826	1602	25
H(16)	11317	8350	1014	23
H(22)	10498	7363	158	24
H(23)	10121	6832	-1001	27
H(24)	8714	6917	-1587	30
H(25)	7680	7532	-1022	31
H(26)	8042	8062	140	25

H(32)	8855	9388	170	25
H(33)	8963	10743	181	32
H(34)	9867	11372	1099	34
H(35)	10681	10654	2016	34
H(36)	10550	9304	2039	29
H(42)	8259	11246	4453	28
H(43)	9325	11669	3800	34
H(44)	10205	10763	3345	39
H(45)	10066	9443	3573	40
H(46)	9027	9012	4255	31
H(52)	7064	9941	3373	25
H(53)	5744	10246	2707	34
H(54)	4618	10631	3299	34
H(55)	4827	10784	4556	31
H(56)	6144	10467	5239	25
H(62)	6629	8626	3999	25
H(63)	6589	7265	3978	33
H(64)	7556	6558	4789	35
H(65)	8581	7191	5605	37
H(66)	8641	8540	5630	31
H(72)	7050	9148	6100	27
H(73)	7018	9587	7283	30
H(74)	7682	10753	7673	27
H(75)	8412	11465	6899	26
H(76)	8453	11038	5712	23

REFERENCES

(1) Harvey, E. L. Dissertation (Ph.D.), California Institute of Technology, 1990.

(2) Durrell, A. C.; Keller, G. E.; Lam, Y.-C.; Sykora, J.; Vlček, A.; Gray, H. B. *J. Am. Chem. Soc.* **2012**, *134*, 14201.

(3) Lam, Y.-C., Caltech, 2015.

(4) Lam, Y.-C.; Darnton, T. Unpublished results.

(5) Pinto, M. A. F. D. R.; Sadler, P. J.; Neidle, S.; Sanderson, M. R.; Subbiah, A.; Kuroda, R. *J. Chem. Soc. Chem. Comm.* **1980**, 13.

(6) Lakowicz, J. R. *Principles of Fluorescence Spectroscopy*; Springer US, 2006.

(7) Dawson, W. R.; Windsor, M. W. *J. Phys. Chem.* **1968**, *72*, 3251.

(8) Ware, W. R.; Baldwin, B. A. *The Journal of Chemical Physics* **1965**, *43*, 1194.

(9) Crosby, G. A.; Demas, J. N. *J. Phys. Chem.* **1971**, *75*, 991.

(10) Brouwer, A. M. *Pure and Applied Chemistry* **2011**, *83*.

(11) Murov, S. L., University of Chicago, 1967.

(12) Lampert, R. A.; Chewter, L. A.; Phillips, D.; O'Connor, D. V.; Roberts, A. J.; Meech, S. R. *Analytical Chemistry* **1983**, *55*, 68.

(13) Eaton, D. F. *Pure and Applied Chemistry* **1988**, *60*, 1107.

(14) Greiner, G. *Journal of Photochemistry and Photobiology A: Chemistry* **2000**, *137*, 1.

(15) Milder, S. J.; Brunschwig, B. S. *J. Phys. Chem.* **1992**, *96*, 2189.

(16) Armarego, W. L. F.; Chai, C. L. L. In *Purification of Laboratory Chemicals (Sixth Edition)*; Butterworth-Heinemann: Oxford, 2009, p 88.

(17) Che, C. M.; Butler, L. G.; Gray, H. B. *J. Am. Chem. Soc.* **1981**, *103*, 7796.

(18) Pangborn, A. B.; Giardello, M. A.; Grubbs, R. H.; Rosen, R. K.; Timmers, F. J. *Organometallics* **1996**, *15*, 1518.

(19) Che, C. M.; Schaefer, W. P.; Gray, H. B.; Dickson, M. K.; Stein, P. B.; Roundhill, D. M. *J. Am. Chem. Soc.* **1982**, *104*, 4253.

(20) Sheldrick, G. *Acta Crystallographica Section A* **1990**, *46*, 467.

(21) Sheldrick, G. M. *Acta Crystallogr A* **2008**, *64*, 112.

(22) Müller, P. *Crystallography Reviews* **2009**, *15*, 57.

(23) Cobas, J. C.; Sardina, F. J. *Concepts in Magnetic Resonance Part A* **2003**, *19A*, 80.

CHAPTER 3: PHOTOREDUCTION OF Pt(POP-BF$_2$)$^{4-}$

To quantitatively probe the excited-state oxidizing power of Pt(pop-BF$_2$)$^{4-}$, a series of luminescence quenching experiments was carried out.

3.1 Analysis of quenching

Quenching in a chemical sense may be described as any process which decreases the fluorescence intensity of a substance. There are two basic types of quenching: static and dynamic. Both static and dynamic (diffusional) quenching require physical contact between the fluorophore and the quencher.[1]

Static quenching occurs when a nonfluorescent ground-state complex containing both fluorophore and quencher exists prior to excitation of the fluorophore; this is often achieved by the formation of ion pairs utilizing oppositely charged quenchers and fluorophores. When such a complex absorbs light, it returns to the ground state without emitting a photon. In the case of static quenching, the dependence of fluorescence intensity on quencher concentration may be derived by calculating the association constant for complex formation, K_S.[1]

$$K_S = \frac{[F-Q]}{[F][Q]} \qquad (1)$$

In equation (1), $[F-Q]$ is the concentration of the fluorophore-quencher complex, $[F]$ is the concentration of uncomplexed fluorophore, and [Q] is the concentration of uncomplexed quencher. If the complex is nonfluoroescent, then the fraction of remaining fluorescence F/F_0 is equivalent to the fraction of total fluorophores not complexed. As the total concentration of fluorophore is $[F]_0 = [F] + [F-Q]$, substitution into equation (1) and subsequent rearrangement yields equation (2):

$$\frac{F_0}{F} = 1 + K_s[Q] \qquad (2)$$

Of particular importance is the fact that because static quenching stops a fraction of available fluorophores from emitting without affecting the remaining uncomplexed fluorophores, the fluorophore lifetime is unaffected and $\tau_0 = \tau$.

Dynamic, or diffusional, quenching occurs when the decrease in fluorescence intensity is caused by collisional encounters between fluorophore and quencher. As such, the fluorophore and quencher must diffuse together within the timeframe dictated by the excited state lifetime τ_0. Collisional quenching is described by the Stern-Volmer equation:

$$\frac{F_0}{F} = 1 + k_q\tau_0[Q] = 1 + K_D[Q] \qquad (3)$$

In equation (3), F_0 and F are the fluorescence intensites in the absence and presence of quencher, k_q is the bimolecular quenching constant, τ_0 is the lifetime of the fluorophore without quencher, $[Q]$ is the concentration of quencher and K_D is the Stern-Volmer quenching constant. As F_0/F is expected to have a linear dependence on $[Q]$, quenching data are typically presented as a plot of F_0/F versus $[Q]$; this yields a line with a y-intercept of 1 and a slope of K_D.[1] A linear Stern-Volmer plot is indicative of a single fluorophore, all of which are equally accessible to quencher molecules.

Inspection of equation (2) shows that static quenching behavior may also yield a linear relationship between F_0/F and $[Q]$. Therefore, in order to unambiguously assign a type of quenching behavior, the fluorescence lifetimes in the presence and absence of quencher (τ_0 and τ) must be measured.

3.2 Fluorophore lifetime measurements

The excitation of a fluorophore with an infinitely short pulse of light results in an initial population N_0 of fluorophores in the excited state. At any time t after the initial excitation, the number of excited molecules may be described as $N(t)$. As time passes, this population decays at a rate dependent on the emissive rate γ and the non-radiative decay rate k_{nr}:

$$\frac{dN(t)}{dt} = -(\gamma + k_{nr})N(t) \tag{4}$$

As $N(t = 0) = N_0$, equation (4) may be integrated to yield

$$N = N_0 e^{-1/\tau} \tag{5}$$

in which τ is the lifetime of the excited state. The fluorescence lifetime is generally defined to be the time required for the intensity to decay to $1/e$ of its original value; or,

$$\tau = \frac{1}{\gamma + k_{nr}} \tag{6}$$

Finally, the fluorescence intensity measured by an instrument, $F(t)$, is proportional to the excited state population:

$$N(t) \cong F(t) \tag{7}$$

Thus, the slope of a plot of $\log F(t)$ versus t will be $-1/\tau$.

3.3 Quenching of $^3[Pt(pop\text{-}BF_2)^{4-}]^*$ phosphorescence

The excited-state lifetimes of the $[Pt(pop\text{-}BF_2)]^{4-}$ singlet and triplet states were measured by Durrell and coworkers in 2012. The triplet state has a lifetime of 8.4 μs with an emission maximum at 512 nm; meanwhile, the singlet state has a lifetime of 1.6 ns with an emission maximum of 393 nm.[2] The length of the triplet lifetime affords ample time for diffusional quenching to occur. The presence of diffusional quenching may be observed as a decrease in either luminescence lifetime or steady-state luminescence intensity at the triplet emission wavelength maximum of 512 nm. As shown in Figure 1, after the triplet excited state of $Pt(pop\text{-}BF_2)^{4-}$ is produced following excitation with 355 nm light, it may return to the ground state either by emission of a photon or by reacting with an electron-transfer type quencher molecule to produce the oxidized quencher and reduced $Pt(pop\text{-}BF_2)^{5-}$. The degree to which the nonemissive path is favored over the emissive pathway is demonstrated by the relative magnitude of the decrease in luminescence intensity. After quenching occurs, it is possible for the products to react to reform the reactants, Q and $Pt(pop\text{-}BF_2)^{4-}$, provided that Q^+ does not decompose.

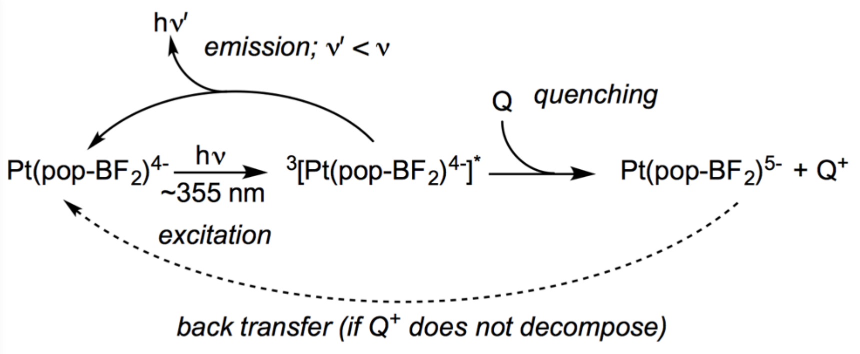

Figure 1: Dynamic (diffusional) reductive quenching scheme.

The excited-state behavior of $Pt(pop)^{4-}$ is well known and has been deeply investigated,[3-12] while that of $Pt(pop\text{-}BF_2)^{4-}$ remains relatively unexplored.[13,14] Furthermore, as yet the only extant data on the oxidizing power of $Pt(pop\text{-}BF_2)^{4-}$ excited states are estimates based on spectral data (see Chapter 1).[2,13,15] By tracking how the quenching rate of an emissive state changes based on the oxidation potential of the selected quencher molecule, a good estimate of the potential of the excited state may be obtained.[16-18] As such, the emissive properties of $Pt(pop\text{-}BF_2)^{4-}$ were studied in the presence of various organic amine quenchers. The specific amines used in this section were chosen as quenchers because of their lack of absorption bands in the areas of Pt(pop-BF$_2$)$^{4-}$ absorption, their ranges of oxidation potential, and their solubility in acetonitrile.[14]

Briefly, solutions of Pt(pop-BF$_2$)$^{4-}$ of a fixed concentration (~10 μM) were prepared such that the total absorbance at the 355 nm excitation wavelength was between 0.05 and 0.1; these solutions were spiked with increasing concentrations of quencher and their steady-state luminescence profiles were recorded using fluorimetry. Quencher-only solutions were also prepared and analyzed to ensure that the quencher was not luminescing due to excitation from the 355 nm probe wavelength. The singlet emission intensity was measured and used as a normalization factor, as the 1.6 ns lifetime of the singlet state hampers it from participating in diffusional quenching; furthermore, noted deviation in the singlet-state intensity from spectrum to spectrum was within instrument error.[2] Finally, the solutions were monitored by UV-Vis spectroscopy during the course of the experiment to check for any possible decomposition; no such decomposition was observed. Stern-Volmer type quenching behavior was observed, and values for k_q were calculated for each quencher by plotting I_0/I (referred to as F_0/F in the equations of section 3.1) vs [Q]. Results are summarized in Figure 2, Figure 3, and Figure 4.

N,N,N′,N′-tetramethyl-para-phenylenediamine (TMPD)
+0.35 V vs NHE
$k_q = 2.80 \times 10^9\ M^{-1}\ s^{-1}$

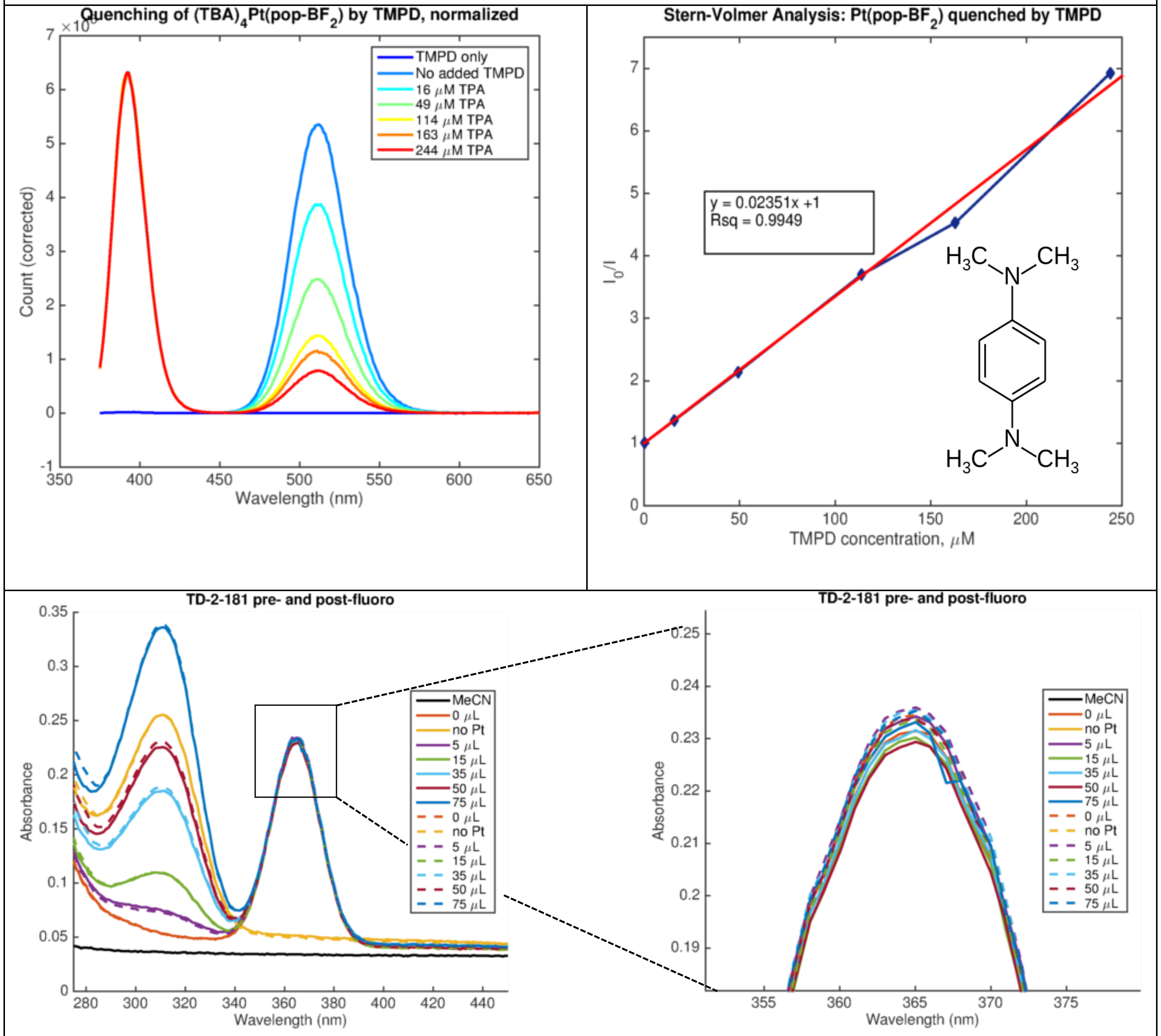

The absorption features at ~315 nm in the lower left plot is attributable to TMPD. This is not expected to affect the quenching results as the excitation wavelength (355 nm) was outside the region of TMPD absorbance; further, the “TMPD only” sample with [TMPD] ≈ 160 μM showed no luminescence activity (dark blue line in upper left plot).

Figure 2: Luminescence behavior of $^3[Pt(pop\text{-}BF_2)^{4-}]^*$ in the presence of TMPD

4-dimethylaminopyridine (DMAP)
+1.1 V vs NHE
$k_q = 5.51 \times 10^8\ \mathrm{M^{-1}\ s^{-1}}$

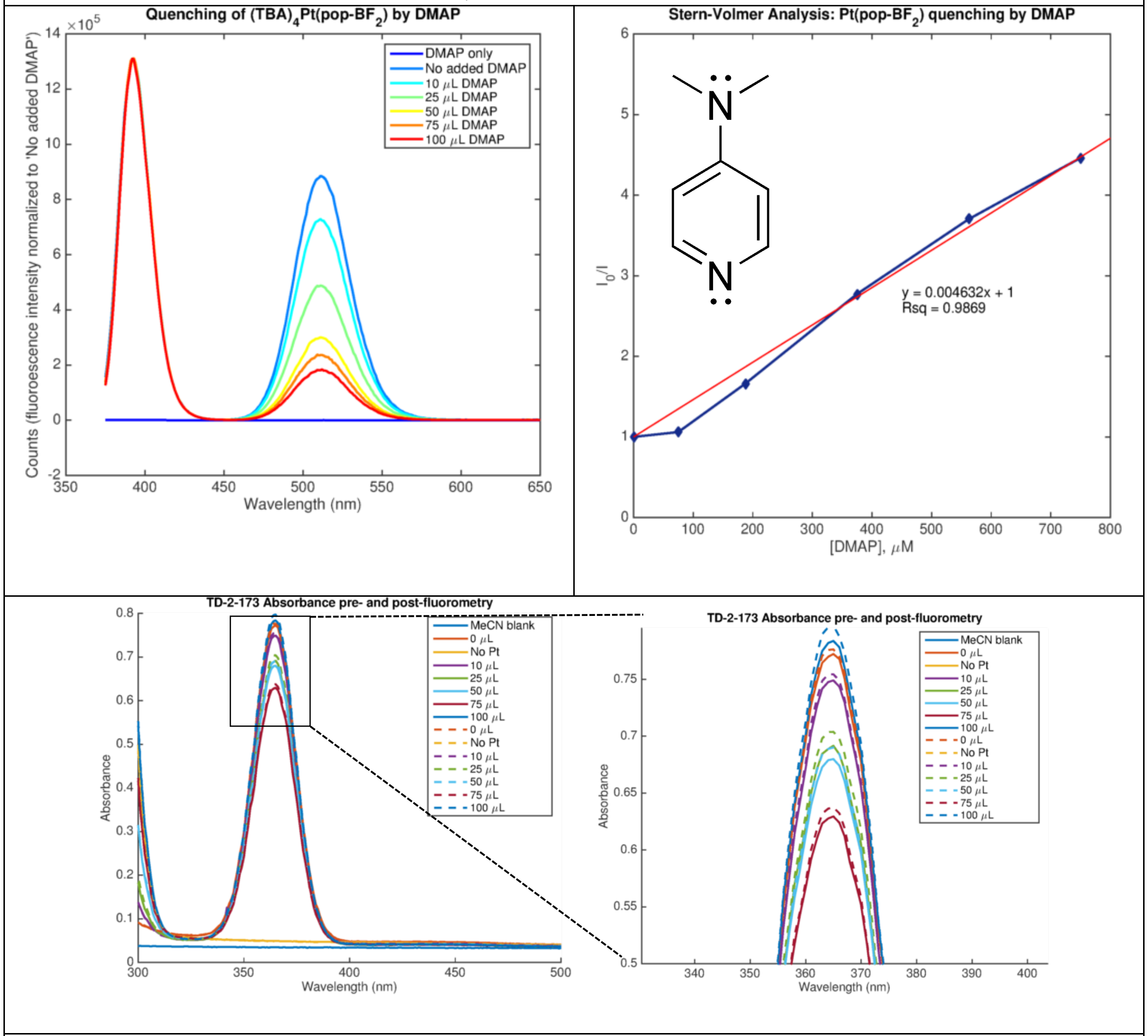

Figure 3: Luminescence of $^3[\mathrm{Pt(pop\text{-}BF_2)}^{4-}]^*$ in the presence of DMAP

Triphenylamine (TPA)
+1.16 V vs NHE
$k_q = 8.97 \times 10^8\ M^{-1}\ s^{-1}$

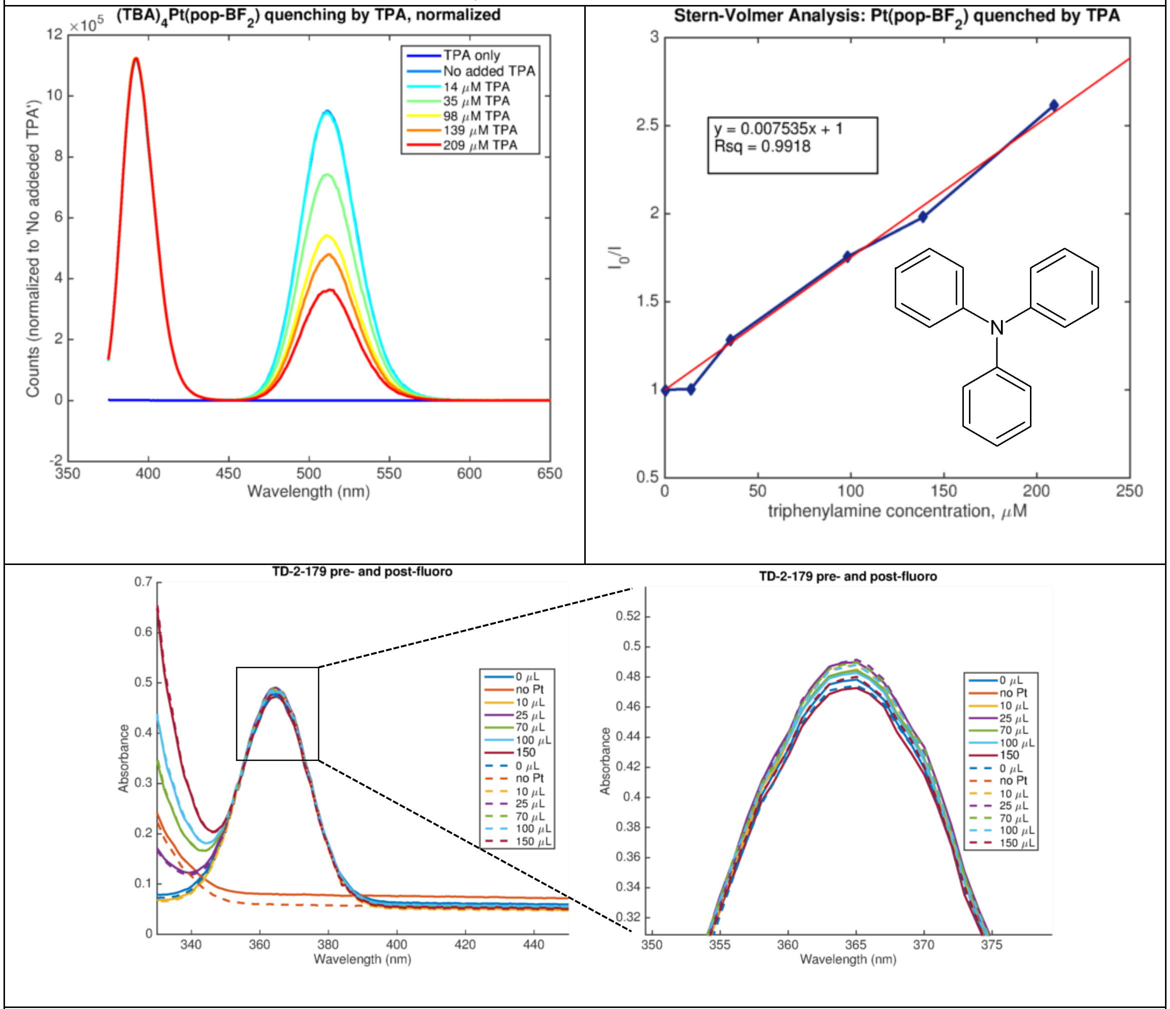

Figure 4: Luminescence of $^3[Pt(pop\text{-}BF_2)^{4-}]^*$ in the presence of TPA

The data obtained for these three quenchers demonstrate that the rate of quenching of the triplet state roughly tracks with the oxidation potential of the selected quencher; that is, when a quencher is easier to oxidize, the quenching rate increases. Data with more quenchers as well as additional trials with these three quenchers are needed to confirm the exact excited state potential of $^3[Pt(pop\text{-}BF_2)^{4-}]^*$, but it is possible that Marcus-type behavior will be observed for $Pt(pop\text{-}BF_2)^{5-}$

/Q+ recombination as in the case of the d^8-d^8 Ir_2 phosphonite complexes studied by the Gray group in the 1990s.[16]

3.4 Quenching of $^1[Pt(pop\text{-}BF_2)^{4-}]^*$ fluorescence

Because of the predicted extraordinary oxidizing power of the $Pt(pop\text{-}BF_2)^{4-}$ singlet excited state,[2,14,19] efforts were undertaken to both observe and quantify the rate of singlet quenching. Due to the very short 1.6 ns lifetime of the singlet state, diffusional quenching was not expected to be favorable; correspondingly, to favor static quenching, a cationic metal complex was used as an acceptor molecule. Given the large negative charge on $Pt(pop\text{-}BF_2)^{4-}$, it was expected that ion pairs would readily form between fluorophore and quencher (Figure 5).

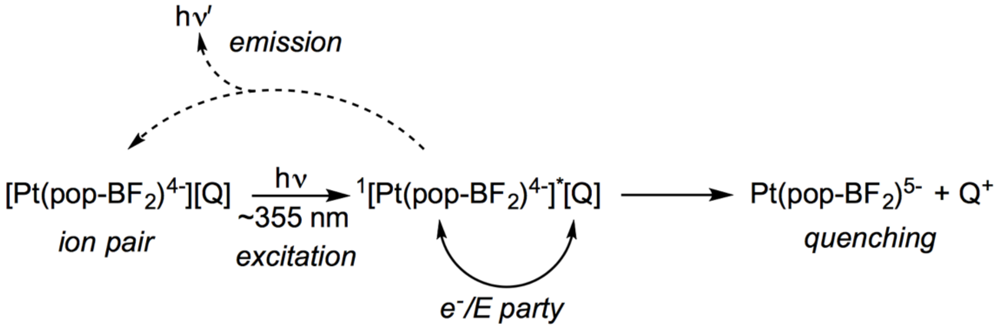

Figure 5: Reductive static quenching schematic

These predictions notwithstanding, analogous experiments to those presented in 3.3 were undertaken using tris(2,2'-bipyridine)cobalt(II) di(hexafluorophosphate), $[Co^{II}(bpy)_3](PF_6)_2$, as the quencher in order to fully rule out the possibility of diffusional quenching. Initial steady-state fluorimetry measurements demonstrated an approximately linear relationship between quencher concentration and intensity of singlet emission, while the concomitant triplet emission deviated significantly from a linear relationship (Figure 6). This deviation in the case of the triplet emission is likely due to a second-order dependence on quencher concentration, as diffusional and static quenching are both possible decay pathways. Such deviations from linearity, demonstrating concavity toward the y-axis, are well-documented in the literature as being ascribable to a combination of static and dynamic quenching.[1]

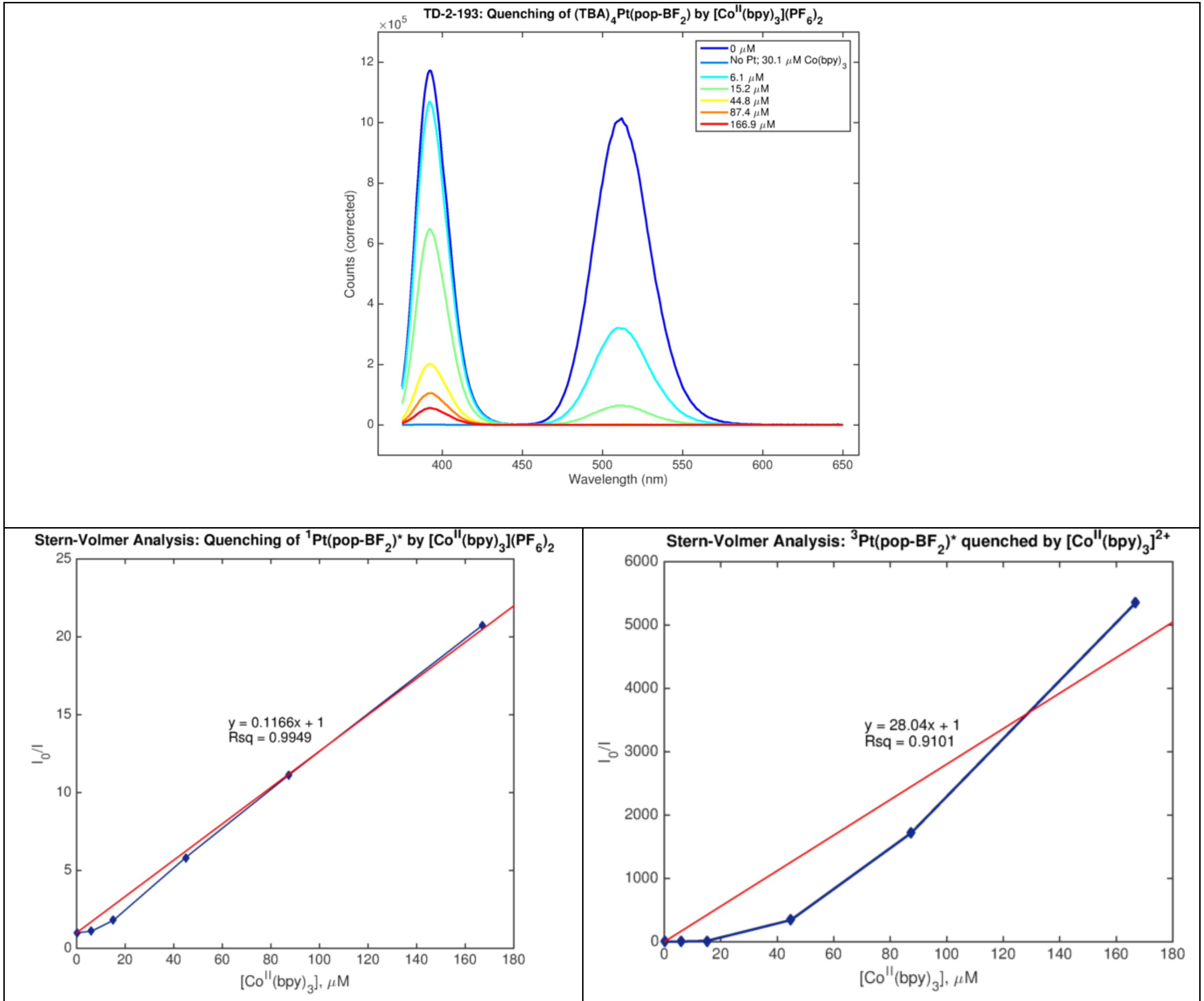

$k_q = 7.3 \times 10^{13}\ M^{-1}\ s^{-1}$

k_q not applicable; S-V relationship does not apply to non-linear relationship

Figure 6: Luminescence behavior of $Pt(pop\text{-}BF_2)^{4-}$ in the presence of $Co(bpy)_3^{2+}$

A putative singlet quenching rate exceeding 10^{13} M^{-1} s^{-1} was also calculated, seemingly ruling out the possibility of a wholly diffusional quenching mechanism given that the diffusion limit in acetonitrile is on the order of 10^{11} M^{-1} s^{-1}. However, close investigation of the plot of I_0/I vs [Q] indicates a very slight deviation from linearity at lower concentrations. A possible explanation for this deviation could be that at low [Q] there is little to no quenching, as the singlet lifetime is too short to allow for diffusional quenching and [Q] could be too low to create a sizable population of quencher-fluorophore complexes. Contrastingly, at high [Q], rapid quenching (i.e. quenching rates in excess of the diffusion limit) could be attributed to static quenching behavior resulting from the favored formation of quencher-fluorophore complexes (Figure 7).

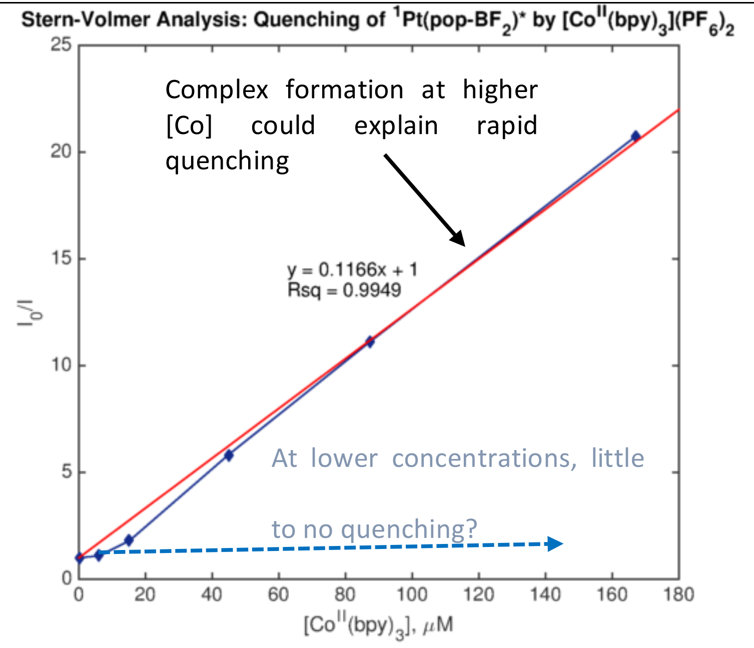

Complex formation at higher [Co] could explain rapid quenching

At lower concentrations, little to no quenching?

Figure 7: Indication of possible bimodal quenching behavior

In an effort to further illuminate this behavior, quencher concentrations were lowered to <20 μM to attempt to disfavor fluorophore-quencher complex formation and to add more data points to the plot in Figure 7. However, with the additional data at lower concentrations, the deviation from linearity was even more distinct for both the singlet and triplet states (Figure 8).

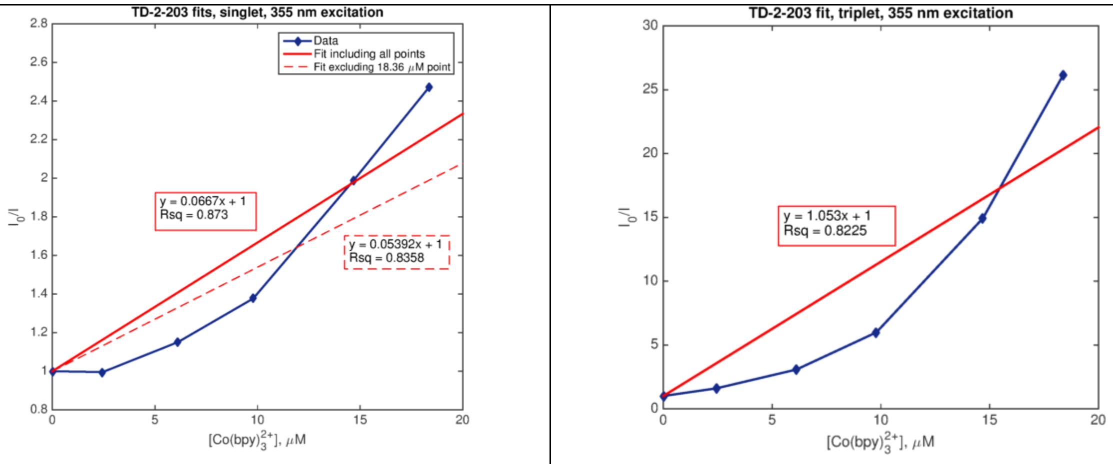

Figure 8: Substantial quenching of Pt(pop-BF$_2$)$^{4-}$ singlet and triplet emission continues at low values of [Q]

Furthermore, the additional data points taken at lower concentrations follow the same pattern observed previously (Figure 9).

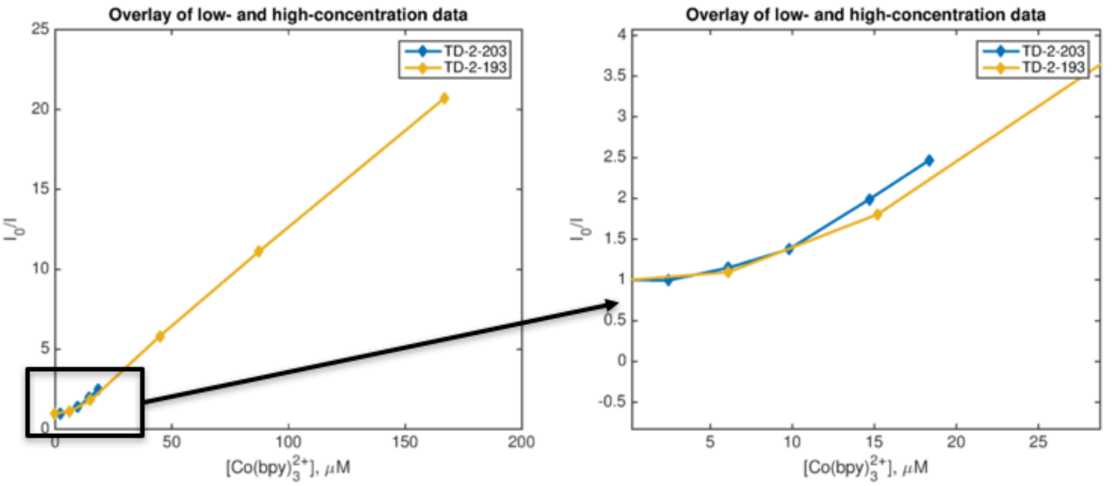

Figure 9: Overlay of quenching data obtained with [Q] = 0 – 170 μM (yellow) and [Q] = 0 – 20 μM (blue).

Finally, the excitation wavelength was moved to 370 nm to further reduce the very limited possibility of emission from the Co^{II} complex, which has an absorbance maximum at 305 nm ($\epsilon \approx$ 63,000 L mol^{-1} cm^{-1}). The red-shift in excitation wavelength also had no effect on the quenching behavior (Figure 10), which is not particularly surprising given the Co^{II} complex's molar absorptivity constant of <6000 L mol^{-1} cm^{-1} at 355 nm.

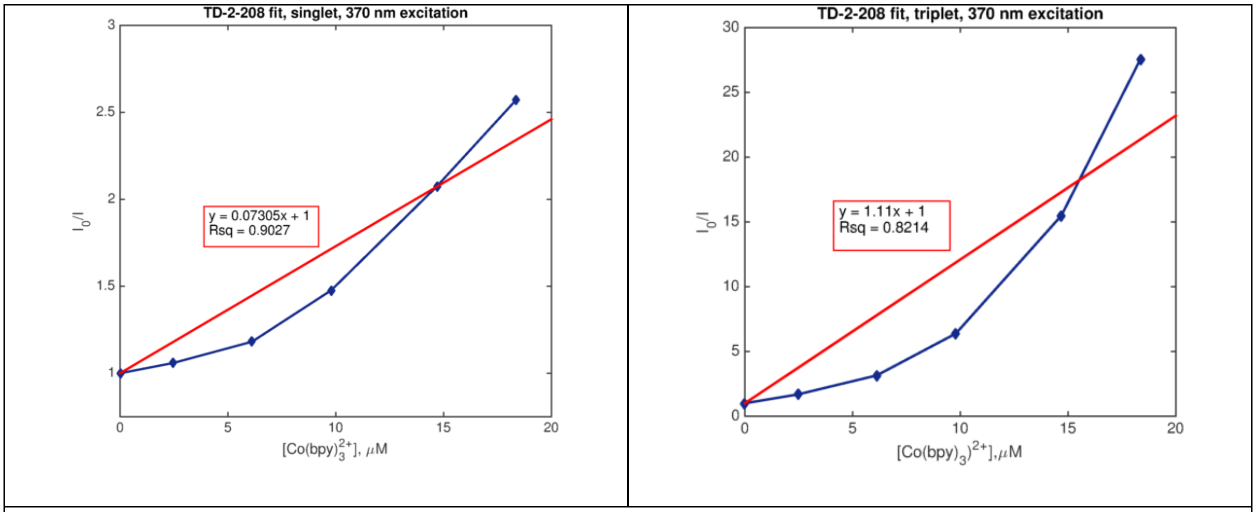

Figure 10: No change in observed second-order behavior with 370 nm excitation.

The diffusion rate limit in acetonitrile is on the order of 10^{10} - 10^{11} M^{-1} s^{-1},[1] so the k_q's calculated for the singlet cannot be attributed solely to diffusional quenching. As a decrease in the emission intensity of the singlet was nevertheless observed in the presence of Co(bpy)$_3^{2+}$, the quenching behavior must be attributed at least in part to non-diffusional energy and/or electron transfer between ^{1}[Pt(pop-BF$_2$)$^{4-}$]* and [Co(bpy)$_3$]$^{2+}$. Steady-state techniques are insufficient to analyze this type of behavior; time-resolved experiments were undertaken.

3.4.1 *Time-resolved analysis: ^{1}[Pt(pop-BF$_2$)$_{4-}$]* and ^{3}[Pt(pop-BF$_2$)$^{4-}$]* luminescence quenching by Co(bpy)$_3^{2+}$*

As described in 3.3, solutions of Pt(pop-BF$_2$)$^{4-}$ (~ 8 μM) in acetonitrile were prepared and spiked with (Co(bpy)$_3$)$^{2+}$ to yield quencher concentrations from 0 – 170 μM. Absorbance spectra were recorded before and after the experiment to monitor for compound decomposition.

Using 355 nm excitation, luminescence decay spectra were recorded at 512 and 400 nm (the approximate emission maxima of the triplet and the singlet, respectively).[i] The intensity decays were fitted to mono- or bi-exponential equations, as appropriate, and values for the excited-state lifetimes were calculated (see 3.2 for background). The lifetime of the triplet state decreased from an initial value of 9.1 μs without quencher to 0.018 μs when [Q] = 170 μM. Decay traces and fitting equations are shown in Figure 11.

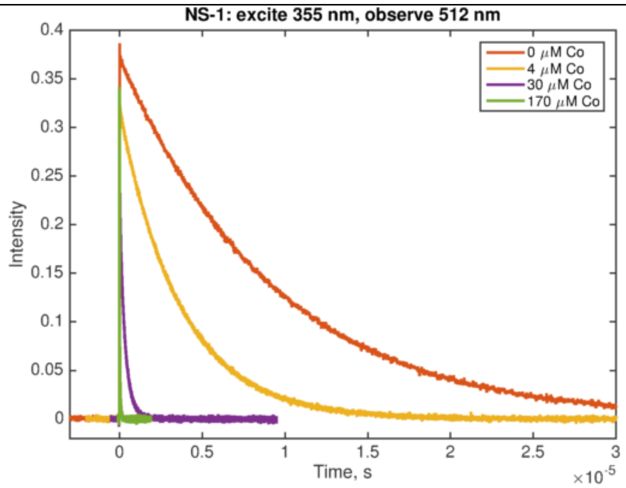

---

[i] The time-resolved data in section 3.4.1 were collected with the kind assistance of Oliver S. Shafaat.

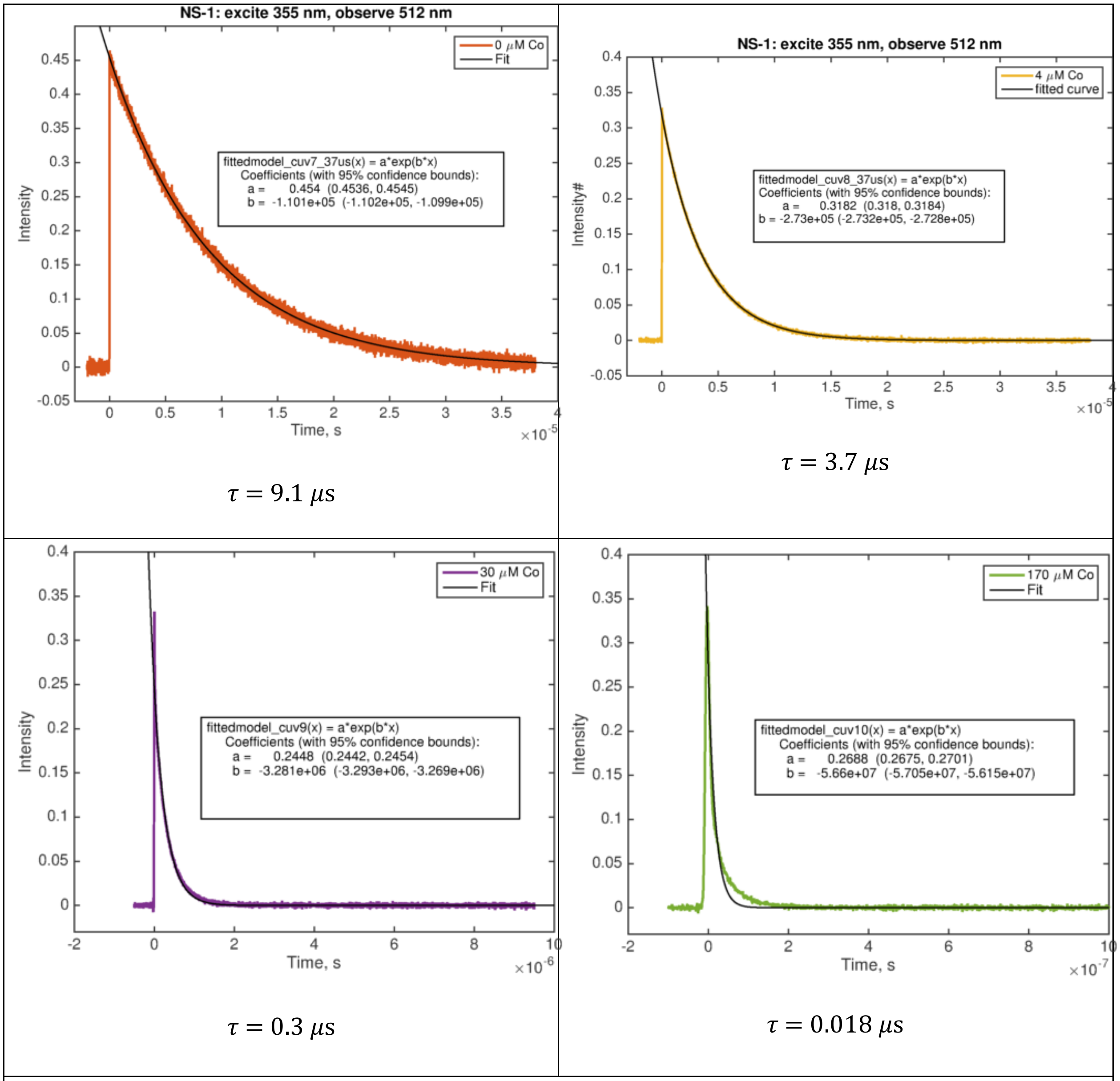

```
fittedmodel_cuv7_37us(x) = a*exp(b*x)
  Coefficients (with 95% confidence bounds):
    a =      0.454  (0.4536, 0.4545)
    b =  -1.101e+05  (-1.102e+05, -1.099e+05)
```

$\tau = 9.1\ \mu s$

```
fittedmodel_cuv8_37us(x) = a*exp(b*x)
Coefficients (with 95% confidence bounds):
    a =      0.3182  (0.318, 0.3184)
b = -2.73e+05 (-2.732e+05, -2.728e+05)
```

$\tau = 3.7\ \mu s$

```
fittedmodel_cuv9(x) = a*exp(b*x)
  Coefficients (with 95% confidence bounds):
    a =      0.2448  (0.2442, 0.2454)
    b =  -3.281e+06  (-3.293e+06, -3.269e+06)
```

$\tau = 0.3\ \mu s$

```
fittedmodel_cuv10(x) = a*exp(b*x)
  Coefficients (with 95% confidence bounds):
    a =      0.2688  (0.2675, 0.2701)
    b =  -5.66e+07  (-5.705e+07, -5.615e+07)
```

$\tau = 0.018\ \mu s$

Figure 11: $^3[\mathrm{Pt(pop\text{-}BF_2)^{4-}}]^*$ lifetime dependence on $[\mathrm{Co(bpy)_3^{2+}}]$

The behavior of the singlet was also investigated; data collection windows from 5 to 50 ns were utilized so as to record both the early- and late-times behavior with sufficient resolution. These decay traces as well as the fitting equations and calculated lifetimes are shown in Figure 12. The majority of the spectra were described well by a single-term exponential; however, others required the application of a second exponential term to acquire appropriate fitting equations. Lifetimes obtained from these biexponential fits are italicized in Figure 12. If one considers only the data sets which could be reasonably described by a simple exponential decay, the lifetime for $^1[Pt(pop\text{-}BF_2)^{4-}]^*$ with 4 μM $[Co(bpy)_3^{2+}]$ was nearly identical ($\tau \approx 1.65 - 1.73$ ns) to the unquenched τ_0 value of 1.67 – 1.70 ns. When $[Co(bpy)_3^{2+}]$ increased to 30 μM, the singlet lifetime decreased measurably to ≈ 1.55 ns. If the only quenching mechanism in action is static quenching, τ should equal τ_0. A possible explanation is that for $[Co(bpy)_3^{2+}] \lesssim 30$ μM, only static quenching is at work. When $[Co(bpy)_3^{2+}]$ increases beyond that, complex formation may no longer be favored as proscribed by K_S, equation (1). This could occur, for instance, if $[Co(bpy)_3^{2+}] \gg [Pt(pop\text{-}BF_2)^{4-}]$. If complex formation is not favored and uncomplexed quencher still remains in solution, that excess quencher could facilitate diffusional quenching.

While it is unlikely that quencher and fluorophore could diffuse over long distances in the span of less than two nanoseconds, it is possible to have quencher and fluorophore close enough to each other at the time of excitation to cause near-instantaneous quenching.[1] This "sphere of action"-type behavior implicates a more complex quenching mechanism involving different degrees of static and diffusional quenching depending on the quencher concentration. To fully deconvolute the behavior, more data are needed; a potential analytical scheme is presented in section 3.5. Repeating the experiments described in this section with a broader range of quencher concentrations would provide needed information about exactly when τ begins to deviate from τ_0. Furthermore, investigating the effects of temperature and solvent choice on the fluorophore-quencher interaction would allow the use of more accurate calculations that account for diffusional and static quenching behavior simultaneously.[1]

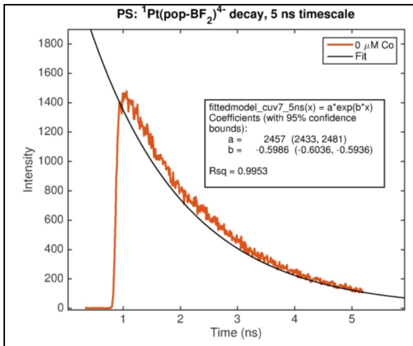

```
fittedmodel_cuv7_5ns(x) = a*exp(b*x)
Coefficients (with 95% confidence
bounds):
       a =       2457  (2433, 2481)
       b =    -0.5986  (-0.6036, -0.5936)

Rsq = 0.9953
```

$\tau_0 = 1.67$ ns

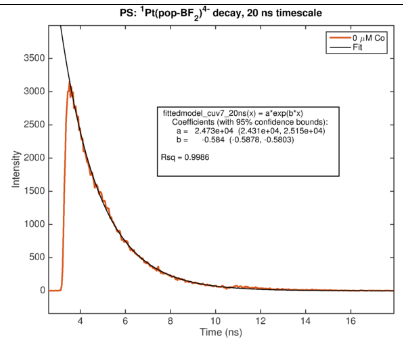

```
fittedmodel_cuv7_20ns(x) = a*exp(b*x)
    Coefficients (with 95% confidence bounds):
     a =   2.473e+04  (2.431e+04, 2.515e+04)
     b =      -0.584  (-0.5878, -0.5803)

Rsq = 0.9986
```

$\tau_0 = 1.71$ ns

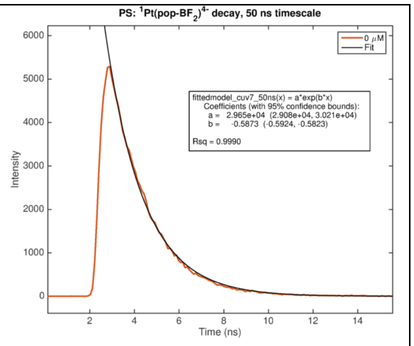

```
fittedmodel_cuv7_50ns(x) = a*exp(b*x)
    Coefficients (with 95% confidence bounds):
     a =   2.965e+04  (2.908e+04, 3.021e+04)
     b =     -0.5873  (-0.5924, -0.5823)

Rsq = 0.9990
```

$\tau_0 = 1.70$ ns

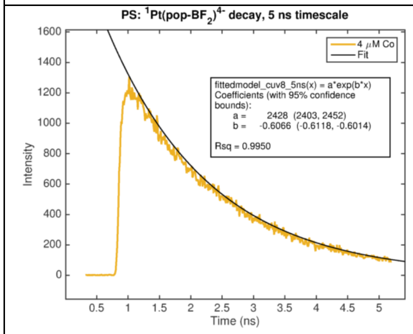

```
fittedmodel_cuv8_5ns(x) = a*exp(b*x)
Coefficients (with 95% confidence
bounds):
       a =       2428  (2403, 2452)
       b =    -0.6066  (-0.6118, -0.6014)

Rsq = 0.9950
```

$\tau = 1.65$ ns

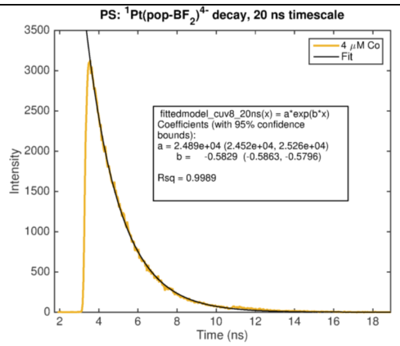

```
fittedmodel_cuv8_20ns(x) = a*exp(b*x)
Coefficients (with 95% confidence
bounds):
a = 2.489e+04 (2.452e+04, 2.526e+04)
       b =    -0.5829  (-0.5863, -0.5796)

Rsq = 0.9989
```

$\tau = 1.72$ ns

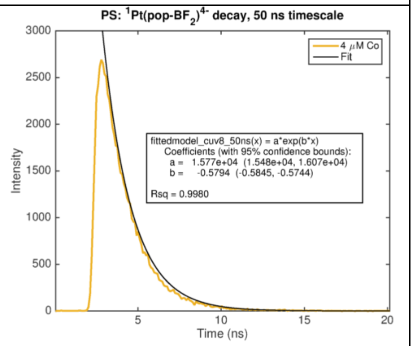

```
fittedmodel_cuv8_50ns(x) = a*exp(b*x)
    Coefficients (with 95% confidence bounds):
     a =   1.577e+04  (1.548e+04, 1.607e+04)
     b =     -0.5794  (-0.5845, -0.5744)

Rsq = 0.9980
```

$\tau = 1.73$ ns

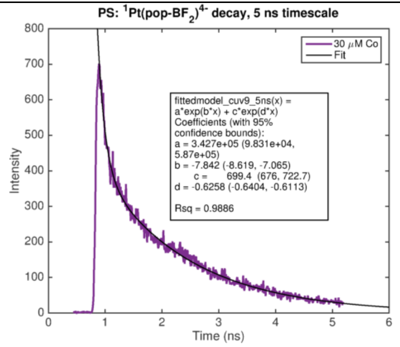

```
fittedmodel_cuv9_5ns(x) =
a*exp(b*x) + c*exp(d*x)
Coefficients (with 95%
confidence bounds):
a = 3.427e+05 (9.831e+04,
5.87e+05)
b = -7.842 (-8.619, -7.065)
      c =       699.4  (676, 722.7)
d = -0.6258 (-0.6404, -0.6113)

Rsq = 0.9886
```

$\tau_a = 1.60\ ns$

$\tau_b = 0.13\ ns$

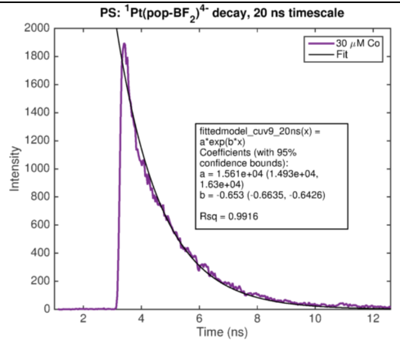

```
fittedmodel_cuv9_20ns(x) =
a*exp(b*x)
Coefficients (with 95%
confidence bounds):
a = 1.561e+04 (1.493e+04,
1.63e+04)
b = -0.653 (-0.6635, -0.6426)

Rsq = 0.9916
```

$\tau = 1.53$ ns

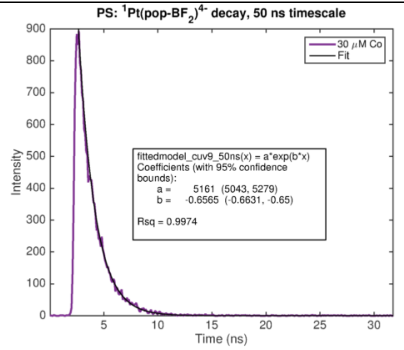

```
fittedmodel_cuv9_50ns(x) = a*exp(b*x)
Coefficients (with 95% confidence
bounds):
       a =       5161  (5043, 5279)
       b =    -0.6565  (-0.6631, -0.65)

Rsq = 0.9974
```

$\tau = 1.52$ ns

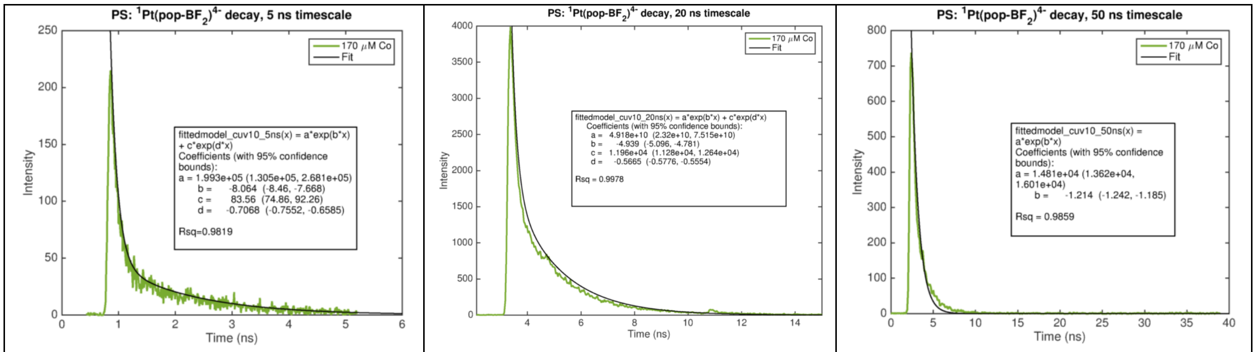

$\tau_a = 1.41\ ns$

$\tau_b = 0.12\ ns$

$\tau_a = 1.94\ ns$

$\tau_b = 0.22\ ns$

$\tau = 0.82$ ns

Figure 12: $^1[Pt(pop\text{-}BF_2)^{4-}]^*$ lifetime dependence on $[Co(bpy)^{2+}]$

Another possible contributing factor to the somewhat puzzling luminescence behavior is sample decomposition, which was unfortunately noted over the course of these laser experiments (Figure 13). The right-hand plot in Figure 13 shows the absorption maximum of $Pt(pop\text{-}BF_2)^{4-}$; decreases in absorption intensity are noted for all samples over the course of the experiment. The full trace on the left additionally shows significant changes in absorption below 300 nm, where bands for both $Pt(pop\text{-}BF_2)^{4-}$ and $Co(bpy)^{2+}$ typically present. The composition of the samples undoubtedly changed during the experiment; the effects of those changes on the luminescence properties are unknown.

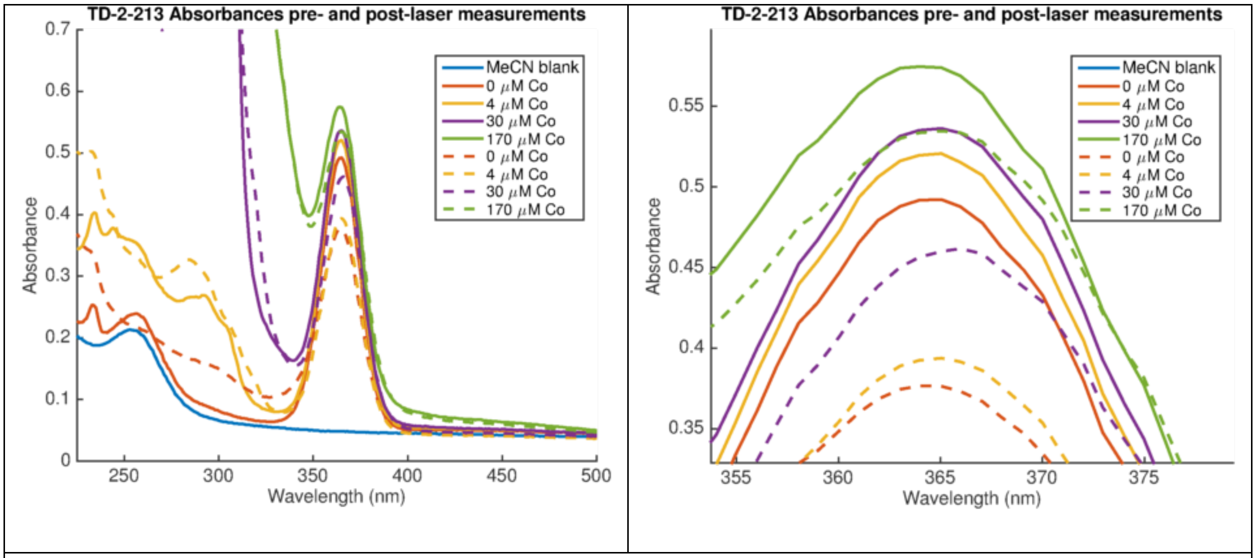

Figure 13: Absorbance spectra of samples before (solid line) and after (dashed line) laser experiments.

3.5 Conclusions

In some instances, a fluorophore may be quenched both by collision with a quencher molecule and by complex formation with the same quencher. Given the presented data collected for the quenching of $^1[Pt(pop\text{-}BF_2)^{4-}]^*$ and $^3[Pt(pop\text{-}BF_2)^{4-}]^*$ by $Co(bpy)_3^{2+}$ and the fact that neither purely diffusional nor purely static analytical techniques describe the behavior observed, it is likely that a more complex mechanism involving both static and dynamic quenching is at play. Such behavior is second-order in [Q], which would also account for the upward curvature observed for the plots of I_0/I vs [Q] presented in Figure 7 through Figure 10.

In these cases, a modified form of the Stern-Volmer equation may be applied:

$$\frac{F_0}{F} = (1 + K_D[Q])(1 + K_s[Q]) \tag{8}$$

As in the equations presented in section 3.1 and 3.2, K_D is the Stern-Volmer quenching constant ($K_D = k_q\tau_0$), K_S is the association constant for fluorophore-quencher complex formation, $[Q]$ is the concentration of quencher, and F_0/F is the ratio of unquenched luminescence intensity to the observed luminescence intensity at any quencher concentration $[Q]$. The dynamic part of the observed quenching may be determined via lifetime measurements:

$$\frac{\tau_0}{\tau} = 1 + K_D[Q] \qquad (9)$$

Combination of equations (8) and (9) yields the following relation:

$$\frac{F_0}{F} = \frac{\tau_0}{\tau_{[Q]}}(1 + K_S[Q]) \qquad (10)$$

The analysis put forward in equation (10) requires a complete set of steady-state and time-resolved quenching data for a single set of samples; lifetimes and steady-state intensities must be acquired that the exact same concentrations of Q. Given the decomposition issues consistently observed with Pt(pop-BF$_2$)$^{4-}$ over the course of time-resolved laser experiments, a complete set of data is not available at this time. That said, Pt(pop-BF$_2$)$^{4-}$ in the presence of amine-type quenchers (as presented in section 3.3) exhibits classic Stern-Volmer-type dynamic quenching behavior of the triplet state. Additional research in this area could lend valuable insight to the mechanism of combined static and dynamic quenching of both the singlet and triplet states of Pt(pop-BF$_2$)$^{4-}$ in the presence of metal complexes like Co(bpy)$_3^{2+}$.

3.6 Materials and methods

Unless otherwise noted, all reagents were obtained from Sigma-Aldrich and used without further purification; all water used was deionized. All manipulations involving Pt(pop-BF$_2$)$^{4-}$ were carried out with standard air-free techniques in an inert-atmosphere glovebox or utilizing a vacuum manifold. Solvents were dried using activated alumina columns according to Grubbs' method.[20] Anhydrous acetonitrile was stored over activated 3 Å molecular sieves; all other anhydrous solvents were stored over activated 4 Å molecular sieves.[21] Molecular sieves were activated by heating to 200 ºC under reduced pressure for 4 hours.

3.6.1 $[Co(bpy)_3](PF_6)_2$ [22,23]

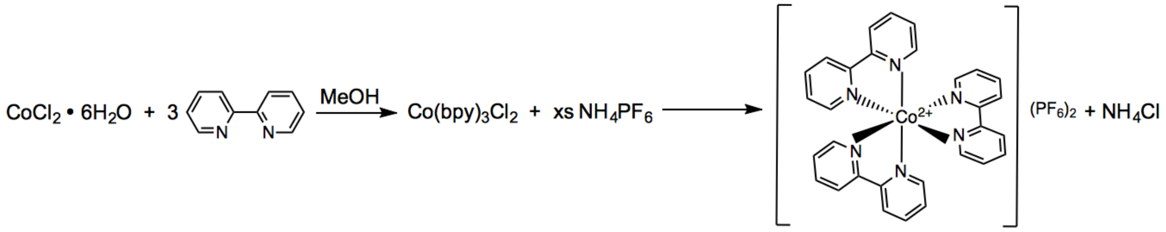

$Co(bpy)_3Cl_2$ was formed by mixing a solution of 3.27 g 2,2′-bipyridine in 100 mL methanol with a solution of 1.66 $CoCl_2 \bullet 6H_2O$ in 50 mL methanol and stirring for one hour. 11.4 g NH_4PF_6 was added to precipitate 8.3 g of a light yellow solid. This product was dissolved in 150 mL CH_2Cl_2 and filtered to remove ~ 2g residual NH_4Cl and NH_4PF_6 as a yellowish-white powder. The mother liquor was reduced in volume via rotary evaporation to yield shiny orange microcrystalline needles, which were rinsed with diethyl ether and dried under vacuum. Further purification may be achieved by recrystallization from acetone/methanol.

3.6.2 Steady-state quenching experiments

Steady-state emission spectra were recorded on a Jobin Yvon Spex Fluorolog-3-11. A 450-W xenon arc lamp was used as the excitation source with a single monochromator providing wavelength selection. Right-angle light emission was sorted using a single monochromator and fed into a Hamamatsu R928P photomultiplier tube with photon counting. Short and long pass filters were used where appropriate. Spectra were recorded on Datamax software.[2]

3.6.3 Time-resolved quenching experiments

To monitor singlet and triplet emission, samples were excited at 355 nm with 8-ns pulses from the third harmonic of a Q- switched Nd:YAG laser (Spectra-Physics Quanta-Ray PRO-Series) operating at 10 Hz. Emission wavelengths were selected using a double monochromator (Instruments SA DH-10) with 1 mm slits. Luminescence was detected with a photomultiplier tube (PMT, Hamamatsu R928). The PMT current was amplified and recorded with a transient digitizer (Tektronix DSA 602). Short- and long-pass filters were employed to remove scattered excitation light. Decay traces were averaged over 500 laser pulses. Instruments and electronics in this system were controlled by software written in LabVIEW (National Instruments). Data manipulation was performed and plotted using MATLAB R2015a (Mathworks, Inc.).[2]

REFERENCES

(1) Lakowicz, J. R. *Principles of Fluorescence Spectroscopy*; Springer US, 2006.

(2) Durrell, A. C.; Keller, G. E.; Lam, Y.-C.; Sykora, J.; Vlček, A.; Gray, H. B. *J. Am. Chem. Soc.* **2012**, *134*, 14201.

(3) Vogler, A.; Kunkely, H. *Angewandte Chemie International Edition in English* **1984**, *23*, 316.

(4) Alexander, K. A.; Bryan, S. A.; Dickson, M. K.; Hedden, D.; Roundhill, D. M.; Che, C. M.; Butler, L. G.; Gray, H. B. In *Inorganic Syntheses*; John Wiley & Sons, Inc.: 1986; Vol. 24, p 211.

(5) Che, C. M.; Butler, L. G.; Grunthaner, P. J.; Gray, H. B. *Inorg. Chem.* **1985**, *24*, 4662.

(6) Che, C. M.; Butler, L. G.; Gray, H. B. *J. Am. Chem. Soc.* **1981**, *103*, 7796.

(7) Che, C. M.; Butler, L. G.; Gray, H. B.; Crooks, R. M.; Woodruff, W. H. *J. Am. Chem. Soc.* **1983**, *105*, 5492.

(8) Stiegman, A. E.; Rice, S. F.; Gray, H. B.; Miskowski, V. M. *Inorg. Chem.* **1987**, *26*, 1112.

(9) Vlcek, A.; Gray, H. B. *J. Am. Chem. Soc.* **1987**, *109*, 286.

(10) Smith, D. C.; Gray, H. B. *Coord. Chem. Rev.* **1990**, *100*, 169.

(11) Sweeney, R. J.; Harvey, E. L.; Gray, H. B. *Coord. Chem. Rev.* **1990**, *105*, 23.

(12) Roundhill, D. M.; Gray, H. B.; Che, C. M. *Acc. Chem. Res.* **1989**, *22*, 55.

(13) Lam, Y.-C.; Darnton, T. Unpublished results.

(14) Harvey, E. L. Dissertation (Ph.D.), California Institute of Technology, 1990.

(15) Lam, Y.-C., Caltech, 2015.

(16) Fox, L. S.; Kozik, M.; Winkler, J. R.; Gray, H. B. *Science* **1990**, *247*, 1069.

(17) Marcus, R. A. *The Journal of Chemical Physics* **1956**, *24*, 966.

(18) Marcus, R. A. *J. Phys. Chem.* **1963**, *67*, 853.

(19) Darnton, T. V.; Hunter, B. M.; Hill, M. G.; Záliš, S.; Vlček, A.; Gray, H. B. *J. Am. Chem. Soc.* **2016**, *138*, 5699.

(20) Pangborn, A. B.; Giardello, M. A.; Grubbs, R. H.; Rosen, R. K.; Timmers, F. J. *Organometallics* **1996**, *15*, 1518.

(21) Armarego, W. L. F.; Chai, C. L. L. In *Purification of Laboratory Chemicals (Sixth Edition)*; Butterworth-Heinemann: Oxford, 2009, p 88.

(22) Hamann, T. W.; Gstrein, F.; Brunschwig, B. S.; Lewis, N. S. *J. Am. Chem. Soc.* **2005**, *127*, 13949.

(23) Feldt, S. M.; Gibson, E. A.; Gabrielsson, E.; Sun, L.; Boschloo, G.; Hagfeldt, A. *J. Am. Chem. Soc.* **2010**, *132*, 16714.

CHAPTER 4: PREPARATION AND CHARACTERIZATION OF $Pt(POP-BF_2)^{5-}$ AND $Pt(POP-BF_2)^{6-}$

Extensive studies of $Pt(pop)^{4-}$ have demonstrated that optical excitation of an electron populates a pσ orbital with bonding character[1], which strengthens the Pt-Pt interaction and causes a shortening of the Pt-Pt distance by 0.21-0.31 Å as determined by both X-ray and optical techniques.[2-4] Theoretical work performed by Lam in collaboration with Vlček and Záliš predicted an analogous bond shortening of 0.18 Å in $Pt(pop-BF_2)^{4-}$.[5] As in optical excitation, direct reduction of $Pt(pop-BF_2)^{4-}$ was expected to fill the pσ orbital, forming a weak Pt-Pt bond. While reversible electrochemical reduction of the parent compound $Pt(pop)^{4-}$ has never been reported, $Pt(pop)^{5-}$ has nevertheless been generated via pulse radiolysis in aqueous solution.[6,7] Given the lack of easily reduced –O—H···O— groups in $Pt(pop-BF_2)^{4-}$, reversible reduction seemed likely, and electrochemical studies were undertaken.

4.1 Electrochemical reductions

$Pt(pop-BF_2)^{4-}$ in acetonitrile (MeCN) undergoes one-electron reductions at $E_{1/2}$ = -1.68 V and E_p = -2.46 V vs Fc^+/Fc (Figure 1).[i] The first wave is chemically reversible and electrochemically quasireversible at a scan rate of 50 mV/s, as shown by the ΔE_p = 155 mV for the wave of interest vs ~100 mV for Fc^+/Fc under very similar conditions. The second wave is electrochemically irreversible and chemically reversible, indicating formation of a superreduced complex $Pt(pop-BF_2)^{6-}$ which is stable at least at 273 K (see 4.2). Scanning anodically, a 2-electron chemically

---

[i] Electro- and spectroelectrochemical data were collected in collaboration with Bryan M. Hunter and Michael G. Hill.

irreversible oxidation is observed at +0.94 V vs Fc$^+$/Fc. The full-range cyclic voltammogram is shown in Figure 2.

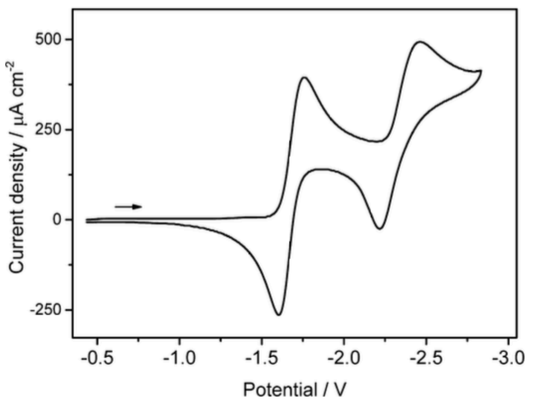	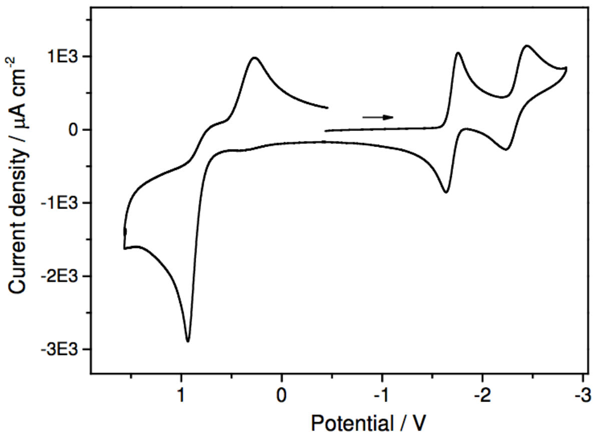
Figure 1: Cyclic voltammogram of Pt(pop-BF$_2$)$^{4-}$ in MeCN containing 0.1 M tetrabutylammonium hexafluorophosphate (Bu$_4$NPF$_6$) at 273 K. Potentials vs Fc$^+$/Fc; scan rate of 50 mV/s.	Figure 2: Full-range cyclic voltammogram of Pt(pop-BF2)4- in MeCN containing 0.1 M (Bu4NPF6) at 273 K. Potentials vs Fc+/Fc; scan rate of 200 mV/s.

The first reduction of Pt(pop)$^{4-}$ has been estimated from reductive quenching kinetics to be approximately -1.8 V, as compared to the -1.68 V obtained for Pt(pop-BF$_2$)$^{4-}$.[8] This difference in potentials is likely attributable to the strong electron-withdrawing effects of the BF$_2$ groups, which may be transmitted to the metal atoms by delocalization of the pσ orbital over the phosphorous atoms acting as donors to the Pt-Pt unit.[9]

Furthermore, potentials for the excited state redox couples can be estimated at 1.57 V for ^{1}[Pt(pop-BF$_2$)$^{4-/5-}$]* and 0.86 V for ^{3}[Pt(pop-BF$_2$)$^{4-/5-}$]* (both versus Fc$^+$/Fc) using spectroscopically determined excited-state energies;[10] continuation of the work described in Chapter 3 could offer further insight into these values.

4.2 Optical properties

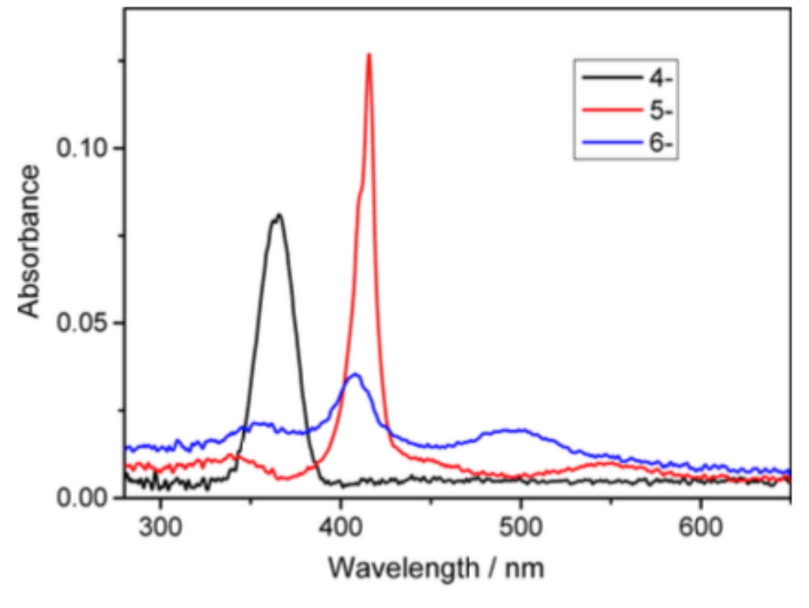

Figure 3: UV-Vis absorption spectra of Pt(pop-BF$_2$)$^{4-}$ (black) and in situ spectroelectrochemically produced Pt(pop-BF$_2$)$^{5-}$ and Pt(pop-BF$_2$)$^{6-}$ (blue; contains ~20% of Pt(pop-BF$_2$)$^{5-}$).

UV-Vis spectroelectrochemistry in acetonitrile at 273 K carried out at the potential of the first reduction showed a sharp decrease in intensity of the characteristic 365 nm absorption band of Pt(pop-BF$_2$)$^{4-}$. This decrease was accompanied by the rise of a sharp band at 416 nm with shoulders at ~411 nm and 450 nm, as well as broad weak bands at ~550 and 338 nm. All of these bands are attributable to Pt(pop-BF$_2$)$^{5-}$ (Figure *3*). Upon anodically switching the

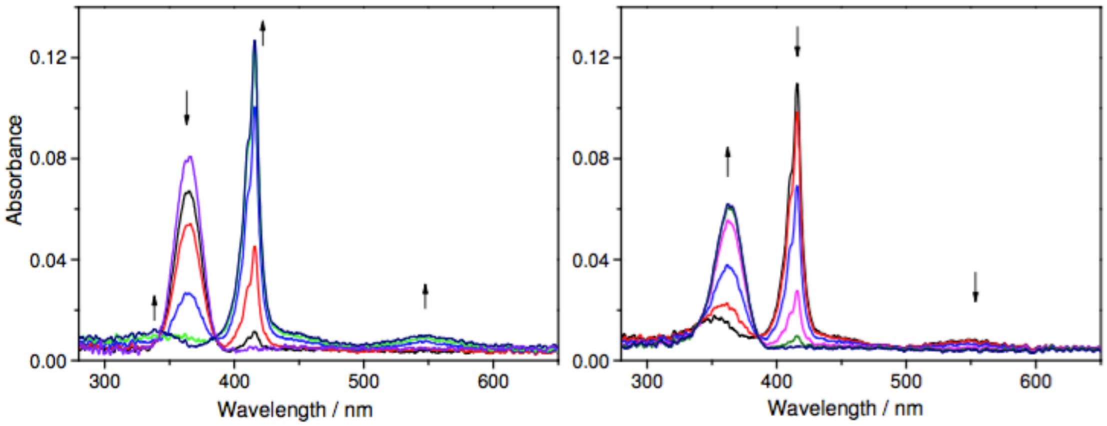

Figure 4: UV-Vis spectra monitored in the course of the first Pt(pop-BF$_2$)$^{4-}$ reduction to Pt(pop-BF$_2$)$^{5-}$ (left) followed by product reoxidation to reform Pt(pop-BF$_2$)$^{4-}$ (right).

potential, the parent complex Pt(pop-BF$_2$)$^{4-}$ is nearly quantitatively recovered (Figure 4). Further reduction at more negative potentials yields a spectrum with distinct features at 356, 408, and 496 nm. Spectra measured during the second reduction indicate an isosbestic point, pointing to conversion to the "superreduced" species Pt(pop-BF$_2$)$^{6-}$ (Figure 5). At low temperature (273 K), reoxidation of this species eventually recovered Pt(pop-BF$_2$)$^{5-}$, while at room temperature a different, unidentified species absorbing at 350 nm is formed upon reoxidation. In both Figure 4 and Figure 5, the slight decrease in absorption intensity upon recovery of the oxidized product may be attributed to diffusion of the compound out of the spectroscopically probed region. Finally, the experimental spectra of both the reduced and superreduced species match the predicted spectra calculated by TD-DFT, supporting the assignments as Pt(pop-BF$_2$)$^{5-}$ and Pt(pop-BF$_2$)$^{6-}$, respectively (Figure 6).[ii]

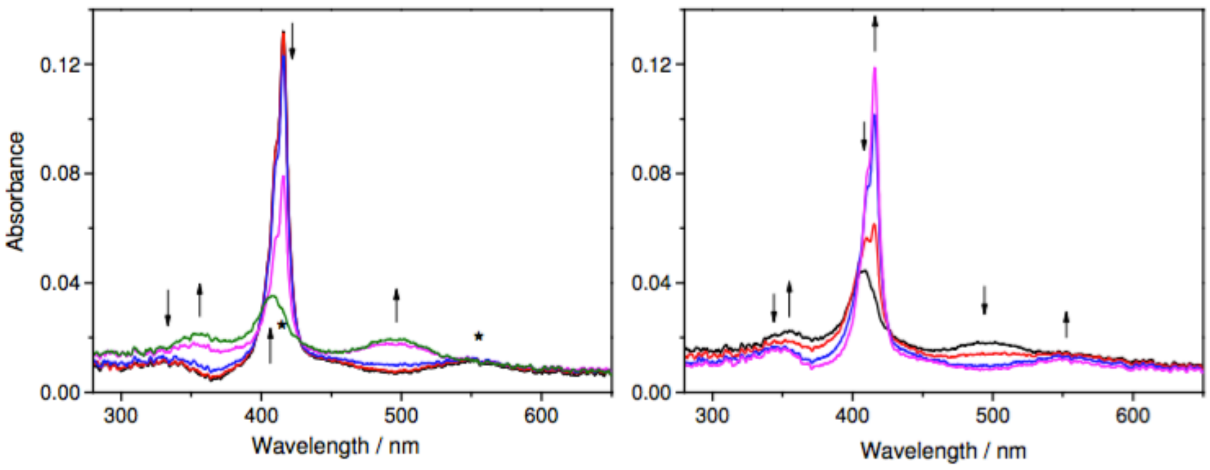

Figure 5: UV-Vis absorption spectra collected in the course of the second reduction to form Pt(pop-BF$_2$)$^{6-}$ (left), followed by reoxidation to form Pt(pop-BF$_2$)$^{5-}$ (right).

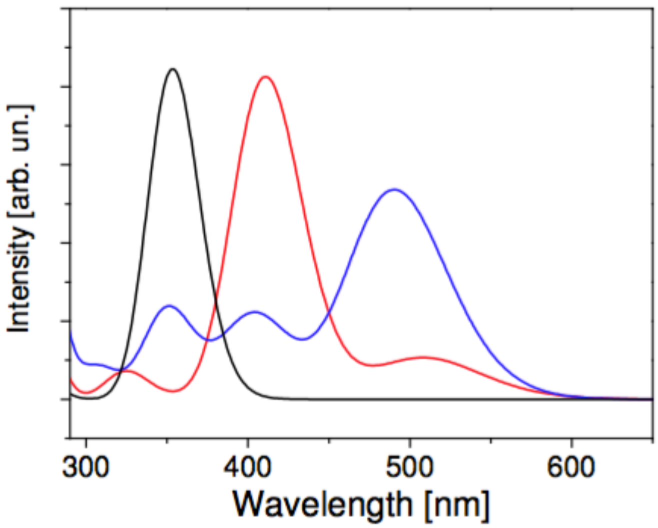

Figure 6: TD-DFT simulated UV-vis absorption spectra of Pt(pop-BF_2)$^{n-}$ (n = 4 (black), 5 (red) and 6 (blue). The same FWHM of 3000 cm^{-1} was assumed for all transitions. TD- DFT (PBE0/PCM-MeCN).[ii]

[ii] Theoretical simulations contributed by S. Záliš and A. Vlček.

4.3 Electron paramagnetic resonance (EPR) characterization

In addition to being generated spectroelectrochemically, Pt(pop-BF$_2$)$^{5-}$ may also be accessed via reduction in acetonitrile with Na/Hg. Reaction of a bright yellow-green acetonitrile solution of Pt(pop-BF$_2$)$^{4-}$ with Na/Hg affords an immediate color change to a red, which deepens in color over ~ 20 min to form a deep wine-red solution. The EPR spectrum of this solution was measured after freezing to 77 K; the experimental and simulated spectra and fitting parameters are shown in Figure 7. The spectrum is characteristic of a spin-doublet state with an axial spin distribution ($g_2 \cong g_3 \neq g_1$). The hyperfine splitting constants due to the two ^{195}Pt nuclei are similar, indicating a nearly symmetrical spin density. Finally, the *g* values are similar to those previously reported for Pt(II) complexes with radical-anion ligands.[11,12] This contrasts with "platinum blue"-type species

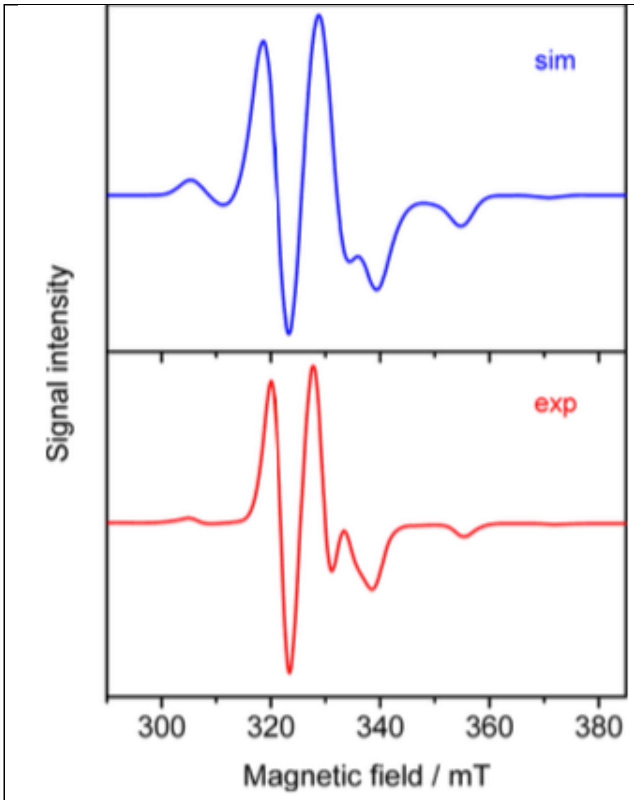

g_1	1.98
g_2	2.03
g_3	2.04
A$_1$(Pt)	900
A$_2$(Pt)	550
A$_3$(Pt)	550
A$_1$(Pt′)	900
A$_2$(Pt′)	500
A$_3$(Pt′)	350

Coupling constants reported in MHz.

Figure 7: Simulated (top) and experimental (bottom) EPR spectra of Pt(pop-BF$_2$)$^{5-}$ and simulation parameters.

in which the unpaired electron is delocalized over four Pt atoms in a molecular orbital with predominantly 5*d* character; such compounds also exhibit axial EPR spectra, but with much larger *g* values in addition to pronounced anisotropy.[13,14] Finally, still larger *g* values have been reported $\mathrm{Pt^I}$ d^9 sites.[15] This suggests that the unpaired electron in Pt(pop-BF_2)$^{5-}$ is delocalized over the two Pt atoms and the ligands in a molecular orbital of 6*p* character.

At room temperature, the EPR-active red solution containing Pt(pop-BF_2)$^{5-}$ decomposes over the course of ~24 hours; the solution turns purple and then brown and the intensity of the EPR signal decreases to a fraction of its original value (Figure *8*). Efforts to isolate Pt(pop-BF_2)$^{5-}$ chemically were unsuccessful, instead yielding yellow-green Pt(pop-BF_2)$^{4-}$ crystals from a red or purple supernatant under a variety of reaction conditions.

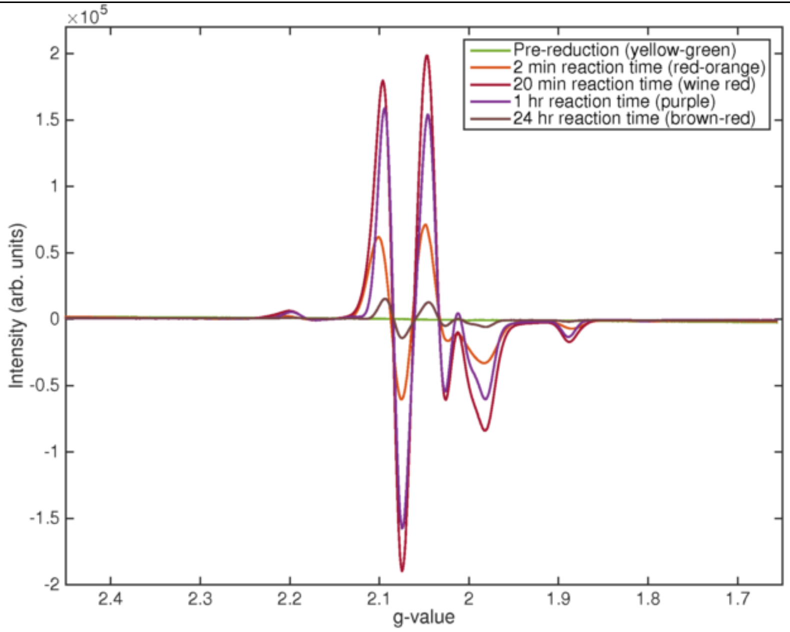

Figure 8: Chemical reduction of Pt(pop-BF_2)$^{4-}$ with Na/Hg monitored by EPR over a 24-hour period.

4.4 Electronic structures

The spectroscopic changes recorded in the course of the reduction together with DFT calculations point to successive filling of the pσ molecular orbital. The strong, sharp dσ*⟶pσ band is the lowest-energy feature in the spectrum of the parent complex. It also is present in the reduced (5-) species with a $(d\sigma^*)^2(p\sigma)^1$ configuration, but it is preceded in energy by a weaker band attributable to pσ excitation. The UV−vis spectral pattern changes completely in the superreduced complex, as the pσ orbital becomes fully occupied. The dσ*⟶pσ transition vanishes, and the spectrum exhibits a series of transitions from the pσ HOMO to higher unoccupied orbitals.

Successive filling of the pσ orbital formally generates a Pt−Pt σ bond without changing the Pt $5d^8$ electronic configuration, making $Pt(pop\text{-}BF_2)^{6-}$ a very rare $6p^2$ σ-bonded binuclear complex. The DFT-calculated Mayer−Mulliken bond orders[iii] show strengthening of the Pt−Pt bonding interaction upon reduction, whereby the bond order increases about 2-fold on going from the 4− parent (0.17) to the 6− superreduced complex (0.34).[9] While significant, the Pt−Pt bonding in $Pt(pop\text{-}BF_2)^{6-}$ is far from a full σ-bond, as the Pt−Pt bonding interaction is limited by several structural and electronic factors. The rigid pop-BF_2 ligand cage does not allow the metal−metal distance to shorten very much, disfavoring effective orbital overlap; the $(5d\sigma)^2(5d\sigma^*)^2(6p\sigma)^2$ configuration places six σ electrons in spatial proximity with one another, producing repulsive electronic congestion along the Pt−Pt axis; and the pσ molecular orbital is only 59% $6p_z$ in character, being delocalized over the Pt−P bonds. Accordingly, Pt−P bond orders

---

[iii] Theoretical simulations contributed by S. Záliš and A. Vlček; further details available in reference 9.

also gradually increase upon reduction. The EPR spectrum of Pt(pop-BF$_2$)$^{5-}$ confirms the delocalized nature of the singly occupied 6pσ molecular orbital, showing axial spin density distribution (see section 4.3).

The Pt–Pt distance was calculated to shorten by 0.08 and 0.06 Å upon the first and second reductions, respectively, while the calculated Pt–Pt stretching frequency ν(Pt–Pt) increases from 128 cm^{-1} in the parent complex to 146 (5–) and 170 cm^{-1} (6–).[9] The reduced species essentially keeps the high symmetry of the parent complex, which is manifested both by the calculation and by the EPR spectrum. The most stable conformer of Pt(pop-BF$_2$)$^{6-}$ shows a small asymmetry, both between the two Pt centers and within each PtP$_4$ unit, where one pair of trans Pt–P bonds is shorter than the other. The HOMO also is distributed slightly asymmetrically, perhaps due to the "frustrated" pσ interaction mentioned above. Nevertheless, the calculated natural charges at the two Pt atoms differ by only 0.035 e$^-$, in accordance with the $(5d\sigma)^2(5d\sigma^*)^2(6p\sigma)^2$ configuration. This behavior contrasts with that of doubly reduced 5d^8-5d^8 Ir$_2$(dimen)$_4$$^{2+}$ (dimen =1,8-diisocyano-p-menthane) that adopts a d^8–d^{10} (Ir^{II}–Ir^0) mixed-valence configuration. In this case, one iridium center maintains a square planar local geometry, while the other distorts toward tetrahedral.[16] Such a distortion avoids the congested $(5d\sigma)^2(5d\sigma^*)^2(6p\sigma)^2$ electronic structure, and its stabilizing effect is manifested by the much smaller difference between the first and second reduction potentials of Ir$_2$(dimen)$_4$$^{2+}$ (0.19 V), as compared to Pt(pop-BF$_2$) (~0.7 V). Such a distortion toward a mixed-valence structure is possible in the Ir$_2$(dimen)$_4$$^{2+}$ case because of the structural flexibility of the dimen bridge,[17] whereas the rigid pop-BF_2 ligand cage of Pt(pop-BF_2)$^{6-}$ enforces a nearly symmetrical structure, producing the unusual partial 6pσ metal–metal bond.

4.5 Materials and methods

Unless otherwise noted, all reagents were obtained from Sigma-Aldrich and used without further purification; all water used was deionized. All manipulations involving Pt(pop-BF_2) were carried out with standard air-free techniques in an inert-atmosphere glovebox or utilizing a vacuum manifold. Solvents were dried using activated alumina columns according to Grubbs' method.[18] Anhydrous acetonitrile (Fisher) was stored over activated 3 Å molecular sieves; all other anhydrous solvents were stored over activated 4 Å molecular sieves.[19] Molecular sieves were activated by heating to 200 ºC under reduced pressure for 4 hours.

4.5.1 Electrochemical experiments

All electrochemical experiments were performed with a CH Instruments model 650A electrochemical analyzer. Bu_4NPF_6 (Fluka) was used as received. Electrolyte solutions were prepared and stored over activated alumina and 4 Å molecular sieves. Cyclic voltammetry (CV) at ambient temperature was measured in a three-electrode configuration consisting of a highly polished glassy-carbon-disk working electrode (A = 0.07 cm^2), a Pt wire auxiliary electrode, and a 1.0 M KCl AgCl/Ag reference electrode, separated by a modified Luggin capillary. Low temperature CV was carried out using a nonisothermal cell configuration, in which the reference electrode was held at ambient temperature, separated from the working compartment by a long glass tube filled with electrolyte, and connected by a Luggin capillary. The temperature was monitored by a thermocouple placed in the working compartment. The ferrocenium/ferrocene couple has $E^{0\prime}$ = 0.434 V, measured at identical experimental conditions.

4.5.2 *Spectroelectrochemical experiments*

Thin-layer spectroelectrochemistry was carried out in a specular-reflectance mode using a modified IR cell. An Ocean Optics UV−vis light source (DH-2000) and spectrometer (USB2000) were connected to the Y-arms of a bifurcated fiber-optic cable; the end of the cable was connected through a lens housing containing a semispherical collimating lens to the front-face window of the spectroelectrochemical cell at a 90° angle. A drop of mineral oil between the fiber optic and front-face quartz window of the cell ensured refractive-index matching. Spectra were not corrected for front-face reflection. The error in intensity at an absorbance of 0.5 is less than 1%. The glassy- carbon working electrode of the spectroelectrochemical cell was attached with silver epoxy to a brass cooling tube, connected to a circulating variable-temperature bath.

4.5.3 *EPR experiments*

EPR spectra were recorded on a Bruker EMS spectrometer at 9.39 GHz. Samples at ~10 mM concentration were prepared by reduction with Na/Hg in dry acetonitrile under an N_2 atmosphere and frozen with liquid nitrogen prior to the measurements. Spectral simulations were performed with MATLAB using the EasySpin MATLAB toolbox (version 4.5.5). Simulation parameters obtained include: g = [2.04, 2.03,1.98]; HStrain=[180,120,100]MHz; A_{Pt1}=[550,550,900] MHz; A_{Pt2} = [350, 500, 900] MHz.

REFERENCES

(1) Roundhill, D. M.; Gray, H. B.; Che, C. M. *Acc. Chem. Res.* **1989**, *22*, 55.

(2) Che, C. M.; Butler, L. G.; Gray, H. B.; Crooks, R. M.; Woodruff, W. H. *J. Am. Chem. Soc.* **1983**, *105*, 5492.

(3) van der Veen, R. M.; Milne, C. J.; El Nahhas, A.; Lima, F. A.; Pham, V. T.; Best, J.; Weinstein, J. A.; Borca, C. N.; Abela, R.; Bressler, C.; Chergui, M. *Angew. Chem., Int. Ed.* **2009**, *48*, 2711.

(4) Christensen, M.; Haldrup, K.; Bechgaard, K.; Feidenhans'l, R.; Kong, Q.; Cammarata, M.; Russo, M. L.; Wulff, M.; Harrit, N.; Nielsen, M. M. *J. Am. Chem. Soc.* **2008**, *131*, 502.

(5) Záliš, S.; Lam, Y.-C.; Gray, H. B.; Vlček, A. *Inorg. Chem.* **2015**, *54*, 3491.

(6) Bryan, S. A.; Schmehl, R. H.; Roundhill, D. M. *J. Am. Chem. Soc.* **1986**, *108*, 5408.

(7) Che, C. M.; Atherton, S. J.; Butler, L. G.; Gray, H. B. *J. Am. Chem. Soc.* **1984**, *106*, 5143.

(8) Heuer, W. B.; Totten, M. D.; Rodman, G. S.; Hebert, E. J.; Tracy, H. J.; Nagle, J. K. *J. Am. Chem. Soc.* **1984**, *106*, 1163.

(9) Darnton, T. V.; Hunter, B. M.; Hill, M. G.; Záliš, S.; Vlček, A.; Gray, H. B. *J. Am. Chem. Soc.* **2016**, *138*, 5699.

(10) Hofbeck, T.; Lam, Y. C.; Kalbáč, M.; Záliš, S.; Vlček, A.; Yersin, H. *Inorg. Chem.* **2016**, *55*, 2441.

(11) Braterman, P. S.; Song, J. I.; Wimmer, F. M.; Wimmer, S.; Kaim, W.; Klein, A.; Peacock, R. D. *Inorg. Chem.* **1992**, *31*, 5084.

(12) Braterman, P. S.; Song, J. I.; Vogler, C.; Kaim, W. *Inorg. Chem.* **1992**, *31*, 222.

(13) Matsunami, J.; Urata, H.; Matsumoto, K. *Inorg. Chem.* **1995**, *34*, 202.

(14) Hirani, B.; Li, J.; Djurovich, P. I.; Yousufuddin, M.; Oxgaard, J.; Persson, P.; Wilson, S. R.; Bau, R.; Goddard, W. A.; Thompson, M. E. *Inorg. Chem.* **2007**, *46*, 3865.

(15) Schmauke, T.; Einar Möller, E.; Roduner, E. *Chem. Commun.* **1998**, 2589.

(16) Hill, M. G.; Sykes, A. G.; Mann, K. R. *Inorg. Chem.* **1993**, *32*, 783.

(17) Hunter, B. M.; Villahermosa, R. M.; Exstrom, C. L.; Hill, M. G.; Mann, K. R.; Gray, H. B. *Inorg. Chem.* **2012**, *51*, 6898.

(18) Pangborn, A. B.; Giardello, M. A.; Grubbs, R. H.; Rosen, R. K.; Timmers, F. J. *Organometallics* **1996**, *15*, 1518.

(19) Armarego, W. L. F.; Chai, C. L. L. In *Purification of Laboratory Chemicals (Sixth Edition)*; Butterworth-Heinemann: Oxford, 2009, p 88.

APPENDIX 1: MATLAB PROGRAMS

When experiments call for the repeated analysis of large quantities of data, it is essential to have reliable scripts and programs on hand to automatically plot and analyze data. The programs and scripts developed by researchers are usually written to be precisely applicable to the exact experiments they are doing, making them an extraordinary resource for future researchers in the group. Unfortunately, these resources are often lost, either because digital copies are not archived or because the programs lack the appropriate annotations and/or explanations to make them useful to future researchers.

In this appendix, a number of MATLAB functions and/or scripts created and/or expanded upon by the author are presented and explained. These files have also been archived on the Gray Group computer in 327 Noyes.

A.1 Fluorimeter data

The MATLAB script 'import_XLS.m' is a script to import and plot files from the Gray Group fluorimeter in BI 018D. After using the fluorimeter's software to export steady-state luminescence data as Excel files, this script will plot selected files in order in a single plot.

`import_XLS.m`

```
%Program to import .XLS files from the fluorimeter in BI 018D
%Written by Tania V. Darnton on May 20, 2013, borrowing components from
%Oliver Shafaat's import_DX script and James McKone's import_CV script
%
%This function imports multiple fluorimeter data files as a set of 2 column
%vectors labeled "Wavelength" and "Absorbance" and plots them.

Legend = {}; %This needs to stay here or else it doesn't reset the Legend
variable when you run the program again and again, it just appends the new
file names on
%Call getfileinfo first
[filename,pathname,filterindex]=uigetfile('*.*','MultiSelect','on');



%If a single file was selected, the output of filename is stored as char
```

```
%array.  It needs to be converted to a cell in order to ensure output to
%a single format.
%--------------
if isequal(filename,0)
       disp('User pressed cancel');
       return;
end

if ischar(class(filename));
    filename=cellstr(filename);
end
%---------------



 ttl = input('Give your plot a title!  ','s');

for j=1:length(filename) %function will step through each filename
%'char' command changes the pathname and filename entries from cell to
string class
    file = [char(pathname),char(filename(j))];

% Analyze the file to be opened in order to check its extension
    [pathstr, name, ext] = fileparts(file);



% Use STRCMP to compare EXT to '.xls'. If same, STRCMP returns 1.
    if strcmp(ext, '.xls');
        C = xlsread(file);
        Wavelength = C(2:end,1);
        Absorbance = C(2:end,2);
    else error('Error: File is not .xls');
    end;
leg = input('Give the names of your data sets in order  ', 's');
    Legend = strvcat(Legend, leg);
%This will prompt you for the name of the data you just chose
%This appends names of data onto each other for later use in the legend.
% 'Hold all' command causes each plot to be a different color
hold all
plot(Wavelength,Absorbance,'LineWidth',2,'DisplayName',name);
set(gca,'FontSize',14);
xlabel('Wavelength (nm)','FontSize',14);
ylabel('Intensity','FontSize',14);
title(ttl,'FontSize',14);
legend(Legend,'Location', 'Best');
    hold off

end
disp('Plot completed!')
```

A.2 UV-Vis data plotter

The Cary 50 UV-Vis spectrometer in Noyes 327 exports all the data taken in a session in a single Excel file in which the first set of wavelength and absorbance data taken are in columns A and B, the second set are in columns C and D, etc. Given such a file, the script ‘import_CSV.m’ prompts the user for a vector denoting the columns containing the wavelength data for the desired sets. For example, if the user wished to plot the first and third spectra recorded by the Cary, he or she would input the vector [1 5], to indicate that the desired data sets were to be found in columns A and B and columns E and F (columns C and D would contain the wavelength and absorption data for the undesired second spectrum recorded). The script then plots the data sets and allows for adjustment of the axes and normalization of the intensities.[i]

`import_CSV.m`

```
%Program to import .CSV files from the Cary 50 UV-Vis in Noyes
%Written by Tania V. Darnton on June 13, 2013
%
%This function imports a UV-Vis data file as sets of 2 column
%vectors labelled "Wavelength" and "Absorbance" and plots them.
%import_CSV.m

Legend = {}; %This needs to stay here or else it doesn't reset the Legend
variable when you run the program again and again, it just appends the new
file names on
%Call getfileinfo first
[filename,pathname,filterindex]=uigetfile('*.*','MultiSelect','on');


%If a single file was selected, the output of filename is stored as char
%array.  It needs to be converted to a cell in order to ensure output to
%a single format.
%---------------
if isequal(filename,0)
        disp('User pressed cancel.');
        return;
end

if ischar(class(filename));
```

---

[i] These portions of the code were originally written by Oliver Shafaat in his script ‘DXreader.m’

```
    filename=cellstr(filename);
end
%----------------



 ttl = input('Give your plot a title!   ','s');
 %This is not strictly necessary, but I find it helpful as a reminder to
myself because then I know
 %what the length of the vector "wavelengths" should be
 numplots = input('How many data sets do you want to import today?   ');
 wavelengths = input('What columns do your data sets start in? \n Input your
answer as a vector, e.g. [a b c]   ');
 absorbances = wavelengths + 1;
%'char' command changes the pathname and filename entries from cell to
string class
    file = [char(pathname),char(filename)];

% Analyze the file to be opened in order to check its extension
    [pathstr, name, ext] = fileparts(file);

% Open the file.  If file is not opened, FOPEN returns -1.
% Test to make sure file opened correctly.

fid = fopen(file);
if fid==-1
  error('File not found or permission denied.');
end;
% Use STRCMP to compare EXT to '.csv'. If same, STRCMP returns 1.
    if strcmp(ext, '.csv');
        %Snoop the number of commas in one line of the data to see how many
        %columns of data there are
        headertest = textscan(fid, '%s', 1, 'HeaderLines', 20);
        commaindex = strfind(headertest{1},',');
        numcommas = length(commaindex{1});

        %create a string of "%f" such that the number of "%f"s equals the
        %number of data columns there are in the file
        f = repmat('%f ',1,numcommas);

        %must open file again to reset the position of the cursor
        fid2 = fopen(file);
        if fid2==-1
        error('File not found or permission denied.');
        end;

        %Import the entire data file using a comma as the delimiter and
        %skipping the two header lines
        C = textscan(fid2, f, 'Delimiter', ',', 'HeaderLines', 2,
'EmptyValue', 0, 'EndOfLine', '\r\n');

    else error('File is not .csv');
    end;

Normalize = input('Do you want to normalize your data over the selected
wavelength? (y/n)','s');
```

```
for j=1:numplots %Performs these tasks for each data set that you want to
graph

        Wavelength = C{wavelengths(j)};
        Absorbance_temp = C{absorbances(j)};
        if Normalize == 'y'
            minval = min(Absorbance_temp);
            maxval = max(Absorbance_temp);
            norm_abs = (Absorbance_temp-minval)/(maxval-minval);
            Absorbance = norm_abs;
        else Absorbance = Absorbance_temp;
        end

%Prompt for the names of the data to go in the legend
leg = input('Give the names of your data sets in order  ', 's');

%This appends names of data onto each other for later use in the legend.
    Legend = strvcat(Legend, leg);

% 'Hold all' command causes each plot to be a different color
hold all
plot(Wavelength,Absorbance,'LineWidth',2,'DisplayName',name);
set(gca,'FontSize',14);
xlabel('Wavelength (nm)','FontSize',14);
if Normalize == 'y'
    ylabel('Normalized Absorbance','FontSize',14)
else ylabel('Absorbance','FontSize',14);
end
title(ttl,'FontSize',14);
legend(Legend,'Location', 'Best');
    hold off

end

AxisAdj = input('Do you want to look at a specific wavelength range? (y/n)',
's');

while AxisAdj == 'y'
    minlambda = input('What do you want your minimum wavelength to be (in
nm)?');
    maxlambda = input('What do you want your maximum wavelength to be (in
nm)?');
    set(gca, 'Xlim', [minlambda maxlambda]);
    AxisAdj = input('Do you want to change the wavelength range again?
(y/n)', 's');
end

disp('Plot completed!')
```

A.3 Fluorimeter data importer

Given the .XLS fluorimeter file type described in A.1, the function ‘extractxls’ takes user-defined variable names to create matrix variables in the workspace representing the wavelength and intensity data recorded by the fluorimeter. For example, the MATLAB input ‘`[x,y]=extractxls;`’ will open a window for the user to select a fluorimeter data output file and will then create a matrix ‘`x`’ with the data set’s wavelengths and a matrix ‘`y`’ with the accompanying intensity data. This data will then be plotted and the created matrix variables can be saved or called for use in further analyses.

extractxls

```
function[t,y]=extractxls()
[filename,pathname,filterindex]=uigetfile('*.*','MultiSelect','off');
M = xlsread(filename);
t=M(:,1);
y=M(:,2);
plot(t,y)
```

A.4 UV-Vis data importer

Given the file type described in A.2, the function ‘extractcsv’ takes user-defined variable names and a user-defined data location within the Excel file to create matrix variables in the workspace representing the wavelength and absorbance intensity recorded by the spectrometer. For example, the MATLAB input ‘`[x,y]=extractcsv(1);`’ will open a window for the user to select a UV-Vis data output file and will then create a matrix ‘`x`’ with the wavelength data from Column A of that file and a matrix ‘`y`’ with the accompanying absorbance data from Column B of that file. The created matrix variables can be saved or called for use in further analyses.

extractcsv(c)

```
function [ x,y ] = extractcsv( c )
%extract_csv Summary of this function goes here
%
[filename,pathname,filterindex]=uigetfile('*.csv');


%If a single file was selected, the output of filename is stored as char
%array.  It needs to be converted to a cell in order to ensure output to
%a single format.
%---------------
if isequal(filename,0)
       disp('User pressed cancel or file not found');
       return;
end

if ischar(class(filename));
    filename=cellstr(filename);
end
%----------------

 wavelengths = c;
 absorbances = wavelengths + 1;
%'char' command changes the pathname and filename entries from cell to
string class
    file = [char(pathname),char(filename)];

% Analyze the file to be opened in order to check its extension
    [pathstr, name, ext] = fileparts(file);

% Open the file.  If file is not opened, FOPEN returns -1.
% Test to make sure file opened correctly.

fid = fopen(file);
if fid==-1
  error('File not found or permission denied.');
end;
% Use STRCMP to compare EXT to '.csv'. If same, STRCMP returns 1.
    if strcmp(ext, '.csv');
        %Snoop the number of commas in one line of the data to see how many
        %columns of data there are
        headertest = textscan(fid, '%s', 1, 'HeaderLines', 20);
        commaindex = strfind(headertest{1},',');
        numcommas = length(commaindex{1});

        %create a string of "%f" such that the number of "%f"s equals the
        %number of data columns there are in the file
        f = repmat('%f ',1,numcommas);

        %must open file again to reset the position of the cursor
        fid2 = fopen(file);
        if fid2==-1
        error('File not found or permission denied.');
        end;

        %Import the entire data file using a comma as the delimiter and
```

```
        %skipping the two header lines
        C = textscan(fid2, f, 'Delimiter', ',', 'HeaderLines', 2,
'EmptyValue', 0, 'EndOfLine', '\r\n');

    else error('File not .csv');
    end;

        x = C{wavelengths};
        y = C{absorbances};

end
```

A.5 Quantum yield calculations

A.5.1 Fluorimeter intensity integration

Given a set of fluorimetry data in matrix form (as might be output by the code from section A.3), the function ‘fluorointeg’ calculates and reports the area under the entire plot. For example, the MATLAB input ‘`a=fluorointeg[x,y];`’ will calculate the area under the wavelength vs intensity plot created by `x` and `y` and store that value to the variable `a`.

```
fluorointeg(x,y)
```

```
function [area] = fluorointeg(x,y)
%fluorointeg.m
%Written by Tania Darnton on March 17, 2014
%This is a function that will take a set of fluorimetry data in matrix form
%and calculate the area under the curve.
xprime=x(2:end);
yprime=y(2:end);
yzero=max(yprime,0);
area = trapz(xprime,yzero);
fprintf('\n The area under the curve is %s. \n',area)
end
```

A.5.2 Fluorimeter intensity integration: singlet vs triplet

In the case of Pt(pop-BF_2)$^{4-}$, it is often useful to know the relative areas of the singlet and triplet emissions in a set of fluorimetry data. The function ‘fluorointegpartial’ assumes that the singlet emission has reached zero intensity by the 77th value in the matrix; for a scan of Pt(pop-BF_2)$^{4-}$

excited at 355 nm and observed from 375 to 650 nm, this is true. Inputs for ‘fluorointegpartial’ are analogous to those of ‘fluorointeg’.

```
fluorointegpartial(x,y)
```

```
function [area] = fluorointegpartial(x,y)
%fluorointeg.m
%Written by Tania Darnton on March 17, 2014
%This is a function that will take a set of fluorimetry data in matrix form
%and calculate the area under the curve.
xprime=x(2:77);
yprime=y(2:77);
xdoubleprime=x(78:end);
ydoubleprime=y(78:end);
yzero=max(yprime,0);
ydoublezero=max(ydoubleprime,0);
areafluoro = trapz(yzero);
areaphos=trapz(ydoublezero);
ratio = areafluoro/areaphos;
area = areafluoro;
totalarea = areafluoro + areaphos;
fprintf('\n The area under the fluoroescence curve is %s. \n',areafluoro)
fprintf('\n The area under the phosphorescence curve is %s. \n',areaphos)
fprintf('\n The ratio of fluorescence to phosphorescence is %s. \n',ratio)
fprintf('\n The area under the entire curve is %s. \n',totalarea)

end
```

A.5.3 Singlet quantum yield calculation

The script ‘qyanalog’ takes a named set of data from the user and calculates a quantum yield for the singlet state of $Pt(pop\text{-}BF_2)^{4-}$. As upwards of sixteen individual variables must be called, the user must utilize a methodical nomenclature system for their variables so that all the data will be called correctly by the script. Users should give their data systematic names ending in ‘x’ and ‘y’ as appropriate; fluorescence and absorbance data for the same sample should vary only in the addition of an ‘f’ at the beginning of the variable name. For example, a sample analyzed at 10 ºC could have absorbance data imported as ‘10degx’ and ‘10degy’ while the corresponding fluorimetry data might be called ‘f10degx’ and ‘f10degy’. By setting the parent experimental variable name to ‘10deg’, the script will concatenate tags for ‘f’, ‘x’, and ‘y’ to the parent name and call the appropriate variables. This script also requires the subfunction ‘fluorointegpartial_qyanalog’, which is presented in section A.5.3.1.

```
qyanalog.m
```

```
%qyanalog.m
%Written by Tania Darnton on March 15, 2014 (approximately)
%Last revision on: June 6, 2014 --> changed QY of anthracene to be 0.27
%This script uses the function fluorointeg to determine the
%quantum yield of an unknown solution.
%The final function 'Qx' calculates the quantum yield of an unknown compound
%based on a standard
%   This function is from J. Phys Chem, Crosby & Demas, vol 75, number 8,
%   p.991, April 1971. On p 999, a function for calculating the quantum
%   yield of an optically dilute solution is put forward.
empty = [];
Qr = input('\n What is the quantum yield of your reference solution at the
parameters of interest? If you do not input a value, 0.27 (anthracene) will
be used. \n');
if isequal(Qr,empty)
        Qr = 0.27;
    end
nx = input('\n What is the average refractive index of your REFERENCE
solution to the luminescence? If you do not input a value, the RI for EtOH
will be used.\n');
if isequal(nx,empty)
        nx = 1.3611;
end
nr = input('\n What is the average refractive index of your SAMPLE solution
to the luminescence? If you do not input a value, the RI for MeCN will be
used.\n');
if isequal(nr,empty)
        nr = 1.3442;
end

locrabs = input('\n What is the parent variable name of your reference
absorbance data?\n','s');
locrlum = input('\n What is the parent variable name of your reference
luminescence data?\n','s');
locsabs = input('\n What is the parent variable name of your sample
absorbance data?\n','s');
locslum = input('\n What is the parent variable name of your sample
luminescence data?\n','s');

strsx = strcat(locsabs,'x'); % Concatenate absorbance parent variable name
with tags 'x' and 'y'
strsy = strcat(locsabs,'y');
strrx = strcat(locrabs,'x');
strry = strcat(locrabs,'y');
locx = evalin('base',strsx); % Evaluate the new variables (for some reason
it doesn't work without this step; it will keep having strx be a string
instead of the var). 'Base' is the basic workspace
locy = evalin('base',strsy);
```

```
locrx = evalin('base',strrx);
locry = evalin('base',strry);
strflsx = strcat(locslum,'x');% Concatenate fluorometry parent variable name
with tags 'f', 'x' and 'y'
strflsy = strcat(locslum,'y');
strflrx = strcat(locrlum,'x');
strflry = strcat(locrlum,'y');
flsx = evalin('base',strflsx); % Evaluate the new variables (for some reason
it doesn't work without this step; it will keep having strx be a string
instead of the var). 'Base' is the basic workspace
flsy = evalin('base',strflsy);
flrx = evalin('base',strflrx);
flry = evalin('base',strflry);

wavelength = input('At what wavelength do you wish to know the absorbance?
If you do not input a value, 355 nm will be used.');
    if isequal(wavelength,empty) %Having default wavelength be 355 nm
        wavelength = 355;
    end
    c = find(locx >= 355 & locx <= 356); %Find the index of the desired
wavelength in the sample
  Ax = locy(c); %Find the absorbance at the desired wavelength in the sample
 Dx = fluorointegpartial_qyanalog(flsx,flsy); %Find the area under the
fluorescence curve of the sample


   d = find(locrx >= 355 & locrx <= 356); %Find the index of the desired
wavelength in the reference
  Ar = locry(d); %Find the absorbance at the desired wavelength in the
reference
 Dr = fluorointeg(flrx,flry); %Find the area under the fluorescence curve of
the reference

Qx = Qr*(Ar/Ax)*((nx)^2/(nr)^2)*(Dx/Dr);
fprintf('\n The quantum yield is %.4f. \n The following variables were used:
\n Reference data = %s \n Sample data = %s \n Wavelength of interest = %.3f
nm \n Qr (quantum yield of reference) = %.4f \n Ar (absorbance of reference)
= %.4f \n Ax (absorbance of sample)=%.4f \n nx (refractive index of sample)
= %.4f \n nr (refractive index of reference) = %.4f \n Dx (area under sample
fluoroescence curve) = %s \n Dr (area under reference fluoroescence curve) =
%s \n',Qx,locrabs,locsabs,wavelength,Qr,Ar,Ax,nx,nr,Dx,Dr)
```

A.5.3.1

```
fluorointegpartial_qyanalog(x,y)
```

```
function [area] = fluorointegpartial_qyanalog(x,y)
%Written by Tania Darnton on May 1, 2014
%This is a function that will take a set of fluorometry data in matrix
form
%and calculate the area under the fluorescence part of the curve only.
yprime=y(2:77);
yzero=max(yprime,0);
```

```
area = trapz(yzero);

end
```